

This dissertation/thesis/report entitled:

The Behavior of Pit Fires

written by:

Veronica Kimmerly

has been approved for the degree of:

Doctor of Philosophy

in


Fire Protection Engineering

by

Rangwala, Ali S (483978) Digitally signed by Rangwala, Ali S (483978)
Date: 2022.07.20 07:05:37 -0400'

Ali S. Rangwala, PhD, Thesis Director

1 - Advisor Name



Albert Simeoni, PhD, Committee Member

2 - Department Chair or Committee Member Name

member: 765A9D01-CEB8-49FE-AD45-756F9EE13EA9 077AF830-456F-4ECC AD45-756F9EE13EA9-077AF830-456F-4ECC 8566C-8D33918
B69D-BB0391BE35F4 Digitally signed by member: 765A9D01-CEB8-49FE-AD45-756F9EE13EA9-077AF830-456F-4ECC
Date: 2022.05.23 14:54:04 +0100'

Jose L. Torero, PhD, Committee Memeber

3 - Committee Member Name

Michael T Timko Digitally signed by Michael T Timko
Date: 2022.05.24 09:00:17 +02'00'

Michael Timko, PhD, Committee Member

4- Committee Member Name

Laureen Elgert Digitally signed by Laureen Elgert
Date: 2022.05.24 16:28:09 -04'00'

Laureen Elgert, PhD, Committee Member

5 - Committee Member Name

6 - Committee Member Name

May 2022

Month YEAR



The Behavior of Pit Fires

Veronica Kimmerly

A Dissertation Submitted to the Faculty of
WORCESTER POLYTECHNIC INSTITUTE
in partial fulfillment of the requirements for the
Degree of Doctor of Philosophy
in
Fire Protection Engineering

May 2022

Approved:

Prof. Ali S. Rangwala – Major Advisor

Committee Members:

Prof. Lauren Elgert; Social Science and Policy Studies, WPI, USA

Prof. Albert Simeoni; Fire Protection Engineering, WPI, USA

Prof. Michael Timko; Chemical Engineering, WPI, USA

Prof. José Torero; Civil, Environmental, Geomatic, and Environmental Engineering, University
College London, UK

Table of Contents

List of Figures	6
List of Tables	10
List of Equations	10
Nomenclature	13
Vita.....	15
Acknowledgments.....	18
Abstract.....	19
1 Introduction and Problem Discussion.....	22
1.1 Motivation	26
1.2 Current State of Research.....	29
1.2 Objective and Thesis Structure	35
2 Theory and Mathematical Model	36
2.1 Fundamentals of Pit Fire Behavior.....	36
2.2 Idealized Pit Fire	41
2.3 One Zone Model.....	43
2.2.1 Conservation of Mass	47
2.2.2 Conservation of Energy	48
2.2.3 Conditional Equations	50
2.2.4 Conservation of Species	52
2.2.5 Ramp-Up Term.....	53

2.2.6	Final Model Equations.....	53
2.2.7	Parametric Study.....	54
3	Air Flow in Pit Fires	59
3.1	Experimental Setup	59
3.2	Results	63
3.2.1	Centerline and Radial Temperature Profiles	64
3.2.2	Air Entrainment Correlation.....	66
3.2.3	Carbon Monoxide and Carbon Dioxide Production.....	71
3.2.4	Oxygen Penetration and Parameter Characterization.....	73
3.3	Particle Imaging Experiments	79
3.3.1	Objective.....	80
3.3.2	Methodology.....	81
3.3.3	Results.....	83
3.3.4	Discussion.....	86
4	Mass Loss Rates for Pit Fires	88
4.1	Experimental Setup	88
4.2	Results	91
4.2.1	Mass Loss Rate.....	91
4.2.2	Flame Height	94
4.2.3	Centerline and Radial Temperature Profiles	96

4.2.4 Flame Height	99
4.3 Comparison to 1-D model	100
5 Conclusions and Future Work	101
References.....	108
Annex A – Model Code Gas Burner.....	118
Annex B – Model Code Liquid.....	121
Annex C – Model Graphs	125
10 g/min.....	125
U/D = 0.5	125
U/D = 0.75	126
U/D = 1.0	126
U/D = 1.5	128
U/D = 2.0	129
14 g/min.....	130
U/D = 0.5	130
U/D = 0.75	130
U/D = 1.0	131
U/D = 1.5	132
U/D = 2.0	133
18 g/min.....	134
U/D = 0.5	134

U/D = 0.75	135
U/D = 1.0	136
U/D = 1.5	137
U/D = 2.0	138
Kerosene.....	140
U/D = 0.5	140
U/D = 0.75	141
U/D = 1.0	142
U/D = 1.5	143

List of Figures

Figure 1-1 Ideal Refuse Setup Pit from Oxfam [10].....	25
Figure 1-2 - Influence of a flush floor on pool fire air entrainment observed by Wu et al. [26] using smoke visualization for (a) tray with no flush floor and (b) with a flush floor.....	30
Figure 1-3 - Reduction in flame necking in an ice cavity fire [27].....	31
Figure 1-4 - Experimental temperature distribution within an ice cavity for crude oil (ullage = 0.2 m) [27]	31
Figure 2-1 - Instantaneous flame images over a pulsation cycle for ullages of (a) 0D, (b) 0.25D and (c) schematic of stage I flame at 0.25D ullage.....	37
Figure 2-2 - Instantaneous flame images over a pulsation cycle for ullages of (a) 0.5D, and (b) schematic of stage II flame at 0.5D ullage.....	39

Figure 2-3 - Instantaneous flame images over a pulsation cycle for ullages of (a) 0.75D, (b) 1D, and (c) schematic of stage III flame at 0.75D ullage	40
Figure 2-4 - Instantaneous flame images over a pulsation cycle for ullages of 1.5D (top) and schematic of stage IV flame (bottom).....	41
Figure 2-5 - Idealized experimental setup of a pit fire with a gas burner.	42
Figure 2-6 - Than and Savilonis experimental temperature data across the ceiling vent [40].....	44
Figure 2-7 – Than and Savilonis model data across the ceiling vent [40].....	45
Figure 2-8 - One-dimensional pit geometry with control volume outline in red.....	47
Figure 2-9 Critical oxygen concentration as function of cavity temperature for kerosene (solid line) and methane (dashed line)	51
Figure 2-10 – Average temperature, oxygen concentration, and mass flow for a gas burner from one-zone model.....	56
Figure 2-11 – Average temperature, oxygen concentration, and mass flow for a 57 cm diameter kerosene pit fire.....	58
Figure 3-1 - 9 cm x 9 cm Square Pit, Z_{SS} = steady smoke layer height, U = ullage.....	61
Figure 3-2 - Experimental setup – non-premixed methane burner with adjustable fuel injector level. The inset on the right shows locations of thermocouples	63
Figure 3-3 - Air entrainment patterns for different ullages in a circular pit with a methane burner.	64
Figure 3-4 - Plume centerline temperatures in the axial direction at 0D to 1.5D for 10 g/min fuel in a circular pit.	65
Figure 3-5 Radial temperature profiles at z-locations of 47, 49 and 51 cm measured from exit of	66

Figure 3-6 - Experimental versus theoretical entrainment rate for a square pit fire with dotted lines represented +/- 10% error.....	69
Figure 3-7 - Air entrainment as a function of ullage	70
Figure 3-8 - Flapping frequency as a function of ullage with flame emissions, demonstrating a region of enhanced burning for a fuel flow rate of 6 g/min. CO/CO ₂ measured using a Servomex Gas Analyzer of smoke extracted at 40 cm above the pit.	72
Figure 3-9 - Representative variation of (a) boundary layer thickness at $z = U$, and (b) radial diffusion time scale of oxygen with ullage and fuel inlet velocity	75
Figure 3-10 - Schematic showing boundary layer formation and flame width, (b) variation of flame width with ullage for different fuel flow rates (symbols represent experimental values, lines represent the predicted values)	76
Figure 3-11 - Representative variation of (a) dimensional, and (b) non-dimensional axial diffusion scale of oxygen with ullage and fuel inlet velocity	77
Figure 3-12 - Variation of non-dimensional oxygen penetration with ullage	78
Figure 3-13 - Schematic of the flame behavior at ullage (a) U_1 , (b) U_2 , and (c) U_3 [$U_1 < U_2 < U_3$]	79
Figure 3-14 - Experimental setup diagram (left) and photo (right)	82
Figure 3-15 - The theorized relationship between ullage and flame behavior (red arrows signify airflow and blue arrows signify flame movement)	83
Figure 3-16 - Sample recirculation vortex formed next to the cavity wall	84
Figure 3-17 - $U = 2$ cm ($U/D = 0.25$), stage II flames, with airflows highlighted by white arrows	84
Figure 3-18 - $U = 4$ cm ($U/D = 0.5$), stage II flames, with airflows highlighted by white arrows	85

Figure 3-19 - $U = 6$ cm ($U/D = 0.75$), stage IV, with airflows highlighted by white arrows	86
Figure 3-20 - Clumps of seeding particles in the field of view	87
Figure 4-1 - Meso-scale kerosene pool fire setup.....	90
Figure 4-2 - Mass flux rates for meso-scale and small-scale pool fires in pit geometries with varying ullage.....	92
Figure 4-3 Burning rate data from Drysdale [69] with ullage cases from Figure 4-2.	93
Figure 4-4 Non-dimensionalized flame height data from Drysdale [69] with meso-scale ullage cases.	94
Figure 4-5 – Flame heights over time for small-scale [28] and meso-scale pool fires in pit geometries with varying ullage.	95
Figure 4-6 Centerline plume temperatures for meso-scale (57.3 cm diameter) kerosene pool fires.	97
Figure 4-7 Radial plume temperatures for meso-scale experiments at 1.6, 1.8, and 2.0 meters above the “ground” for several ullages.	98
Figure 4-8 Flame height for ullage	100
Figure 4-9 Average Pit Temperature for Meso Scale Experiments and Modelling	101
Figure 5-1 – Comparison of model and experimental temperature results for a 9 cm diameter methane pit fire	103
Figure 5-2 – Comparison of model and experimental results frequency results for a 9 cm diameter 10 g/min methane pit fire	104

List of Tables

Table 1 - Summary of experimental studies into ullage effects in similar geometries (tank fires, pit fires (like tank fires but with the ground around the opening), and trench fires (elongated tanks)) and with several fuel types over a range of ullage to the diameter.....	33
Table 3 -Variables and dimensions for air entrainment analysis.....	67
Table 4 - A reduced row-echelon form of Table 3.	67

List of Equations

$\frac{dm}{dt} + \dot{m}_i - \dot{m}_f = 0$ [2-1].....	47
$\frac{dm}{dt} = \frac{d(\rho V)}{dt} = V \frac{d\rho}{dt}$. [2-2].....	47
$\frac{d\rho}{dt} = \frac{1}{R_{MW}} \frac{d(\frac{P}{T})}{dt}$ [2-3].....	48
$\frac{dm}{dt} \approx \rho_\infty T_\infty V \frac{d(1/T)}{dt}$. [2-4].....	48
$\rho_\infty T_\infty V \frac{d(1/T)}{dt} + \dot{m}_i = \dot{m}_f$. [2-5].....	48
$\frac{dU}{dt} + \dot{m}_i C_p T_i - \dot{m}_f C_p T_f = \dot{Q} - hA_s(T - T_\infty)$ [2-6].....	48
$\frac{dU}{dt} = C_v V \frac{d(\rho T)}{dt} = C_v V \frac{d(P/R)}{dt}$, [2-7].....	48
$R = C_p - C_v$ $\gamma = \frac{C_p}{C_v}$. [2-8].....	49

$$\boxed{\frac{dU}{dt} = \frac{V}{\gamma-1} \frac{dP}{dt}} \quad [2-9] \dots\dots\dots 49$$

$$\dot{m}_f'' = \dot{m}_\infty'' + \frac{h_c \left(\frac{\lambda}{e^\lambda - 1} \right) \left(\frac{\Delta H_c}{c_p r} \right) (1 - X_r) (Y_{O_2} - Y_{O_2, \infty}) + F\sigma(T^4)}{h_{fg} + c_{p,o}(T_v - T)} \quad [2-10] \dots\dots\dots 49$$

$$\frac{V}{(\gamma-1)} \frac{dP}{dt} + \dot{m}_t C_p \{ \eta(\Delta P_t) T + \eta(-\Delta P_t) T_\infty \} - \dot{m}_f C_p T_f = \dot{Q} - hA_s(T - T_\infty) \quad [2-11] \dots\dots\dots 49$$

$$\dot{m}_t'' = \begin{cases} A_o C_d \sqrt{2\rho(t)\Delta P_t}, & \Delta P_t > 0 \\ -A_o C_d \sqrt{2\rho_\infty |\Delta P_t|}, & \Delta P_t \leq 0 \end{cases} \text{ and } T_t = \begin{cases} T(t), & \Delta P_t > 0 \\ T_\infty, & \Delta P_t \leq 0 \end{cases} \quad [2-12] \dots\dots\dots 50$$

$$\rho(t) = \frac{\rho_\infty T_\infty}{T(t)} \text{ and } \Delta P_t = P(t) - P_\infty + (\rho_\infty - \rho(t))gU \quad [2-13] \dots\dots\dots 50$$

$$Q = \begin{cases} \dot{m}_f'' \Delta H_c A_f, & Y_{O_2}(t) > Y_{O_2, crit} \\ 0, & Y_{O_2}(t) \leq Y_{O_2, crit} \end{cases} \quad [2-14] \dots\dots\dots 50$$

$$Y_{O_2, crit} \approx c_p(T_f - T_\infty)(\Delta h_c - L)/r \quad [2-15] \dots\dots\dots 50$$

$$\rho_\infty T_\infty V \frac{d(Y_{ox}/T)}{dt} + (Y_{ox})_{Top Vent} \dot{m}_t = -\dot{Q}/\Delta H_{ox}. \quad [2-16] \dots\dots\dots 52$$

$$\boxed{\rho_\infty T_\infty V \frac{d(Y_{ox}/T)}{dt} + [\eta(\Delta P_t) Y_{ox} - \eta(-\Delta P_t)(0.233)] \dot{m}_t = -\dot{Q}/\Delta H_{ox}} \quad [2-17] \dots\dots\dots 52$$

$$\dot{m}_f = (1 - \exp(-0.1 * t)) * \dot{m}_{fuel}'' * \frac{Y_{ox}(t)}{0.233} \quad [2-18] \dots\dots\dots 53$$

$$\rho_\infty T_\infty V \frac{d(1/T)}{dt} \pm \dot{m}_T - \dot{m}_f = 0$$

$$\frac{V}{\gamma-1} \frac{dP}{dt} \pm \dot{m}_T C_p T = \dot{Q} - hA_s(T - T_\infty) \quad [2-19] \dots\dots\dots 53$$

$$\rho_\infty T_\infty V \frac{d(Y_{ox}/T)}{dt} \pm Y_{ox} \dot{m}_T = \frac{-\dot{Q}}{\Delta H_{ox}}$$

$$F^0 L^0 T^0 \theta^0 \stackrel{\text{def}}{=} \left(\frac{\rho c_p \sigma^{\frac{1}{4}} U^{\frac{7}{2}} f}{\dot{Q}^{\frac{5}{4}}} \right)^{a5} \left(\frac{\dot{Q}^{\frac{3}{2}} \dot{m}_{ent}'''}{(\rho c_p)^2 \sigma^{\frac{1}{2}} U^2} \right)^{a6} \left(\frac{T_{\infty} \sigma^{\frac{1}{4}} U^{\frac{1}{2}}}{\dot{Q}^{\frac{1}{4}}} \right)^{a7} \left(\frac{g(\rho c_p)^2 U^6}{\dot{Q}^{\frac{5}{2}} \sigma^{-\frac{1}{2}}} \right)^{a8} \quad [3-1] \dots 68$$

$$\frac{U^{\frac{7}{2}} f}{\dot{Q}^{\frac{5}{4}}} \propto \frac{\dot{Q}^{\frac{3}{2}} \dot{m}_{ent}'''}{U^2} \quad [3-2] \dots 68$$

$$\dot{m}_{ent}''' \propto \frac{U^{\frac{11}{2}} f}{\dot{Q}^{\frac{11}{4}}} \quad [3-3] \dots 68$$

$$\dot{m}_{ent}''' = 1.6 \left(\frac{U^{5.5} f}{\dot{Q}^{2.75}} \right)^{-0.16} \quad [3-4] \dots 68$$

$$\frac{\partial Y_F}{\partial t} + \frac{\partial(u_F Y_F)}{\partial z} = \wp_{F,O_2} \frac{1}{r} \frac{\partial^2(r Y_F)}{\partial r^2} + \wp_{F,O_2} \frac{\partial^2 Y_F}{\partial z^2} \quad [3-5] \dots 73$$

$$\sim \frac{1}{\tau_F} \quad \sim \frac{u_F}{U} \quad \sim \wp_{F,O_2} \frac{4}{D^2} \quad \sim \wp_{F,O_2} \frac{1}{U^2} \quad [3-6] \dots 73$$

$$\tau_F \sim \left[\frac{U}{u_F} \right] \quad \tau_F \sim \left[\frac{\delta^2}{\wp_{F,O_2}} \right] \quad \tau_F \sim \left[\frac{U^2}{\wp_{F,O_2}} \right]$$

(advection of fuel) (radial diffusion of fuel) (axial diffusion of fuel) [3-7] \dots 74

$$\frac{\partial Y_{O_2}}{\partial t} = D_{O_2,F} \frac{1}{r} \frac{\partial^2(r Y_{O_2})}{\partial r^2} + D_{O_2,F} \frac{\partial^2 Y_{O_2}}{\partial z^2} \quad [3-8] \dots 74$$

$$\sim \frac{1}{\tau_O} \quad \sim D_{O_2,F} \left[\frac{1}{\delta} \frac{\delta}{\delta^2} \right] \quad \sim D_{O_2,F} \left[\frac{1}{U^2} \right] \quad [3-9] \dots 74$$

$$\tau_O \sim \left[\frac{\delta^2}{D_{O_2,F}} \right] \quad \tau_O \sim \left[\frac{U^2}{D_{O_2,F}} \right] \quad [3-10] \dots 74$$

(radial diffusion of O₂) (axial diffusion of O₂)

$$\delta_z = \frac{5z}{\sqrt{\text{Re}_z}} = 5z \sqrt{\frac{u_F}{u_F z}} = 5 \sqrt{\frac{u_F z}{u_F}} \quad [3-11] \dots 75$$

$$\tau_{O_2,D} \sim 25 \frac{v_F}{\varphi_{O_2,F}} \frac{U}{u_F} \sim 25(Sc) \frac{U}{u_F} \quad [3-12] \dots\dots\dots 75$$

$$L_W \sim D - 2\delta_U \Rightarrow \frac{L_W}{D} \sim 1 - \frac{2\delta_U}{D} \quad [3-13] \dots\dots\dots 76$$

$$\tau_{F,A} \sim \left[\frac{L_{O_2}^2}{\varphi_{O_2,F}} \right] \Rightarrow L_{O_2} \sim \sqrt{\tau_{F,A} \times \varphi_{O_2,F}} \Rightarrow L_{O_2} \sim \sqrt{\frac{U}{u} \varphi_{O_2,F}} \quad [3-14] \dots\dots\dots 76$$

Nomenclature

A_s : interior surface area of the enclosure (m^2)

L_f : flame length (m)

L_{O_2} : oxygen penetration depth (m)

m : mass of gas in the enclosure (kg)

\dot{m}_f : fuel mass evaporation rate (kg/s)

\dot{m}_t : mass flow rate out of the top (can be negative to indicate in-flow) (kg/s)

\dot{m}_{ent}''' : volumetric air entrainment rate for a specific direction (kg/m^3s)

\dot{m}_{out}''' : volumetric flow rate of the plume with species concentrations of oxygen, carbon dioxide, and carbon monoxide (kg/m^3s)

\dot{m}_{fuel} : mass flow rate of fuel (kg/s)

f_A : base anchoring frequency (s^{-1})

f_F : flapping (flame opening) frequency (s^{-1})

f_P puffing (vertical flame stretching) frequency (s^{-1})

f_S : side location frequency (s^{-1})

h : overall heat transfer coefficient that accounts for convection, radiation, and conduction effects (W/m^2K)

P_{∞} : ambient air pressure (Pa)

\dot{Q} : fire heat release rate (kW)

\dot{Q}_{conv} : convective heat from hot gases (kW)

\dot{Q}_{rad} : radiative heat from pit walls (kW)

T_{∞} : ambient air temperature (K)

T_t : temperature of the gas flowing out of the top (K)

T_v : temperature of the surface of the liquid fuel (K)

U : internal energy of the enclosed gas (kJ)

V : the volume of the enclosure (m^3)

Y_{ox} : mass fraction of oxygen in the enclosure

ΔH_c : heat of combustion of the fuel (kJ/g)

ΔH_{ox} : heat of combustion per unit mass of oxygen consumed (kJ/g)

ρ_{∞} : ambient air density (kg/m^3)

Vita

Veronica Kimmerly

Worcester Polytechnic Institute

Department of Fire Protection Engineering

100 Institute Road, Worcester, MA 01609

Email: vmkimmerly@wpi.edu, Veronica.Kimmerly@ul.com

Doctorate of Philosophy, Worcester Polytechnic Institute, 2020

Department: Fire Protection Engineering

Committee: Prof. Ali S. Rangwala, Prof. Laureen Elgert, Prof. Albert Simeoni, Prof.

Michael Timko, Prof. Jose Torrero

Dissertation: "The Behavior of Pit Fires"

Master of Science, University of Ghent, Lund University, University of Edinburgh, 2017

Department: International Masters of Fire Safety Engineering

Advisor: Prof. Luke Bisby

Thesis: "Verification and Validation of a Structures in Fire Model"

Bachelor of Science, Virginia Polytechnic Institute and State University, 2015

Departments: Chemical Engineering, Mathematics

Chemical Engineering Capstone Project: "Steam System for Acid Recovery Facility for BAE"

PUBLICATIONS

Journal:

V. Kimmerly, A. Rangwala, "Laboratory-scale Investigation of Air Entrainment in Burn Pits Used for Waste Disposal," *FUEL*, 276 (2020).

V. Kimmerly, S. Nair, A. Rangwala, V. Raghavan, "Characterization of Homogeneous Diffusion Flames in Ullages", *Fire Safety Journal*, (submitted 2022).

Conference:

V. Kimmerly, A. Rangwala, "Laboratory-scale Investigation of Air Entrainment in Burn Pits Used for Waste Disposal," 16th International Congress on Combustion By-Products and Their Health Effects, Ann Arbor, MI, July 10-12, 2019

V. Kimmerly, A. Rangwala, "Effects of ullage on combustion efficiency and plume entrainment of pit fires," 11th U.S. National Combustion Meeting, Pasadena, CA, March 24-27, 2019

V. Kimmerly, A. Rangwala, "Effects of ullage on combustion efficiency and plume entrainment of pit fires," Eastern States Section Combustion Institute Spring Technical Meeting, University Park, PA, March 4-7, 2018

Poster:

V. Kimmerly, A. Rangwala, "Effects of Ullage on Pit Fires," National Fire Protection

Association Conference and Expo, San Antonio, TX, June 17-20, 2019

V. Kimmerly, A. Rangwala, "Effects of Ullage on Pit Fires," Graduate Research Innovation

Exchange WPI, February 6, 2019

V. Kimmerly, A. Rangwala, "Effects of Ullage on Pit Fires," National Fire Protection

Association Conference and Expo, Las Vegas, NV, June 11-14, 2018

Presentation:

V. Kimmerly, "Open Burning of Trash – The Problem No One Wants to Talk About," 3-Minute

Thesis Competition, WPI, 2019 (First Place Winner)

WORK EXPERIENCE

UL LLC, Fire Research and Development, Research Engineer III

Northbrook, IL, November 2020 – Present.

U.S. Army Corps of Engineering, Cold Regions Research and Engineering Lab, Student Trainee,

Hanover, NH, June 2018 – March 2020.

Jensen & Hughes, Research and Development Intern,

Blacksburg, VA, June – August 2016.

DuPont, Tyvek® Building Innovation, Research and Development Co-op Student,

Richmond, VA, August 2012 – May 2013.

Acknowledgments

I want to thank my advisor, Professor Ali Rangwala, for all the guidance and encouragement he has provided me throughout my research and my time at WPI. It has been a joy to be part of the Fire Protection Engineering department, and I finally met Prof. Albert Simeoni after just missing him at the University of Edinburgh. I owe so much to Sharanya Nair for her assistance with experiments and her wonderful insights while writing our paper. I also need to thank Diane Poire for her unfailing support and invaluable resources. I want to thank my colleagues in the combustion lab, Trevor, Li, Pi, Nate, Mahesh, Suhas, and Matt, for always being willing to lend a hand or listen to a question. Without Trevor Borth, my time at WPI would not have been nearly as much fun nor my sanity as intact after writing my thesis. Also, I want to thank Ray and Fritz for their help in working on various projects in both the big lab and the combustion lab. Many thanks to my committee for their helpful comments and different perspectives on my research. I want to thank Prof. Jackie Sung and Kyle Twarog for their time and resources during my time at Dr. Sung's lab at the University of Connecticut. I want to thank my roommates, Alexandra and Annelise, for commiserating with me over grading assignments and ranting with me about research challenges. Also, I want to thank my colleagues at UL for their support and advice during the writing of my thesis. Finally, I want to thank my parents for

always encouraging my academic interests, proofreading every paper I've written in my academic career, and letting me ramble on about my work to them. I wouldn't be an engineer without your inspiration and support.

Abstract

In the past few years research has emerged that identifies open-air waste fires as a significant contributor to global greenhouse emissions and human health hazard with long-term consequences from exposure. Clearly these fires need to be addressed but the context of these fires in low-infrastructure or impoverished regions limits the potential solutions. Given that for many people open-air fires are the only way they can dispose of their waste besides landfilling, it is unlikely that these fires can be eliminated. So, if these fires can't be stopped is there a way they can be improved? Open-air waste fires are typically burned in a pit to limit fire spread and provide thermal protection. Previous research into the effects of a fire in a partially filled pit (ullage is the term for the distance between the fill level and the top of the pit) has found burning is enhanced for some ullage to diameter ratios. If altering the pit geometry and the fuel location within in the pit can improve these fires, either by reducing emissions or reducing exposure time, then it is a highly implementable solution to this hazard.

To investigate the effects of ullage on pit fire behavior, a series of small-scale and meso-scale experiments are performed in conjunction with the development of a one-zone model. The small-scale experiments (9 cm and 10 cm diameters) decoupled the burning rate from the air flow by using a methane gas burner. The first set of experiments analyzed the characteristics of a fire in a pit using an experimental set up comprising of a square burner with fuel (methane) injected into

the burner at different ullages (U) with three flow rates (2, 4, and 6 g/min) to vary the heat release rate. The flame dynamics are captured using high-definition video. Air entrainment is measured using a vent hood, where the products of combustion are collected and detailed temperature measurements within the hood are used to determine the location of the steady smoke layer height. At all fuel flow rates, the flame fluctuates inside the ullage, opening up at the central portion at one time instant and closing down to a conical flame at another time instant. Based on the value of fuel flow rate and ullage value, the frequency of this flame fluctuation varies. At a fuel flow rate of 2 g/min, the flame is diffusion controlled. As the fuel flow rate is increased, convection begins to dominate. Based on the ullage and fuel flow rate, partial premixing of air and fuel occurs within the ullage and a bluish flame is observed showing highly efficient combustion behavior. In summary, for a given ullage, there is a range of fuel flow rates where the airflow into the ullage is strong enough to impart partial premixing. Thus, based on the fuel flow rate or the heat release rate, an appropriate ullage can be chosen to improve the burning performance. The air entrainment depends directly on the heat release rate and inversely on the ullage and fluctuation frequency values. Based on this an engineering correlation based on a similarity analysis is proposed and experimental and theoretical values of air entrainment are within reasonable agreement. The correlation is limited because assumptions of negligible radiation and decoupling of mass transfer are made when using a gas burner in the experiments. However, the correlation is valuable as it led to a systematic study of air entrainment effects on heat release rate in a pit.

The second set of small-scale experiments are conducted to study the effect of pit depth on flame pulsation, anchoring, oxygen penetration, and temperature in buoyant diffusion flames of methane in a cylindrical burner. Depending upon the ullage (i.e., pit depth), four stages of flame behavior are identified. Stage I exhibits stable flames anchored close to the porous plate with

vertical pulsation. At higher ullages, the flame also exhibits a U-shaped flame with a certain pulsation frequency (termed as stage II). At even higher ullages, the anchoring location begins to vertically oscillate in the pit while still exhibiting both vertical and U-shape pulsation (termed stage III). At the highest ullages, oxygen cannot penetrate very far into the pit, causing the flame to anchor towards the top of the pit and only exhibit small vertical oscillations (termed Stage IV). Temperature, vertical pulsation frequency, flame height, and penetration depth determine that Stage III flames are the optimal flame stage and exhibit enhanced burning. A parameter characterization study has also been conducted to explain the diffusive and convective time scales in pit fire. This work indicates that an open-air pit fire can be designed with a certain ullage to diameter ratio that could have Stage III flame behavior and enhance the efficient burning of waste in these pits.

Then meso-scale experiments (57 cm diameter) were conducted with a condensed fuel (kerosene) where mass loss rate is coupled to the air entrainment and radiative heat flux. A constantly replenishing pool system was used to maintain a constant ullage below the fire. These experiments were conducted to determine if stage II fires are still enhanced at the meso-scale and if the trends in plume temperatures from the small-scale persist. The results confirm that stage II flames are enhanced, with comparable mass flux to that seen at 0D (pool fire) but with shorter flames, indicating reduced flame necking leading to a cylindrical shaped flame. The temperature profiles showed a similar trend to that seen at the small-scale with 0.75D having the highest plume temperature despite the shortest flames (and thus further from the TC tree). Finally, the experimental results are compared to data from a simple 1-D model and the model is shown to be accurate enough to use as a tool for designing future large scale experiments with condensed fuels.

In the future, more experiments are needed to determine the fire behavior at the large scale ($D \geq 1$ m) and what ullage to diameter is optimal, to better visualize and model the flow field of the flame with PIV and advanced modelling, to further the understanding of radiative heat flux in the pit with more temperature measurements inside the pit cavity, and finally to determine the chemistry behind the reduction in CO production and if this reduction is significant enough to impact the health and environmental hazards presented by waste fires

1 Introduction and Problem Discussion

In many parts of the world, people's first-hand experience with fire happens in the context of waste disposal fires, mainly burn pits. Recent research has highlighted the environmental and health impacts of these fires, but little work has been raised on combatting this issue. A major hurdle to reducing this hazard is that for many people burn pits are their best or only way to manage solid waste, so they are unlikely to stop this behavior even when informed of the hazards. This thesis seeks to understand the fundamentals of how fire behaves in a pit and if there are simple ways to enhance these waste fires' combustion and thereby reduce the hazards they present.

For millennia, human-generated waste consisted of biomass (plant matter, food scraps, sewage, bone, etc.), and this was either decomposed or burned, with fire being much faster. This

lead to the development of "slash and burn" agriculture, where a fire is used to eliminate undesired biomass while the ash provides nutrients to the soil [1]. Historically, smaller-scale fires (e.g., not acre-sized) occurred in pits, which helped contain the fire to one area and contain the heat for both protection and other uses (e.g., cooking, pottery making, metal refining, etc.). A burn pit is extremely easy to construct, and soil or rock is a good insulator that allows for heat to be trapped within the pit. This trapped heat is then used for other purposes and enhances the combustion of the solid waste fuel. As we enter the modern era of waste, beginning at the end of the 19th century, as industrialization and cities grow, fire as a waste disposal method persists because it effectively reduces solid waste volume. In the U.S., "as recently as 1960, almost a third of U.S. municipal solid waste was incinerated" [2]. Also, "many sanitation authorities believed that the most hygienic and efficient way to deal with trash was to burn it, ... British and other European cities had experimented successfully with this method beginning in the 1870s" [3]. Fire is the most efficient means of reducing the amount of solid waste, with incineration shown to reduce the volume by 80% and mass by 70% [4]. This is the primary motive of many who set waste fires, "another negative phenomenon developed during the uprising is the frequent open burning of waste accumulated in municipal solid waste dumps within city boundaries, primarily to reduce waste volume [4]". However, early incinerators were inefficient and a significant pollution source, which came to outweigh their volume-reducing benefits compared to landfills.

However, in the present day, the rapidly growing population generates 1 to 2 billion metric tons of municipal solid waste per year globally [3], quickly outpacing landfills' capacity. Additionally, the nature of this waste has shifted to include increasing amounts of plastics and electronic waste, neither of which breaks down in landfills, causing them to fill up even quicker. The growing environmental movement has also brought societal changes in acceptable waste

disposal methods, such as banning open dumps or focusing on recycling over disposal. Traditionally waste has been disposed of by placing it in a specific location, with higher-income areas burying waste in landfills and the lower-income regions using open dump areas [3]. However, rapid population growth means less available land for dumps and higher energy demand, which has brought incineration back into mainstream waste management strategies. Modern technology [5] has made large-scale incinerators more efficient through better waste processing and collection and cleaner through increased air scrubbing. Thus incineration has become popular in countries with limited area for landfills or where more environmentally friendly methods are desirable (e.g., Germany, Sweden, Norway, etc.) [5]. However, such large-scale facilities are costly to construct and require an extensive infrastructure (trash collection, power supply, etc.) to operate, limiting their effectiveness outside of the global north.

Most open-air waste fires (meaning not in industrial incinerators) occur in remote or poor regions where the cost of other waste disposal methods is prohibitive or other methods do not exist. Therefore these people use the space and tools available to them and construct burn pits, "Contemporary backyard composting and the burn pile at the corner of the rural yard echo long-standing practices of using the margins of personal space for disposal" [3]. Residential burning of waste is a regular practice in developing and developed countries where waste collection prohibits the removal of waste to a central location for treatment or disposal [6]. Establishments such as healthcare institutions [7] and military bases [8] sometimes use open-air fires for waste disposal due to a lack of alternatives and the hazards of merely dumping such waste. Fire is also used as a rudimentary way to recover metals from electronic waste [9] in more impoverished regions.

People using burn pits for waste disposal are aware that the smoke is an irritant and take steps to avoid it by locating the pit such that the smoke moves away from settlements. From an

Oxfam pamphlet [10] for refugee settlements, "Burning or incineration of waste is often used for the disposal of combustible wastes. However, this should be used as a last option and should only take place off-site or at a considerable distance downwind of dwellings. Burning of waste near dwelling can cause nuisance from smoke and can be a fire hazard. Even away from dwellings burning waste creates an environmental hazard concerning the gases, especially CO₂, emitted to the atmosphere. However, burning of waste can reduce the volume of waste when there is limited space for burial or landfill. If the burning of waste is undertaken, it should take place in pits and covered in soil once burnt as with burial. The constraints, which apply for siting household refuse pits also apply here."

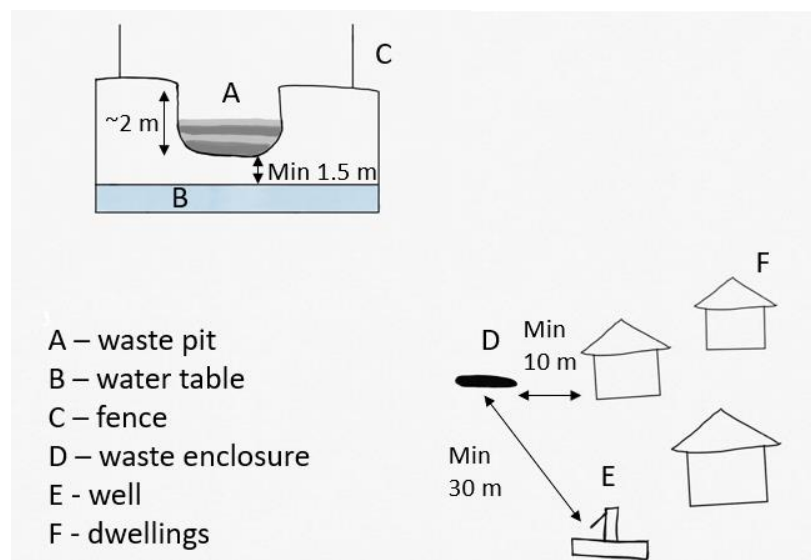


Figure 1-1 Ideal Refuse Setup Pit from Oxfam [10]

A more recent phenomenon is the use of open-air fires to "recycle" electronic waste or, more accurately, burn the plastics away to collect valuable metals from various electronics. "Wire is often burned in the open to remove the plastic insulation to facilitate copper recovery. Circuit boards are also often burned with supplemental fuels in outdoor fires to reduce them to metals.

Subsequently, these metals (primarily copper and tin) are separated from the ash by water floatation. The remaining waste and unusable materials, including the CRT glass, acid solutions, and miscellaneous parts, are either dumped or burned. [9]" These fires are particularly hazardous because of the large amounts of plastics being burned. Just as with waste fires, it is unlikely that people conducting electronic waste fires can be persuaded to stop this behavior, so steps should be taken to make it safer.

1.1 Motivation

Recently, scientists have begun investigating the hazards of open-waste fires and discovered that they significantly contribute to greenhouse gases and long-term health risks. "Emissions from open burning, on a mass pollutant per mass fuel (emission factor) basis, are greater than those from well-controlled combustion sources. Some types of open burning (e.g., biomass) are large sources on a global scale in comparison to other broad classes of sources (e.g., mobile and industrial sources) [11]". Open-air fires tend to produce more hazardous by-products such as aromatic compounds, carbon monoxide, carbon dioxide, and ammonia [11] than controlled fires such as those in incinerators. "Considerable uncertainty exists in the inventory of polychlorinated dibenzodioxin and dibenzofuran (PCDD/F) emissions from uncontrolled combustion sources such as "backyard" burning of domestic waste. These sources' contribution to the worldwide PCDD/F balance may be significant, but few quantitative sampling programs have yet assessed the potential for emission from these sources [12]". Research into uncontrolled (i.e., open-air) waste fires reveals that the emissions typically contain known health hazards such as dioxins, furans, volatile organic compounds, fine particulates, and phenyl compounds [6], [9], [12]–[20]. As Wiedinmyer et al. [6] state, the emissions from waste incinerators are reported in

both national and global inventories of emissions and pollutants, but open-air waste fires are not included. Their research found that in developing regions, CO₂ production from waste fires is a substantial portion of total emissions, and thus efforts to curb emissions should address open-air waste fires. A common hurdle to studying these fires is the wide variety of fuels burned. "There are probably large variations in the amounts and composition of waste combusted in backyard burning both between countries (due to differences in legislation and waste assessment policies) and within countries (due to variations in the availability of regulated waste handling facilities, lifestyle, etc.). However, the scientific literature on these activities is very scant. Apart from a few studies from Belgium (2) and Japan (3, 4), the majority and the most profound published studies reflect conditions in the United States, where legislation often permits the burning of household waste in backyard barrels, and it is a common practice in some areas" [21].

The U.S. Environmental Protection Agency's efforts to reduce emissions from solid-fuel cookstoves found that improving the combustion by altering stove design did reduce the total amount of emissions. However, the emission factors were still in an unsafe range (comparable to a diesel engine [22]). Therefore, reducing the net amount of emissions is unlikely to limit the health hazards of open-air waste fires, but enhancing the burning rate can reduce exposure significantly. A design is desired that reduces exposure time to emissions and reduces the number of emissions. Therefore, a low-cost low-infrastructure method to improve the burning rate of open-air burn pits is greatly needed. It is not possible to completely halt these hazardous fires, but they can be improved.

In addition to the environmental hazards that these open-air waste fires present, they also present significant health hazards. Recent studies conducted by the U.S. Department of Defense into the consequences of open-air burn pits in the Middle East have revealed that even being on

the same base as a burn pit can hurt a person's health [23], [24]. These fires are used because there isn't the existing infrastructure for other waste disposal methods, and if there are, they present security concerns. "Management of U.S. military solid waste at deployed locations has traditionally been a logistical challenge, and failure to manage such waste can reduce personnel combat effectiveness through exposure to pathogens and vector-borne illnesses. The lack of sufficient and safe off-base waste treatment methods in the deployed environment, combined with limited numbers of waste management devices such as incinerators, have forced continued reliance on open burning in "burn pits" as an expedient method of volume reduction and treatment for solid waste during the conflicts in Afghanistan and Iraq or even during training exercises. As one of the most extreme examples, records show that civilian contractors at Joint Base Balad, Iraq, one of the largest military bases and central logistics hub in Iraq at the time, were burning nearly 200 short tons per day of solid waste during peak troop levels [21]". Unlike other burn pits often located in remote or impoverished regions and thus understudied, the U.S. military deals with any health consequences personnel incur while serving. This cost leads to research into reducing these hazards.

Additionally, open-air waste fires can occur accidentally due to overheating or accidental ignition in traditional landfills [16],[14]. A typical example is tire stockpiles which are known to self-ignite, and "these fires, some of which may be started intentionally, generate large amounts of heat and smoke and are difficult to extinguish. This is partly due to the fact that tires, in general, have more heat energy by weight than does coal (37 600 vs. 27 200 kJ/kg) (4). Some tire fires have burned continuously for months, such as the 9-month Rhinehart tire fire in Winchester, VA [25]. The emissions from such fires affect not only the atmosphere but also the land and groundwater due to the liquefaction of the rubber during the combustion process [22]". These fires occur for a

similar reason to other burn pits; the volume of solid waste presents a problem, and fire, whether accidental or intentional, reduces this volume.

1.2 Current State of Research

When reviewing the existing literature on pit fires, extensive research on tank fires is found, but little is found on pit fires. Table 1 presents a comprehensive literature review of studies on or relating to open-air burn pits. From this review, three fire shapes are found: pit, tank, and trench. The earliest research is on tank fires and the effects of ullage, defined as the distance between the tank's opening and the fuel level inside the container. This interest in the impact of ullage on tank fires arose from safety concerns in the chemical industry. Later, interest in trench fires resulted after the tragic fire at the King's Cross train station in the U.K., where the trench shape of the escalators is theorized to have played a critical role in the fire behavior. Experimental results further confirmed the effects of ullage (in this case, trench depth) on the burning rate. Interest in pit fires is a more recent development as the growing hazard of burn pits is identified [6], [8]. The pit shape is unique as there is ground around the vessel opening that alters the fire's airflow. Early work into the effects of ullage on pit fires has also found enhancements in the burning rate.

There are two critical features of the pit geometry: the ullage and the ground. Wu et al. [26] were the first to qualitatively show the change in the behavior of air entrainment into a pool fire set into a flush floor (i.e., with flat ground) vs. a tank (absence of flush floor) using smoke visualizations on a 10 cm square SAE30W oil fire (Figure 1-2). In the absence of the fuel's flush floor, clear eddies could be observed at the edges of the fuel tray. However, when the floor was added, the eddies disappeared, and a random upward flow of gases was observed. Wu et al. did not vary the depth of the fuel surface (ullage). Several studies (see Table 1) have been conducted

on the effects of ullage on tank and trench fires. A few studies have addressed pit fires, possessing both ground and ullage, and are limited in their scope. Therefore, more work is needed to determine the fundamentals of fire behavior in the pit geometry.

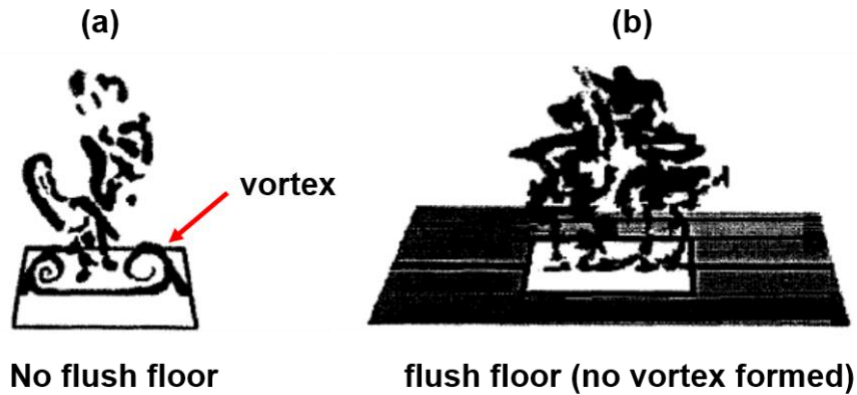


Figure 1-2 - Influence of a flush floor on pool fire air entrainment observed by Wu et al. [26] using smoke visualization for (a) tray with no flush floor and (b) with a flush floor.

Akin to Wu et al.'s study, Rangwala et al.'s work on crude oil fires in ice cavities found a reduction in flame necking in the presence of a pit-like cavity (Figure 1-3), meaning the reaction zone of the fire is wider. This wider reaction zone allows for a flatter (i.e., more uniform) temperature profile across the flame instead of the more typical Gaussian distribution across the radius (Figure 1-4). This combination of higher plume temperatures across the pool diameter and increased reaction area help explain the enhancements in burning seen for increased ullage.

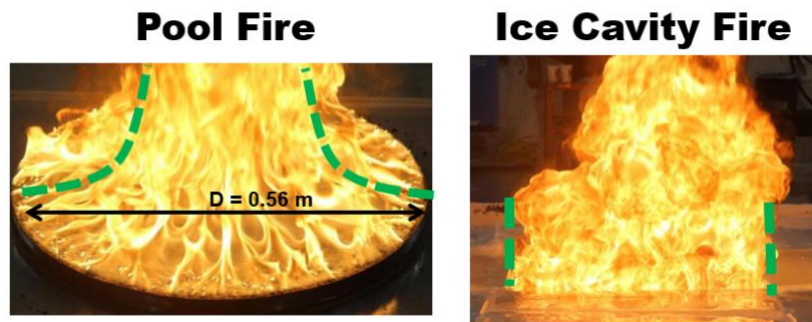


Figure 1-3 - Reduction in flame necking in an ice cavity fire [27]

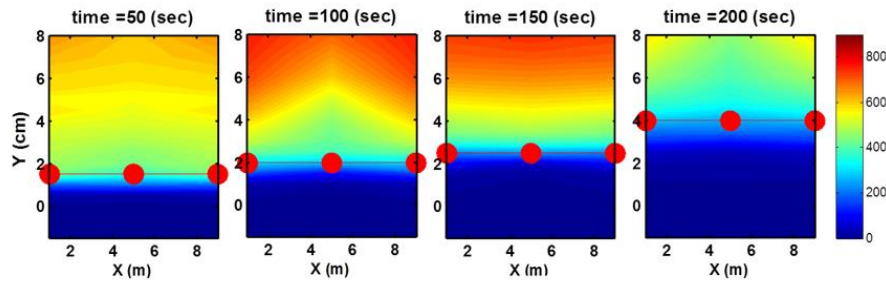


Figure 1-4 - Experimental temperature distribution within an ice cavity for crude oil (ullage = 0.2 m) [27]

Table 1 shows that previous research into pit-like geometries has only been done for liquid fuels where the mass loss rate was found to decrease and increase with increasing ullage [27], which differs from tank fires. The boundary conditions in previous studies have varied from adiabatic due to insulation (Shi et al. [28]) to natural convection (on steel: Kuang et al. [29], Wu et al. [26]; on glass: Dlugogorski et al. [30], Artemenko et al. [31], Gao et al. [32]; on other: Liu et al. [33], Drysdale et al. [34]) to ice (Shi et al. [27], [35]). If the study's aim is tank fires, then natural convection as a boundary condition is realistic. Still, if the study's objective is burn pits, then an adiabatic boundary condition is practical. The thermal conductivity of soil depends on the grain size, moisture content, and ingredients. Overall, it is a better insulator than air (around 3x higher when exposed to 90°C) [36]; therefore, an adiabatic boundary condition mimics that of a burn pit. The experiments discussed in this paper will use insulated pit walls like Shi et al. [28].

As far as existing fire models, the closest examples to pit fires are ceiling vents in compartment fires [37], [38]. The pit's top experiences a similar bi-directional flow to that seen in compartments with ceiling vents. However, the proximity of the vent to the seat of fire differs between these two scenarios. Additionally, the walls of a pit are typically non-combustible,

unlike walls in a compartment fire. These models present an excellent jumping-off point for developing a simple model of a pit fire.

Some experiments with liquid fuels have been performed with a constant ullage by using a constantly replenishing system. In contrast, others have examined free burns where the ullage increases throughout the burn. Experiments without a constant ullage make it difficult to pinpoint the specific ullages where burning is enhanced. The existence of a critical ullage in pit fires where the mass loss rate is increased supports the concept of an optimized burn pit for waste management. Shi et al. [28] theorized that this critical ullage enhances burning due to changes in the flame behavior that increases the amount of premixing between air and gaseous fuel. The fundamental gap in knowledge exists for several points:

- The effects of ullage on flame location inside the pit have not been investigated by either Shi et al. [28] or Kuang et al. [29].
- Any existing studies have not addressed the effect of ullage on emissions.
- No mathematical model exists that describes air entrainment into a pit fire.
- No model exists to describe pit fire behavior; although ceiling vent models are similar, few exist [38]–[42].

This thesis seeks to determine how ullage affects flame behavior in a pit, from flame front location to flame shape to plume temperatures and develop models to describe the air entrainment into a pit fire and describe the pulsation behavior seen in pit fires.

Table 1 - Summary of experimental studies into ullage effects in similar geometries (tank fires, pit fires (like tank fires but with the ground around the opening), and trench fires (elongated tanks)) and with several fuel types over a range of ullage to the diameter

<i>Year</i>	<i>Authors</i>	<i>Shape</i>	<i>Scale</i>	<i>U/D</i>	<i>Fuel Type</i>	<i>Constant Ullage?</i>	<i>Fuel</i>	<i>Frequency (Hz)</i>	<i>Emissions</i>	<i>Regression Rate (cm/s)</i>	<i>Mass Flux Rate (kg/m²s)</i>
2020	Kimmerly[43]	Pit	Small	0 - 2	Gas	Yes	Methane	1.0 - 3.0	C.O., CO ₂	-	0.0033 – 0.01
2019	Kimmerly et al.	Pit	Small	0 - 2	Gas	Yes	Methane	0.12 - 0.34	-	-	0.026-0.047
2017	Shi et al.[27]	Pit	Meso	0.1 - 0.2	Liquid	No	Crude Oil	-	-	0.375 - 0.5	0.029 - 0.039
2017	Shi et al.[28]	Pit	Small	0.25 - 2.4	Liquid	Yes	Methanol	-	-	-	0.01 - 0.025
2019	Kuang et al.[29]	Pit	Small	0.25 - 2	Liquid	Yes	Heptane	-	-	-	0.005 - 0.05
2019	Kimmerly	Pit	Small	0 - 1	Liquid	Yes	Methanol	-	-	-	-
2020	Kimmerly	Pit	Meso	0 - 1.25	Liquid	Yes	Kerosene	-	-	-	0.01 - 0.05
1998	Wu et al.[26]	Pool with Ground	Small	0.05	Liquid	No	Crude Oil	-	-	-	-

1961	Magnus[44]	Tank	Meso	0 - 1.33	Liquid	No	Ethanol, Gasoline	-	-	0.0887 - 0.908	-
1968	Artemenko, Blinov[31]	Tank	Small	0 - 1.86	Liquid	No	Aviation Gasoline, Isoamyl alcohol	-	-	0.072 - 0.08	-
2000	Dlugogorski, Wilson[30]	Tank	Small	0.22 - 2.01	Liquid	Yes	Ethanol	-	-	0.046 - 0.25	0.02 - 0.004
2020	Liu et al. [33]	Tank	Small	0 - 2.2	Liquid	Yes	Heptane, Ethanol	1.5 - 5.6	-	-	0.0027 - 0.013
2019	Gao et al.[32]	Trench	Small	0.2 - 1.2	Liquid	No	Ethanol, Diesel	2.25 - 4.5	-	-	-
1992	Drysdale, Macmillan[45]	Trench	Meso	0.71	Solid	No	Plywood	-	-	-	-

1.2 Objective and Thesis Structure

This thesis seeks to address open-air waste fires by exploring how fire behaves in a pit. The first chapter has provided an overview of the problem and the current state of research in this field. Chapter 2 covers the theory behind pit fires and the development of a simple one-zone model. Chapter 3 covers a series of experiments to describe and quantify the air entrainment into a pit fire. Chapter 4 covers experiments to describe and quantify mass loss for a pit fire at a larger scale. Finally, Chapter 5 will summarize the experiments' results and compare these results to those from the one-zone model.

2 Theory and Mathematical Model

2.1 Fundamentals of Pit Fire Behavior

Despite the small amount of experimental work on pit fires, enough evidence exists to identify the existence of flame behaviors unique to pit fires as an effect of the ullage to diameter ratio. One such behavior is a U-shaped or twin-peak flame; it has been discovered in small-scale experiments with liquid and gaseous fires when an ullage is present. However, this paper will address other behaviors unique to pit fires, specifically the flame anchoring location higher up in the pit cavity and the narrowing of the flame base. This section seeks to explain the physical mechanisms behind this behavior and extrapolate them to possible fire enhancements. detailed description of the fluid mechanics behind each stage and a sketch are given for each stage.

Stage I Flames ($U/D \sim 0-0.25$)

The flame photographs for methane flames in zero ullage (0D) and 0.25D ullage are portrayed in Figs. 2.1(a) and 2.1(b), respectively. Normal diffusion flames are visible in this stage with the flames being anchored close to the fuel injection plate. The flame base occupies the whole burner surface. Air for these flames entrains through the periphery. Both axial (puffing) and lateral (flapping) fluctuations are observed. The flame necking phenomenon as a consequence of the air entrainment and buoyant plume is observed and is consistent with the literature for pool flames [46], [47]. These flames are categorized as stage I flames. For a flame with the ground around the fuel, two significant flows occur hot gaseous fuel with strong upwards buoyancy and cool ambient air flowing radially into the hot gas. This cool airflow is due to an oxygen gradient across the flame front with oxygen diffusing from high to low concentrations. Two types of instabilities occur for this fire: Rayleigh-Taylor (R-T) instabilities arise due to the density gradient in the axial direction,

and Kelvin-Helmholtz (K-H) instabilities arise due to the velocity difference between the fuel and air flows. These two instabilities combine to form a rotating vortex that necks the flame inward and forms a bulge above this vortex as shown in Fig. 2-1(c). This toroidal bulge grows larger as it is driven upwards by the dominant buoyant flow. The vortex diameter increases to conserve angular momentum as the rotational velocity decreases. This vortex grows large enough that a section of the flame completely detaches and forms a flame ball while the anchored flame begins the process again. This phenomenon is well studied and termed as "puffing" [46], [48], [49].

Increasing the ullage from 0D to 0.25D does alter the airflow, but this alteration is not significant enough to change the flame behavior, as seen in Fig. 2-1. The flame base is seen close to the fuel base inside the ullage portraying that oxygen diffuses into the pit near the burner rim. It is also seen that the flame base is as wide as the burner, showing minimal effects of the boundary layer thickness due to the small flow development length for the low ullage.

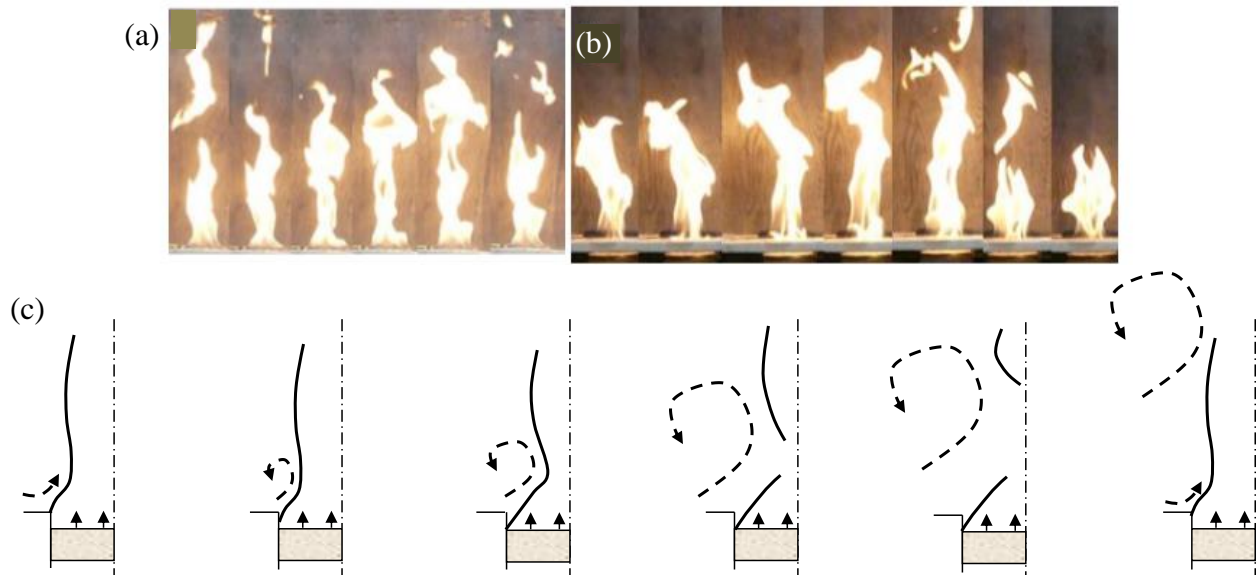


Figure 2-1 - Instantaneous flame images over a pulsation cycle for ullages of (a) 0D, (b) 0.25D and (c) schematic of stage I flame at 0.25D ullage

Stage II Flames ($U/D = 0.5-0.75$)

The flame photograph for flame in 0.5D ullage is shown in Fig. 2.2. The flame anchors close to the fuel injection plate, but the base area has decreased when compared to Stage I, due to the growing boundary layer on the burner walls. The air can entrain towards the fuel injector surface outside the flame surface and partly premix with the fuel being injected there through recirculation zones from the ullage [28]. As the ullage increases from 0.25D to 0.5D, the puffing phenomenon is visible as shown by the departing flame fragments. Additionally, in these flames, the flame tip opens up and splits the flame into two relatively large flame tongues (Fig. 2.2). This flame tip opening differs from the smoke-point flame tip opening seen in premixed and diffusion flames [50]–[54]. The smoke-point flame tip opening seen in laminar diffusion flames is caused by the strain as the flame sharply curves at the tip. Additionally, flame tip opening is caused by diffusional stratification, reducing the fuel concentration at the tip below the limiting value [50]. These U-shaped flames are reported in the literature for pool fires where an ullage is present [30], [55] and are distinct from tulip-shaped flames [56]–[58]. Tulip-shaped flames occur for premixed flames in closed or half-closed tubes, and while a half-closed tube is analogous to pit fire, a premixed flame is not analogous. Flames in a tube open into a tulip shape because of competition between the forward and backward flows. Burned gases are directed backward in the tube close to the central axis, and unburned gases are accelerated forward down the tube near the walls. These combine to cause the "tulip-shape" with the flame's center drawn backward, and the edges are drawn forward [56]. Thus, U-shaped flames for pit fires are distinct from flame-tip opening and tulip-shaped flames. In literature, the U-shape seen for pit fires is attributed to a combination of the heated walls accelerating the flow near the wall (Swami et al. [59]) and airflow into the flame,

forming a cavity in the center of the flame due to the hydrodynamic effects of this flow (Dlugogorski and Wilson [30]).

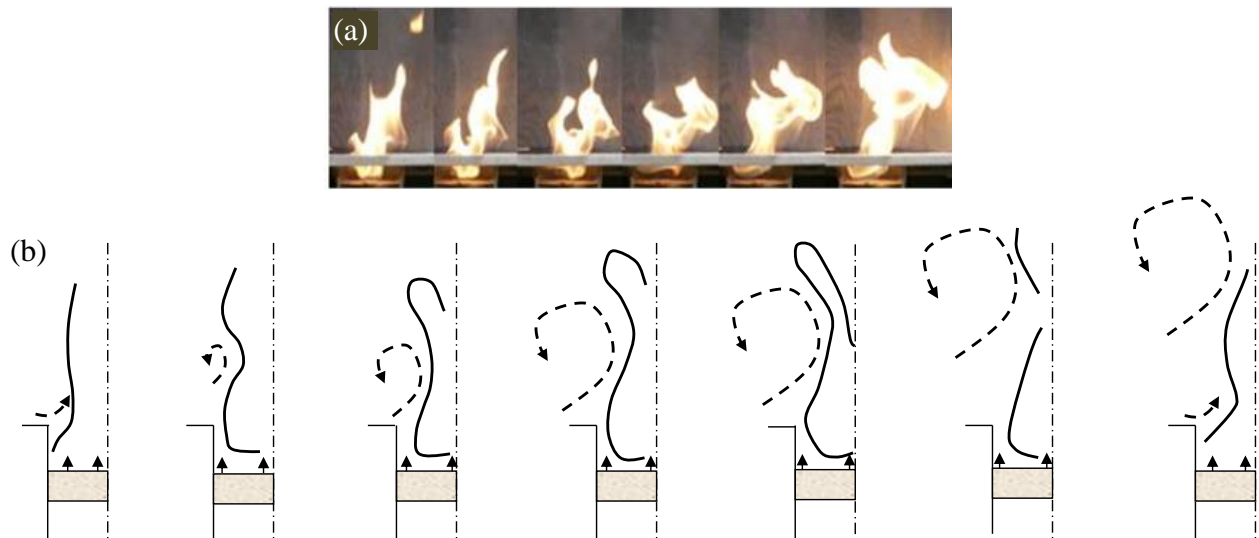


Figure 2-2 - Instantaneous flame images over a pulsation cycle for ullages of (a) 0.5D, and (b) schematic of stage II flame at 0.5D ullage

The flame photographs in the present study suggest that the flames are slightly lifted from the fuel inlet due to the reduction in the oxygen diffusion length with respect to ullage as shown in Fig. 2-3(b). However, the radial diffusion time for oxygen within the ullage is higher for 0.5D ullage as compared to 0.25D ullage (Fig. 2.1b), leading to reduction in flame width in the ullage. The U-shaped flames could be due to local quenching of the flame near the axis due to slow mixing of the reactants. On the contrary, away from the axis, accelerated fuel due to the heated walls of the burner mixes with ambient air and can sustain reactions in the periphery. Moreover, shorter flames are observed as compared to 0D and 0.25D ullage.

Stage III Flames ($U/D \sim 1.0$)

As the ullage is increased to $0.75D$ and $1D$ (Figs. 2-3(a) and 2-3(b)), the flames lift-off the fuel injector surface. As the flame area is lesser than the glass tube area, air entrainment into the pit occurs, and the flame base is sustained as a partially premixed flame where the Damkohler number is close to unity. The lift-off height varies with time as the flame bases oscillate in the vertical direction. Vigorous flame oscillations and puffing phenomenon are seen in this stage, called Stage III (Fig. 2-3). For stage III flames, the pit's vortex becomes too weak to entrain sufficient oxygen at the fuel surface consistently. The weak vortex causes the flame to move vertically in the pit, with the flame moving upwards when there isn't enough oxygen in the pit and downwards as more oxygen is drawn into the pit. This vertical pulsation corresponds with the formation and collapse of the twin-peak structure. As the air flows into the pit, the flame moves lower down the pit, and the flow begins the formation of the twin-peak structure. Then as the twin peak structure decays and the majority of airflow comes vertically the flame moves upward in the pit.

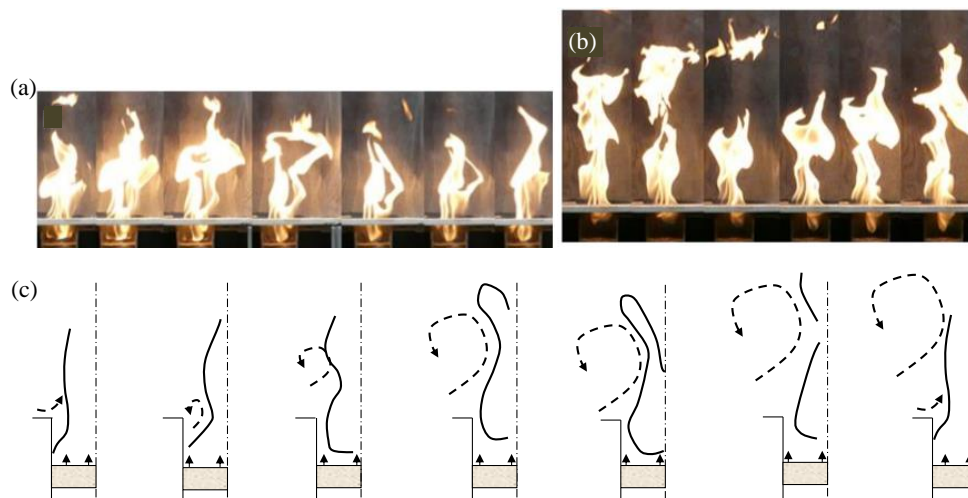


Figure 2-3 - Instantaneous flame images over a pulsation cycle for ullages of (a) $0.75D$, (b) $1D$, and (c) schematic of stage III flame at $0.75D$ ullage

Stage IV Flames ($U/D \sim 1.5$)

At a higher ullage of 1.5D (Fig. 2-4), the flame sustains as a lifted flame near the glass tube's opening, and the flame base does not oscillate much. Air penetrates only through a small distance down the pit. This regime is designated as stage IV (Fig. 2-4). The flame oscillation patterns are similar to the case of 1D. Finally, as the ullage increases from 1.0D to 1.5D, the twin-peak behavior is still seen, but the flame base is now anchored at the top of the pit. The vortex is insufficient to draw enough oxygen into the pit to sustain combustion there.

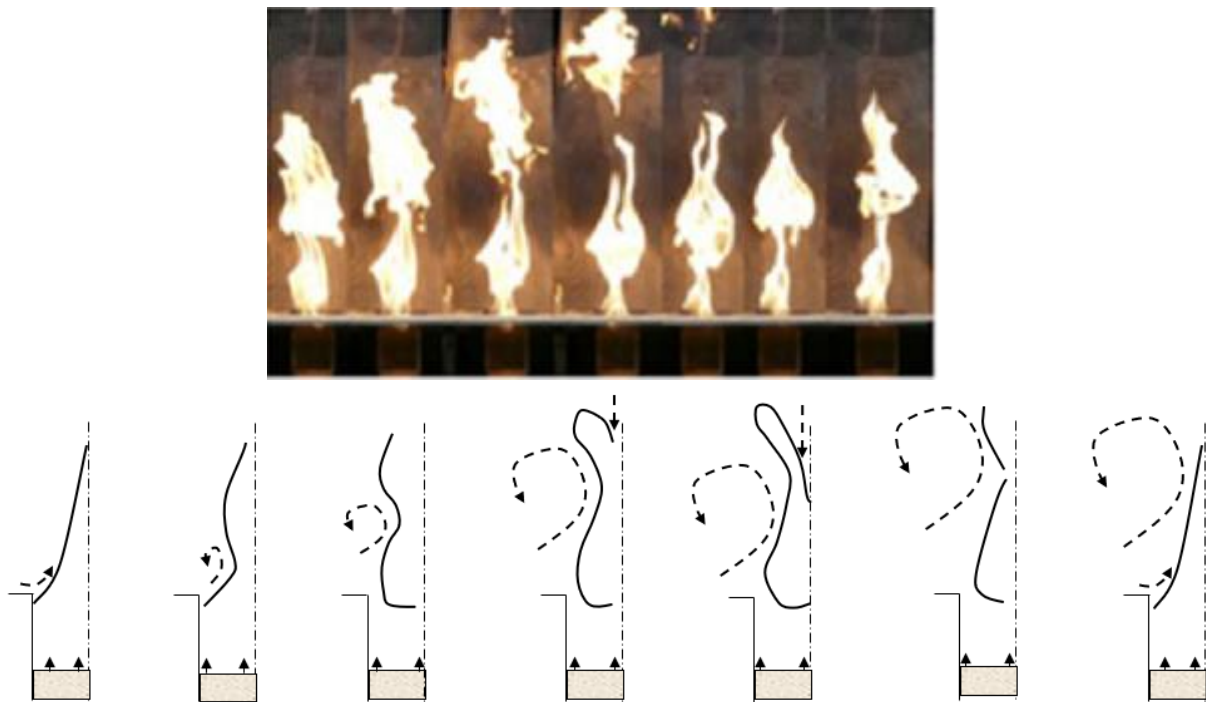


Figure 2-4 - Instantaneous flame images over a pulsation cycle for ullages of 1.5D (top) and schematic of stage IV flame (bottom)

2.2 Idealized Pit Fire

In designing experimental setups to investigate the effects of ullage, the first step was to develop an idealized pit fire and elucidate the relevant parameters (Figure 2-5). The red box

identifies the control volume around the flame, and airflow into the control volume is the volumetric air entrainment rate (\dot{m}_{ent}''') with arrows to show the direction of airflow into the flame, notably in the central region for a twin-peak flame and in the pit cavity. The major parameters from Figure 2-5 affecting the flame behavior are identified as the airflow into the fire, the frequency of pulsation of the flame (which previous work has tied to airflow), and the flame anchoring location.

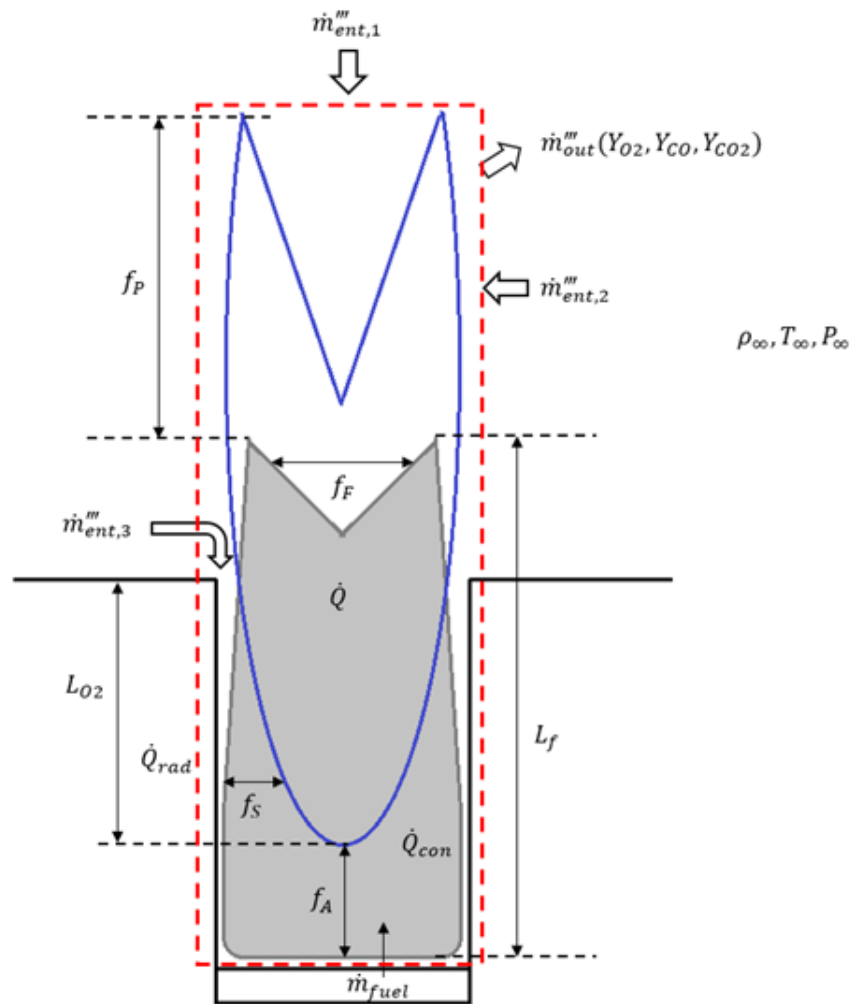


Figure 2-5 - Idealized experimental setup of a pit fire with a gas burner.

Based on the idealized pit fire, it was determined that an experimental setup must first capture the flame dynamics with a gas burner where the mass loss rate is decoupled from the airflow to isolate the effects of ullage. Cetegen and Ahmed [46] used a gas burner to study pool fires' puffing behavior, as the puffing frequency is independent of fuel type. Their non-reacting plume experiments indicated that the puffing's intensity depends on local heat release, so a gas burner allows precise control of the heat release rate. Additionally, Zhang et al. [60] performed experiments to design a gas burner that can emulate condensed phase fuels burning at a steady state. Both studies seek to use gas burners as they produce more consistent results than condensed phase fuels as there is no heat of vaporization to contend with, which significantly simplifies the problem. Experiments with liquid fuels are needed at the meso-scale to test a broader range of ullage to diameter ratios because no existing work has been done at a ratio similar to that of the critical ullage to diameter ratio seen in small-scale testing. If meso-scale experiments have results that show improvements in the burning rate at certain ullage to diameter ratios, this further supports the concept of an optimized burn-pit that is safer by reducing exposure time to hazardous emissions.

2.3 One Zone Model

The over-arching goal of this research is to address the possible use of optimized burn pits for solid waste disposal, and as such large-scale experiments are necessary to determine if the improvements seen at the small-scale ($D < 0.5$ m) persist at the scale of most burn pits in the field ($D \geq 1$ m). However, these large-scale experiments are difficult and time-consuming to design and set up. Therefore, a mathematical model would allow for quicker parameter analysis to determine which experimental conditions should be tested and what instrumentation should be used to collect

the most interesting data. A fully developed CFD (computational fluid dynamics) model would be too computationally intensive (e.g., days to run the model for one set of inputs) to use as a design tool for experiments so a simpler model is developed for this purpose. Thus, a 1-dimensional model based on conservation equations with the pit as the control volume was developed and coded into Wolfram Mathematica 8.0.0.

In developing the pit model, ceiling vent models were used as a starting point as they have a similarly altered air flow. Numerical models describing fire behavior in a room with a ceiling vent have been developed since the early 1990s as interest in extending existing fire models of rooms with doors to new geometries [61]. In 1993, Than and Savilionis from WPI [40] published a paper comparing a ceiling vent model to experimental results. They found that temperatures across the vent opening fluctuated quite regularly (Fig. 2-6) which shows the flame is periodically drawing cooler ambient air into the enclosure or allowing hot smoke to leave the enclosure.

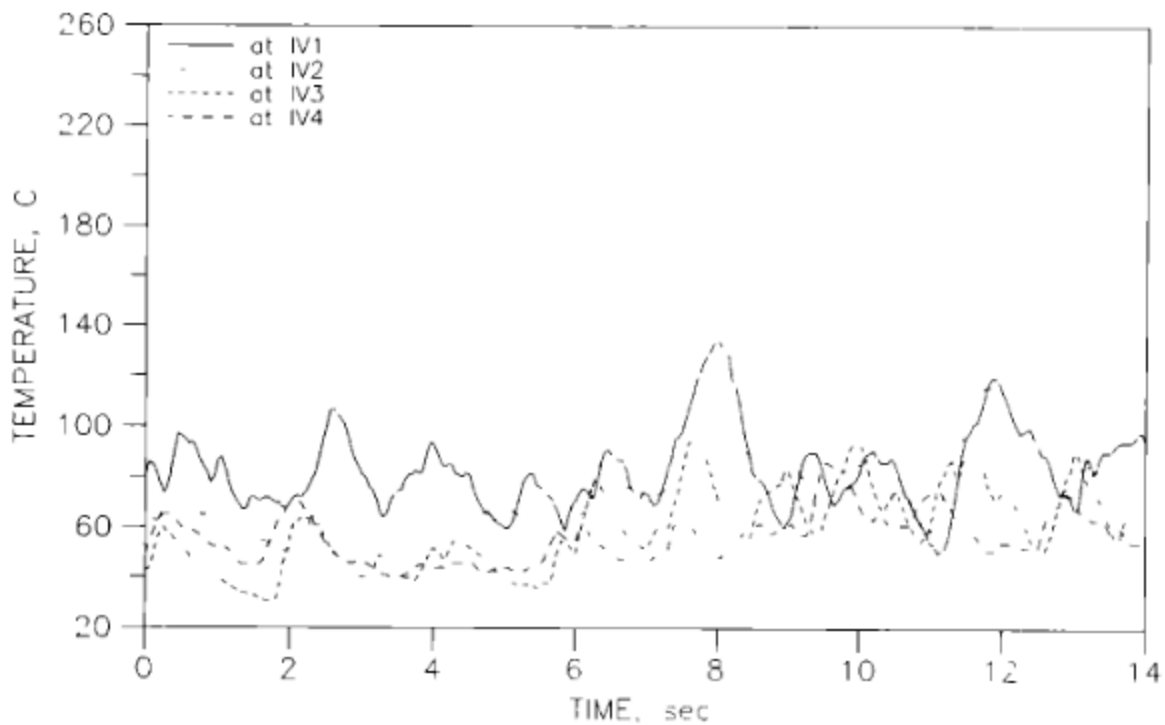


Figure 2-6 - Than and Savilionis experimental temperature data across the ceiling vent [40]

In their model, they set flow at the vent to be in one direction (i.e., in or out, not both) at any given time in agreement with their temperature data. Furthermore, they assumed that the hot gasses leaving the enclosure mix with ambient air above the vent and that air drawn into the enclosure is warmer than ambient due to this mixing and defined an arbitrary mixing ratio (λ) to determine the “warmed” inflow. The model gave considerably more variation in the vent temperature than that seen in the experiment; they attributed this variation to a slow thermocouple response but also numerical oscillations inherent to the modelling equations.

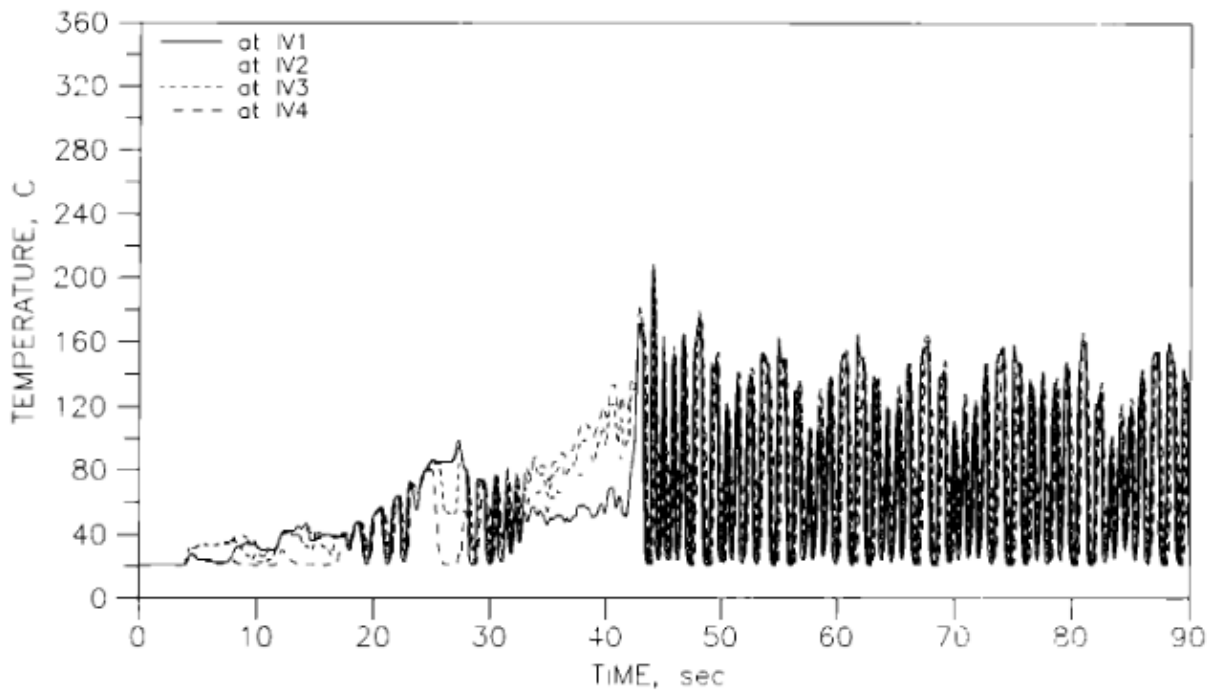


Figure 2-7 – Than and Savilonis model data across the ceiling vent [40]

In 1998, Kerrison et al. published a paper with a similar model to Than and Savilonis, but their model doesn't use a mixing ratio [42] and instead allowed the CFD model to predict the temperature of the warmed air that flows into the compartment. However, they still saw

considerable fluctuations in the vent temperatures, well beyond that seen in the experimental data. Later in 2009, Chow and Gao published an article on the oscillatory airflow in the ceiling vent and used a sinusoidal wave function to model this buoyancy and pressure-driven oscillation [39]. In 2014, He et al. presented the results of experimental studies on fires in ceiling-vented compartments, and the results can be used to validate a numerical model [38]. Finally, in 2018, Chen and Lu published a comprehensive review of oscillation across a ceiling vent in a compartment fire and related the vent oscillation frequency to the flame pulsation frequency [41]. These previous models helped identify relevant parameters and assumptions.

The 1-D pit model will provide pressure, temperature, and mass flux as a function of time for a pit geometry with gaseous and liquid fuels. Figure 2-8 shows a simple sketch of the model geometry, with fuel flowing into the pit (\dot{m}_{fuel}'') and a single flow (\dot{m}_t'') capturing airflow into the pit and combustion products leaving the pit. This single flow at the top the pit will change sign from a positive outflow of smoke to a negative inflow of air, as the fire consumes all the available oxygen in the cavity causing the fire to “extinguish” and as the pressure within the cavity changes sign. A theoretical framework is described here, and work is being done to solve the equations using Wolfram Mathematica 8.0.0.

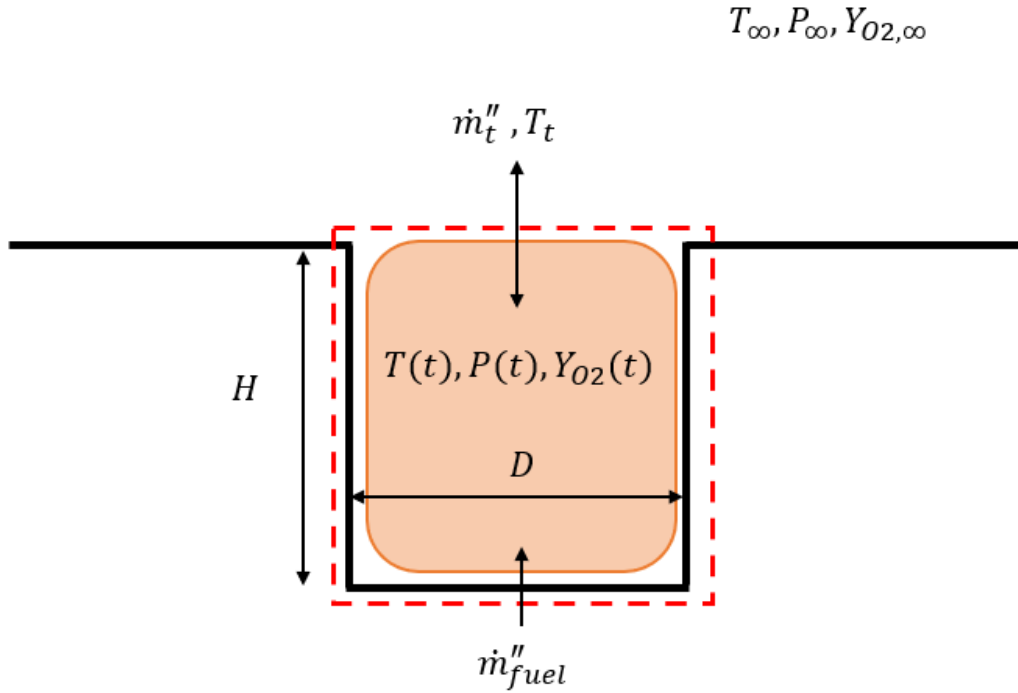


Figure 2-8 - One-dimensional pit geometry with control volume outline in red.

The basis of the model are the conservation of mass, energy, and species. The simplifications of the general equations are given below.

2.2.1 Conservation of Mass

The general conservation of mass equation [2-1] has the change in mass with time plus the flow in from the top of the pit and minus the flow of mass into the pit from the fuel.

$$\frac{dm}{dt} + \dot{m}_t - \dot{m}_f = 0 \quad [2-1]$$

Now, the mass term is converted to a volumetric term as $m = \rho V$ and since the volume of the pit is constant it can be simplified as:

$$\frac{dm}{dt} = \frac{d(\rho V)}{dt} = V \frac{d\rho}{dt} \quad [2-2]$$

Then assuming an ideal gas ($PV = nRT = \frac{m}{MW}RT$ or $\rho = \frac{m}{V} = \frac{P*MW}{T*R}$) the density and volume terms can be converted to pressure and temperature with the molecular weight of the fuel (MW) combined with the ideal gas constant R to form R_{MW} .

$$\frac{d\rho}{dt} = \frac{1}{R_{MW}} \frac{d\left(\frac{P}{T}\right)}{dt} \quad [2-3]$$

Pressure in the enclosure does not change much relative to the atmospheric pressure, hence $\rho T \approx \rho_{\infty} T_{\infty}$. Therefore,

$$\frac{dm}{dt} \approx \rho_{\infty} T_{\infty} V \frac{d(1/T)}{dt}. \quad [2-4]$$

Finally, the conservation of mass can be written as:

$$\boxed{\rho_{\infty} T_{\infty} V \frac{d(1/T)}{dt} + \dot{m}_i = \dot{m}_f}. \quad [2-5]$$

2.2.2 Conservation of Energy

The general conservation of energy equation relates internal energy (U) to the heat contained in the two mass flows, to the heat release rate of the fire (\dot{Q}), and the heat absorbed by the pit ($hA_s(T - T_{\infty})$).

$$\frac{dU}{dt} + \dot{m}_i C_p T_i - \dot{m}_f C_p T_f = \dot{Q} - hA_s(T - T_{\infty}) \quad [2-6]$$

Then the internal energy can be converted to a function of pressure since the volume of the pit is constant, given the following:

$$\frac{dU}{dt} = C_v V \frac{d(\rho T)}{dt} = C_v V \frac{d(P/R)}{dt}, \quad [2-7]$$

where

$$R = C_p - C_v$$

$$\gamma = \frac{C_p}{C_v} \quad [2-8]$$

So, the general equation can be written as

$$\boxed{\frac{dU}{dt} = \frac{V}{\gamma-1} \frac{dP}{dt}} \quad [2-9]$$

Then the heat release rate of the fire differs for a gaseous or liquid fuel. For a gas burner, the heat release rate is based on the fuel flow rate, $\dot{Q} = \Delta H_c \dot{m}_f$. For a liquid pool fire, a stagnant layer model is used with radiative effects included. The mass flux can be written as follows (from [62]), and it includes the heat of vaporization and convection into the air.

$$\dot{m}_f'' = \dot{m}_\infty'' + \frac{h_c \left(\frac{\lambda}{e^\lambda - 1} \right) \left(\frac{\Delta H_c}{c_p T} \right) (1 - X_r) (Y_{O_2} - Y_{O_2, \infty}) + F \sigma (T^4)}{h_{fg} + c_{p,o} (T_v - T)} \quad [2-10]$$

Where \dot{m}_∞'' is the burning rate under ambient conditions, $Y_{O_2, \infty}$ is the ambient oxygen concentration, $\lambda = \frac{c_p \dot{m}_f''}{h_c}$, h_c is the convective coefficient at ambient, c_p is the heat capacity of the fuel, X_r is the radiative fraction of the heat release, F is the radiative view factor, T_v is the vaporization temperature of the fuel, and h_{fg} is the convection coefficient at the fire temperature.

Then all of this gives the following equation for conservation of energy in terms of pressure,

$$\frac{V}{(\gamma-1)} \frac{dP}{dt} + \dot{m}_i C_p \{ \eta(\Delta P_i) T + \eta(-\Delta P_i) T_\infty \} - \dot{m}_f C_p T_f = \dot{Q} - h A_s (T - T_\infty) \quad [2-11]$$

where $\eta(x)$ is defined as a step function. It accounts for the flow reversals based on the pressure differentials across the vents. $\eta(x) = 1$ for $x \geq 0$, and $\eta(x) = 0$ for $x < 0$. The formulation of the vent flow equations is further discussed in the section below.

2.2.3 Conditional Equations

The model uses a conditional statement (shown as the step-function in [2-11]) based on the pressure within the pit to capture the flame pulsation behavior:

$$\dot{m}_t'' = \begin{cases} A_o C_d \sqrt{2\rho(t)\Delta P_t}, & \Delta P_t > 0 \\ -A_o C_d \sqrt{2\rho_\infty |\Delta P_t|}, & \Delta P_t \leq 0 \end{cases} \text{ and } T_t = \begin{cases} T(t), & \Delta P_t > 0 \\ T_\infty, & \Delta P_t \leq 0 \end{cases} \quad [2-12]$$

For the above conditional,

$$\rho(t) = \frac{\rho_\infty T_\infty}{T(t)} \text{ and } \Delta P_t = P(t) - P_\infty + (\rho_\infty - \rho(t))gU \quad [2-13]$$

This conditional statement allows the sign of the flow through the cavity opening to change based on the pressure within the cavity and changes the temperature of this inflow to reflect if smoke is flowing out or cool ambient air is flowing into the cavity.

A second conditional statement checks if there is sufficient oxygen entrained into the pit to sustain combustion, with the approximate critical oxygen concentration [63].

$$Q = \begin{cases} \dot{m}_f'' \Delta H_c A_f, & Y_{O_2}(t) > Y_{O_2,crit} \\ 0, & Y_{O_2}(t) \leq Y_{O_2,crit} \end{cases} \quad [2-14]$$

The critical oxygen concentration is calculated using extinction theory in Quintiere [64] and gives the following for a liquid fuel (i.e. diffusion flames).

$$Y_{O_2,crit} \approx \frac{c_p(T_f - T_\infty)}{(\Delta h_c - L)/r} \quad [2-15]$$

Where T_f is the flame temperature (taken as 1300°C for a diffusion flame), L is the effective heat of gasification for a liquid fuel (0.67 MJ/kg for kerosene [64]), T_∞ is the cavity temperature, and r is the stoichiometric fuel to oxygen mass ratio (0.57 if kerosene is assumed to be $C_{10}H_{22}$). This simple linear model relates the amount of oxygen necessary to sustain flaming to the temperature within the cavity and is seen in Figure 2-9. This model is based on a stagnant layer gas-gas phase

and conservation equations supported by experimental data. The coefficients in the equation are based on the heat of gasification of the fuel and the fuel stoichiometry. For a gaseous fuel (i.e., premixed flames), the equation is even simpler, and the critical oxygen concentration is a function of the flammability limits of the fuel, for instance for methane the upper flammability limit is 14% volume in air which gives a critical oxygen mass fraction of 0.08 (see the dashed line in the Figure 2-9). These two models for determining the critical oxygen concentration in the pit are important as they are part of the “trigger” for switching the direction of flow at the pit opening and drawing air into the pit, and they control where the fire is “on” or “off” which effects the temperature and pressure in the pit which also effect the flow condition at the opening.

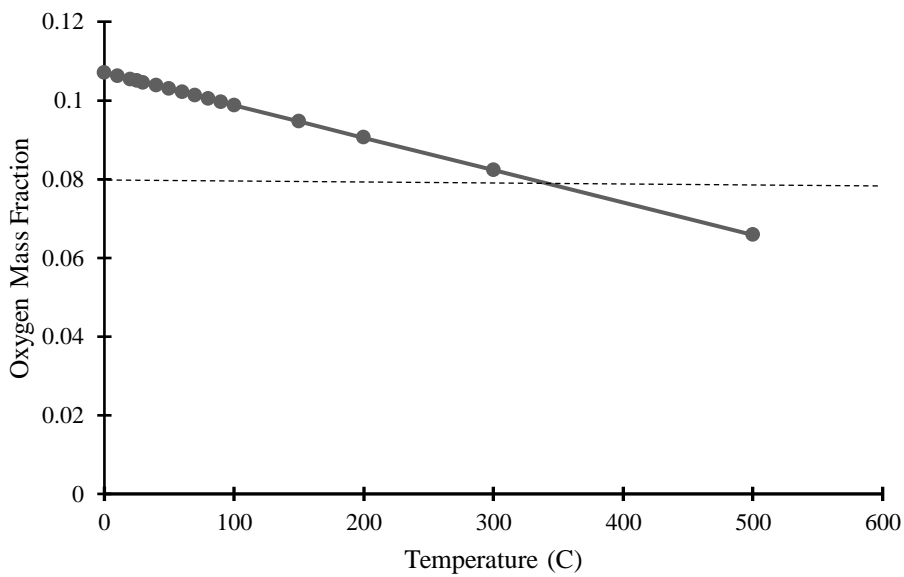


Figure 2-9 Critical oxygen concentration as function of cavity temperature for kerosene (solid line) and methane (dashed line)

Overall, the critical oxygen condition works as a switch on the fire, if there is sufficient oxygen inside the cavity to sustain burning then the fire is fully “on” and the fire heats up the gases in the cavity causing the cavity pressure to raise above the ambient pressure causing hot gases to flow

out of the cavity (with the pressure conditional), but if there insufficient oxygen the fire is “off” and the gases in the cavity cool off and the pressure in the cavity decreases until it is below ambient which causes ambient air (oxygen-rich) to flow into the cavity. So, the flow at the top of the cavity is controlled by both the critical oxygen concentration and the pressure difference between the cavity and the ambient. For a liquid fuel, the oxygen switch is a function of the cavity temperature because it must evaporate, while for a gas it is a constant value.

2.2.4 Conservation of Species

Finally, the general equation for the conservation of species on oxygen is:

$$\rho_{\infty} T_{\infty} V \frac{d(Y_{ox}/T)}{dt} + (Y_{ox})_{Top Vent} \dot{m}_t = -\dot{Q} / \Delta H_{ox}. \quad [2-16]$$

This can be solved using the vent flow equation at the top to give:

$$\boxed{\rho_{\infty} T_{\infty} V \frac{d(Y_{ox}/T)}{dt} + [\eta(\Delta P_t) Y_{ox} - \eta(-\Delta P_t)(0.233)] \dot{m}_t = -\dot{Q} / \Delta H_{ox}}. \quad [2-17]$$

The pit is a circular pit of diameter D and height/ullage U , so the pit volume is $V = \frac{\pi}{4} D^2 U$, the pit surface area is $A_s = \pi D U$, and the area of the opening at the top of the pit is $A_o = \frac{\pi}{4} D^2$. The walls of the pit are assumed to be adiabatic. The bottom of the pit is either a gas burner or a pool fire. If it is a gas burner, it is supplying fuel (with a heat of combustion of ΔH_c) at a rate of \dot{m}_f to an area of $A_f = \frac{\pi}{4} D^2$ giving a flux of $\dot{m}_f'' = \dot{m}_f / A_f$.

A vent parameter (C_d) addresses alterations to the airflow into the pit caused by the edges of the opening. The ambient conditions are described by temperature (T_{∞}), density (ρ_{∞}), pressure (P_{∞}), oxygen concentration (Y_{Ox}), specific heat ratio (γ), and heat capacity (c_p).

2.2.5 Ramp-Up Term

Additionally, a ramp-up term is included to simulate the ignition process (see equation [2-18]).

The term is a simple exponential function and is added to the mass flow rate equations to increase the amount of fuel vapor slowly.

$$\dot{m}_f = (1 - \exp(-0.1 * t)) * \dot{m}_{fuel}'' * \frac{Y_{ox}(t)}{0.233} \quad [2-18]$$

2.2.6 Final Model Equations

It is seen from the above analysis that three differential equations are developed:

$$\begin{aligned} \rho_{\infty} T_{\infty} V \frac{d(1/T)}{dt} \pm \dot{m}_T - \dot{m}_f &= 0 \\ \frac{V}{\gamma - 1} \frac{dP}{dt} \pm \dot{m}_T C_p T &= \dot{Q} - hA_s(T - T_{\infty}) \\ \rho_{\infty} T_{\infty} V \frac{d(Y_{ox}/T)}{dt} \pm Y_{ox} \dot{m}_T &= \frac{-\dot{Q}}{\Delta H_{ox}} \end{aligned} \quad [2-19]$$

With the following variables and constants:

- State variables: $1/T$, P , and Y_{ox}/T .
- Control variables: A_f (Area of fuel), U (ullage), A_s (Area of the surface of walls),
- Constants (properties from NIST database online):

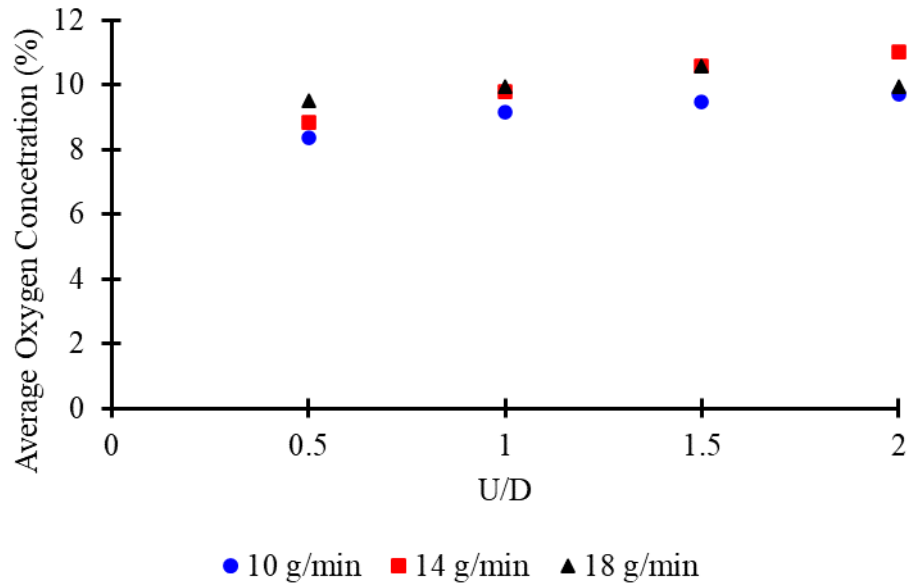
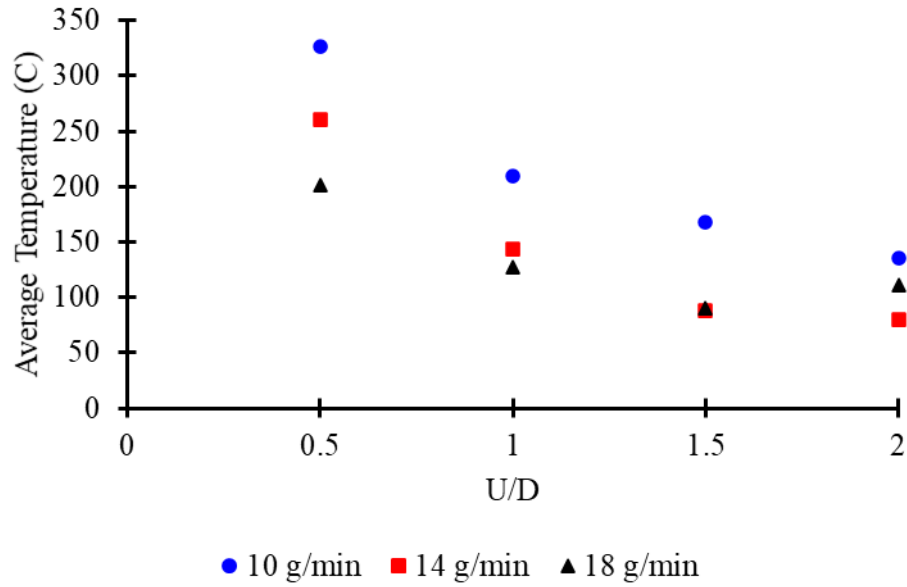
<u>Property</u>	<u>Methane</u>	<u>Kerosene</u>
σ Stefan Boltzman constant	5.67x10 ⁻¹¹ kW/m ² -K	
$Y_{ox,\infty}$ Ambient oxygen concentration	0.233	
C_p Specific heat of air	1 kJ/kg-K	
$\gamma = C_p/C_v$ Ratio of specific heats	1.4	
ρ_∞ Density of ambient air	1.2 kg/m ³	
ΔH_c Heat of combustion	55.51 kJ/g	43.00 kJ/g
ΔH_{cox} Heat of combustion of oxygen	13 kJ/g	
C_d orifice factor	0.7	
T_{out} Ambient temperature	300 K	
L heat of gasification	N/A	0.25 kJ/g

To recap, the model assumes: 1-dimension, radiative heating of the fuel, unidirectional flow at the top of the cavity governed by pressure and oxygen concentration, adiabatic cavity walls, complete combustion of the fuel, an exponential ramp-up of the mass flow at the start of the model, and constant ambient parameters. Additionally, the model assumes a fully premixed flame within the cavity, but experimentally this is not always valid during the fire, so the model is limited in its ability to fully describe the pit fire. This model will allow for quick analysis of various fuels, pit diameters, and pit depths to be conducted prior to experimentation and give an indication of which values would be best to investigate experimentally. This will hopefully, streamline the development of large-scale experiments which are costly and time-consuming to set up.

2.2.7 Parametric Study

The gas burner version of the model is run for three fuel rates (10, 14 and 18 g/min) and three ullage to diameter ratios (0.5, 1, and 1.5) for a 9 cm diameter circular burner. The average pit temperature, average oxygen concentration, and average inflow from the top of the pit are

calculated and shown below in Figure 2-10. The average inflow into the pit is calculated by averaging all the negative values (greater than 0.00001 kg/s) of the mass flow (negative indicating flow into the pit) at the top of the pit.



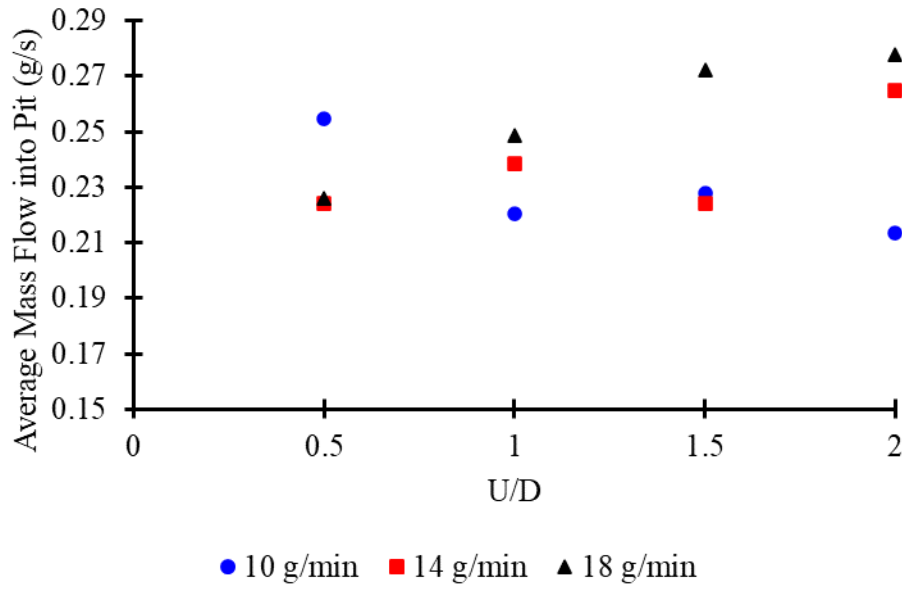
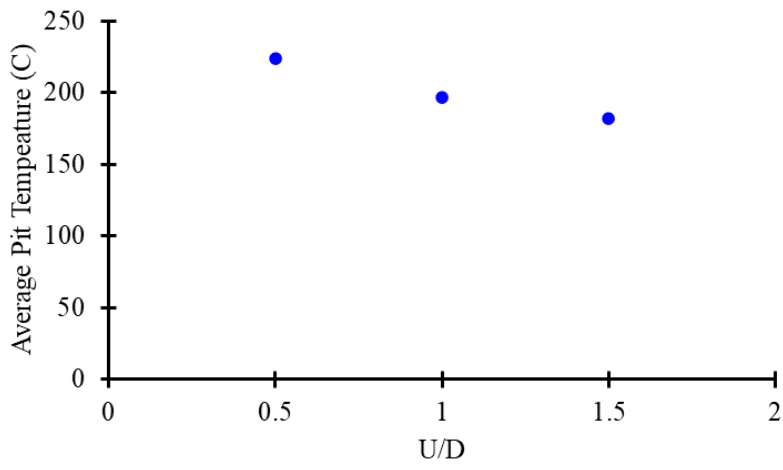
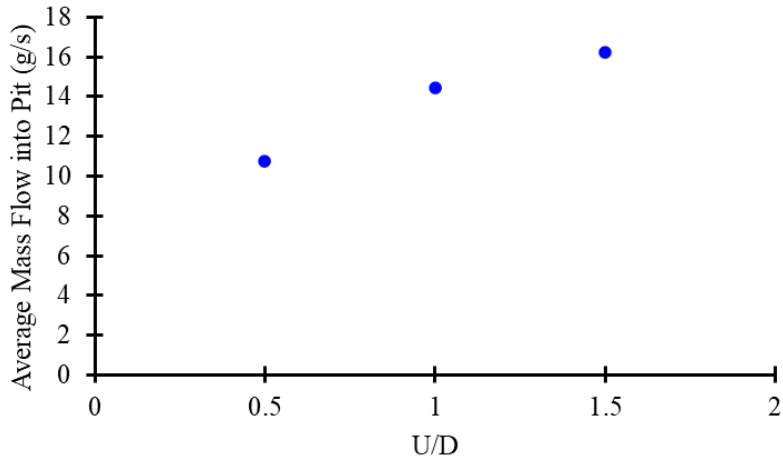


Figure 2-10 – Average temperature, oxygen concentration, and mass flow for a gas burner from one-zone model

From these parametric trials, we see that as the ullage to diameter ratio increases the average pit temperature decreases, the average mass flow out the top of the pit increases, and the average oxygen concentration within the pit increases. The increase in oxygen and the mass flow at the top of the pit are tied to together, as the mass flow out the top increases the inflow also increases as the fire draws in more oxygen and this leads to the increase in average oxygen concentration in the pit. The average temperature decreases because more ambient air is drawn into the cavity, and from the flame stages the anchoring location has likely moved further up inside the pit so the heat generation within the pit is decreased (i.e., more flame outside of the pit at higher ullages).

Then for a liquid pool fire, kerosene is taken as the fuel (heat of combustion of 43.2 kJ/g). Figure 2-11 shows the average temperature and average oxygen concentration in the pit over the whole computational time. From these, we can see that a similar trend to that seen for the small-

scale gas burners in Figure 2-10 with decreasing temperature and increasing oxygen concentration as ullage increases.



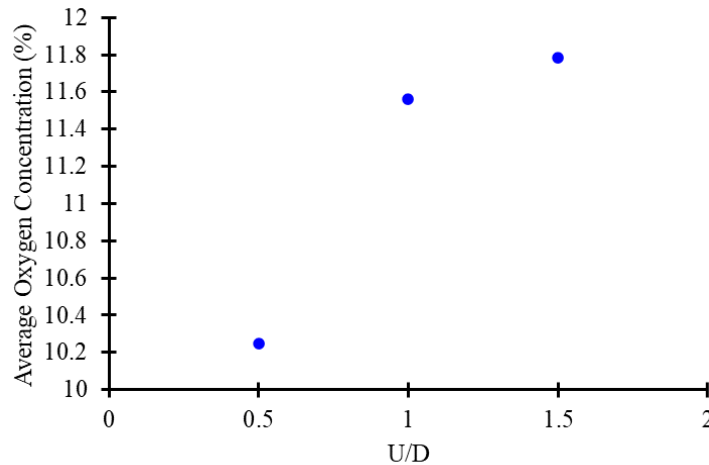


Figure 2-11 – Average temperature, oxygen concentration, and mass flow for a 57 cm diameter kerosene pit fire

To recap, the 1-D model shows that increasing the ullage to diameter ratio leads to increasing air flow into the pit (both mass and oxygen concentration) and decreasing average temperature in the pit. These two trends are related as cooler ambient air being drawn into the pit leads to lower average temperatures. This increasing inflow with a deeper cavity is because, even though the amount of fuel is the same, as more of the flame is contained within the cavity, the more air that must be drawn into the cavity to the flame base to sustain the flame. The proportion of flame within the cavity is found to be a function of the ullage as the model assumes the flame anchors at the fuel surface.

This one-zone model's end goal is to provide a platform for quick parameter and scaling analyses on pit fires. This model will allow users to determine what experimental studies should be conducted based on small-scale and meso-scale results. The development of a functional design for large-scale burn pits depends on the rapid production of experimental results. The model will also help determine the physics behind the flame behavior seen in the empirical studies mentioned above. However, there are limitations to the model, such as the assumption of a fully premixed

flame within the cavity, the 1-D assumption of airflow at the cavity opening is vastly simplified, the radiative heat effects for the liquid fuel are very simplified, and finally, the model assumes the fire is axisymmetric which the small-scale shows are only true for two axes not three during the pulsation of the flame shape.

3 Air Flow in Pit Fires

When burning liquid and solid fuels, the airflow into the flame is coupled to the heat release rate and thus the gasification rate of the fuel. This coupled behavior makes it difficult to isolate the effects of ullage on airflow. Therefore, a gas burner where the burning rate can be fixed and decouple the heat release rate from the airflow is needed in experiments for a close examination of ullage effects on flame behavior. These experiments on ullage with small-scale gas flames [43] conducted by the author, found that the mass-loss rate affects the flame anchoring location, which was not seen in the previous work [28]. In addition to determining flame behavior, the emissions are analyzed, as this has not been addressed in the literature.

3.1 Experimental Setup

The first set of experiments was a small-scale gas burner to decouple mass loss and airflow to clarify how ullage affects flame behavior. These experiments' setup is based on Zukoski, Kubota, and Cetegen's [65] experimental setup to determine air entrainment into fire plumes. Their setup consisted of a gas burner under a vent hood with a controlled extraction rate. The extraction rate is varied until a steady smoke layer is established inside the hood and verified with a thermocouple tree in the hood; this layer indicates that the amount of smoke extracted is equal to the amount of air entrained into the plume. In the current study, Zukoski et al.'s [66] experimental

setup was altered to include a variable ullage parameter rather than a variable cavity height. The pit fire experiments were done in the 10 cm x 10 cm square pit under a vent hood to determine ullage effects on air entrainment and emissions. The pit consists of a square cross-sectional (10 cm × 10 cm) cavity with a depth of 20 cm, made of borosilicate glass resting on a 6 mm thick gypsum board. A square cross-section was chosen to lessen distortion flame visualization inside the pit. The pit's top surface is kept flush with a square plate (30 cm × 30 cm) of a 6 mm gypsum board to simulate ground around the opening of a burn pit. The ullage is tested in 1 cm increments from 0 to 20 cm (0 to 2 times the pit diameter). The walls are insulated with 0.635 cm thick mineral wool on three sides, with the front side left uninsulated so that the camera can record the direct flame videos. A wire mesh is kept surrounding the top plate over the burner to reduce ambient air disturbances. The pit setup is placed underneath a square vent hood (41 cm × 41 cm) located 40 cm above the pit's opening.

The hood has a controllable extraction rate and sends emissions to a gas analyzer. Three fuel flow rates, 2, 4, and 6 g/min, are tested for each ullage to simulate different fuel loadings. Each set of parameters (fuel flow rate and ullage) is tested three times. High-definition direct videos are captured at a rate of 30 frames per second during the experiments. From the videos, direct flame images are extracted, and the flame fluctuations in the lateral direction are studied to determine its frequency. Gas analyzer data is recorded for 2 minutes, and the values are averaged across this period. Sixteen K-type 32-gauge (0.02 cm diameter) chromel-alumel thermocouples are arranged in a vertical array with 1 cm spacing on a wall of the hood to determine the presence and location of the hot smoke layer. The presence of a continuous smoke layer in the hood is used in determining the entrainment rate. Another K-type thermocouple is located after the gas sampling port to record the exhaust gas temperature. Experimental results were used to develop an air

entrainment correlation based on ullage and flapping frequency and examine the effects of ullage on the CO/CO₂ ratio.

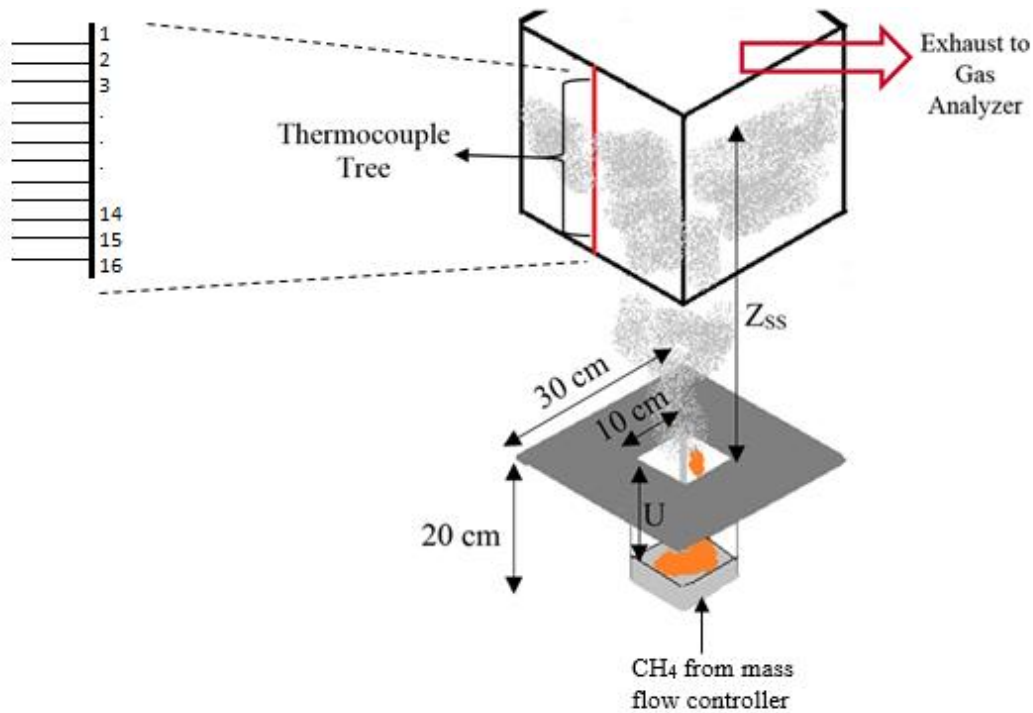


Figure 3-1 - 9 cm x 9 cm Square Pit, Z_{ss} = steady smoke layer height, U = ullage.

The second set of small-scale experiments were designed to capture flame behavior better and to investigate plume temperatures. They were done in a 9 cm diameter circular pit with a methane gas burner. A circular pit was selected to rule out any corner effects on flame behavior. The pit is made of a borosilicate glass tube (0.5 cm thickness, 9 cm diameter (D), 28 cm length) with a rigid ceramic-wool insulation flange (28 cm by 28 cm square, 1 cm thick) at the top of the tube. Methane flows through a bottom valve with sufficient pressure to diffuse through the ceramic block (fuel injector plate) at 10, 14, and 18 g/min. The ceramic block's top surface's location in the glass tube can be manually adjusted to create different ullages. Direct flame videos are recorded at 30 frames per second using a camera. Thirteen K-type thermocouples (0.2 mm diameter) are

arranged as an array in the plume region (47 cm above the top of the glass tube). Experiments are done at ullages (U) from 0 to 18 cm, corresponding to zero to 2D, respectively. Each experiment has been performed at least three times. The temperature data is recorded for 30 s after 5 minutes since the ignition has passed. It is time-averaged for each trial and is averaged over three trials for each ullage. The frequency data is the average of six cycles in the 30 s of video recording for each ullage. Flame height is estimated by image processing using the diameter of the cylinder as a reference. The height is measured in every frame in three of the cycles and used to determine the frequency. This second set of experiments is used to determine how ullage affects flame behavior and relate emissions data to flame behavior and plume temperatures to determine if ullage can lead to enhanced burning for a fixed mass loss rate.

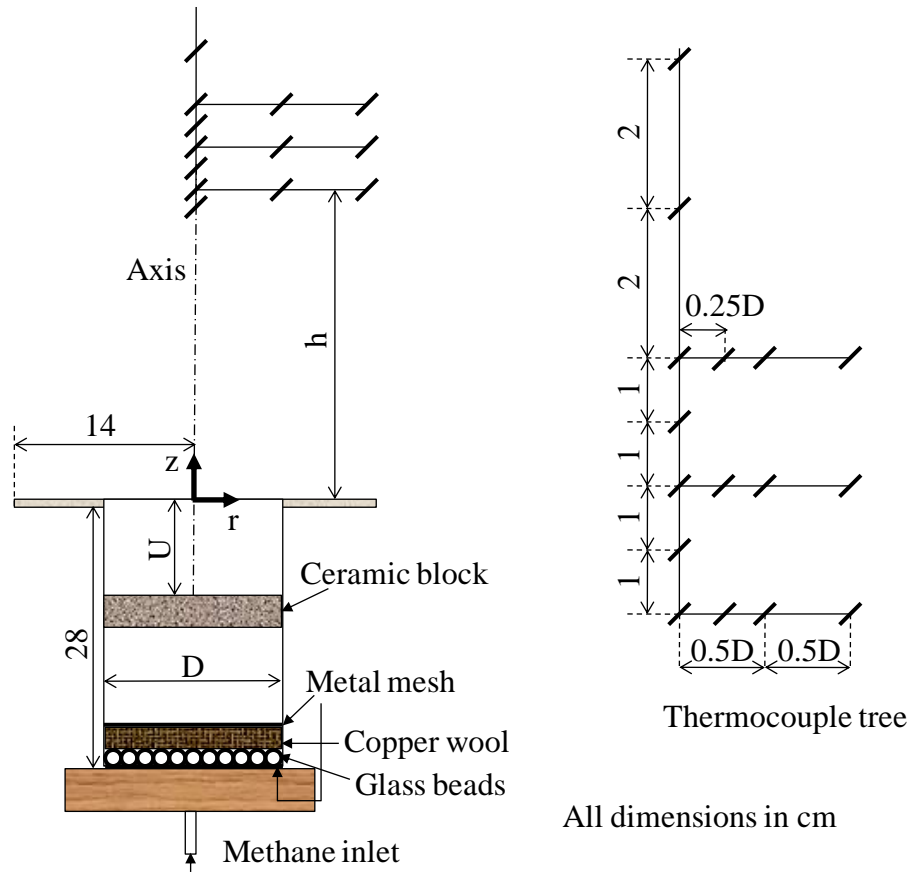


Figure 3-2 - Experimental setup – non-premixed methane burner with adjustable fuel injector level. The inset on the right shows locations of thermocouples

3.2 Results

Figure 3-3 shows experiments with a circular (9 cm diameter) methane burner in a quartz cylinder. These experiments found that a twin-peak flame structure appears at certain ullages for a given mass loss rate. This behavior agrees with the four stages theorized in Figure 2-1 and section 2.1.

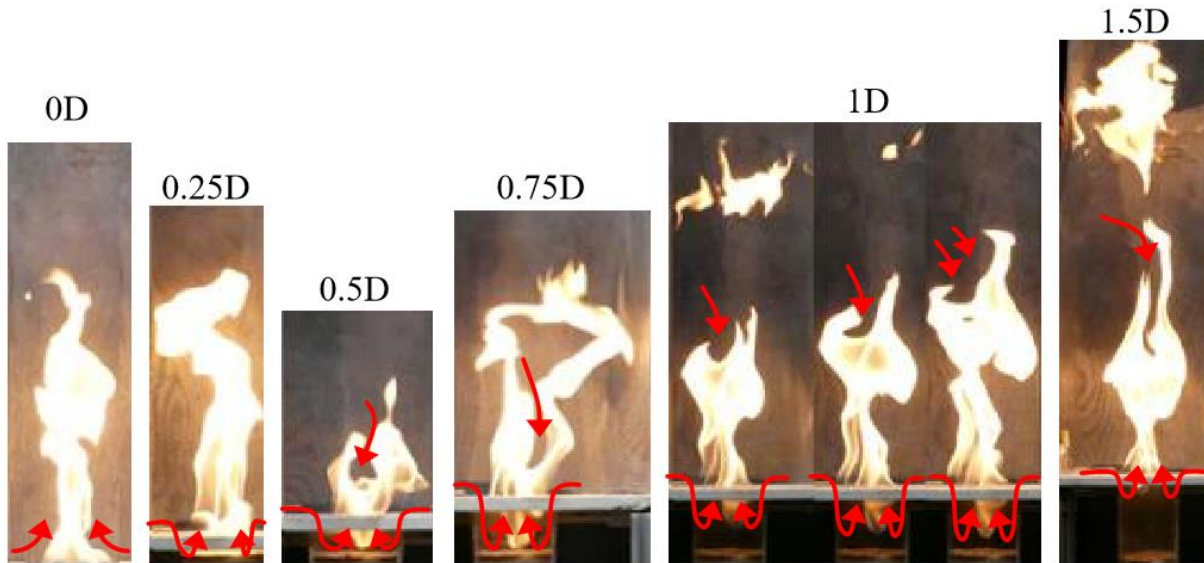


Figure 3-3 - Air entrainment patterns for different ullages in a circular pit with a methane burner.

3.2.1 Centerline and Radial Temperature Profiles

Figure 3-4 shows that as ullage increases, the highest centerline temperatures are at ullage ratios of 1 and 1.5. However, there is a shift in behavior from 0.5 to 0.75, where the temperature begins increasing with increasing ullage. It is determined that the optimum stage is Stage II (U/D from 0.5 to 0.75), where the flame is anchored to the burner surface and exhibits a twin-peak flame structure that allows oxygen to penetrate the flame center. Both aspects of flame behavior lead to increased premixing of the fuel and oxygen. The anchoring at the bottom of the pit allows more oxygen to enter the pit and mix with the fuel. The flame tip's opening into the twin-peak structure allows oxygen to mix with the flame's fuel-rich center. Figure 3-4 shows that increased premixing is reflected in an increase in plume temperature for these ullages.

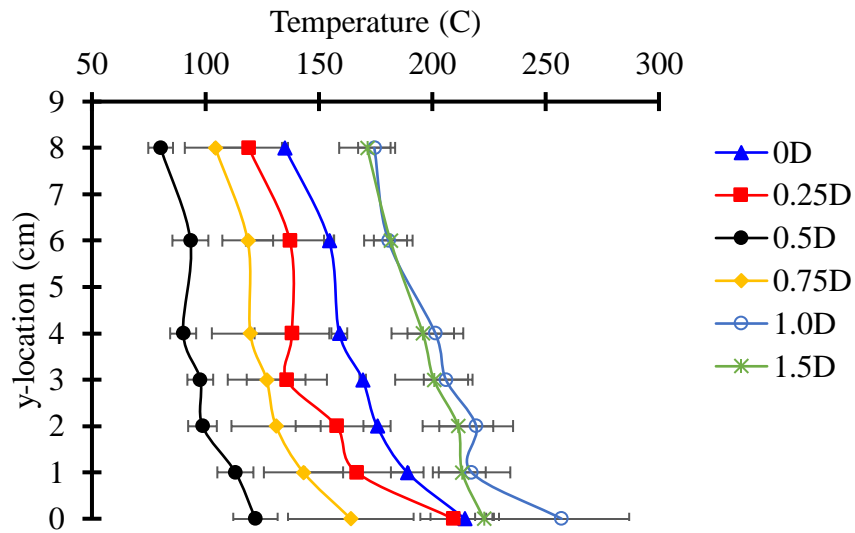


Figure 3-4 - Plume centerline temperatures in the axial direction at 0D to 1.5D for 10 g/min fuel in a circular pit.

When the radial temperatures are examined in Figure 3-5, the same trend seen for the centerline temperatures is also seen with the highest plume temperatures seen at an ullage to diameter ratio of 1.0. Additionally, the plume is less Gaussian at $U/D = 1.0$, with higher temperatures near the centerline.

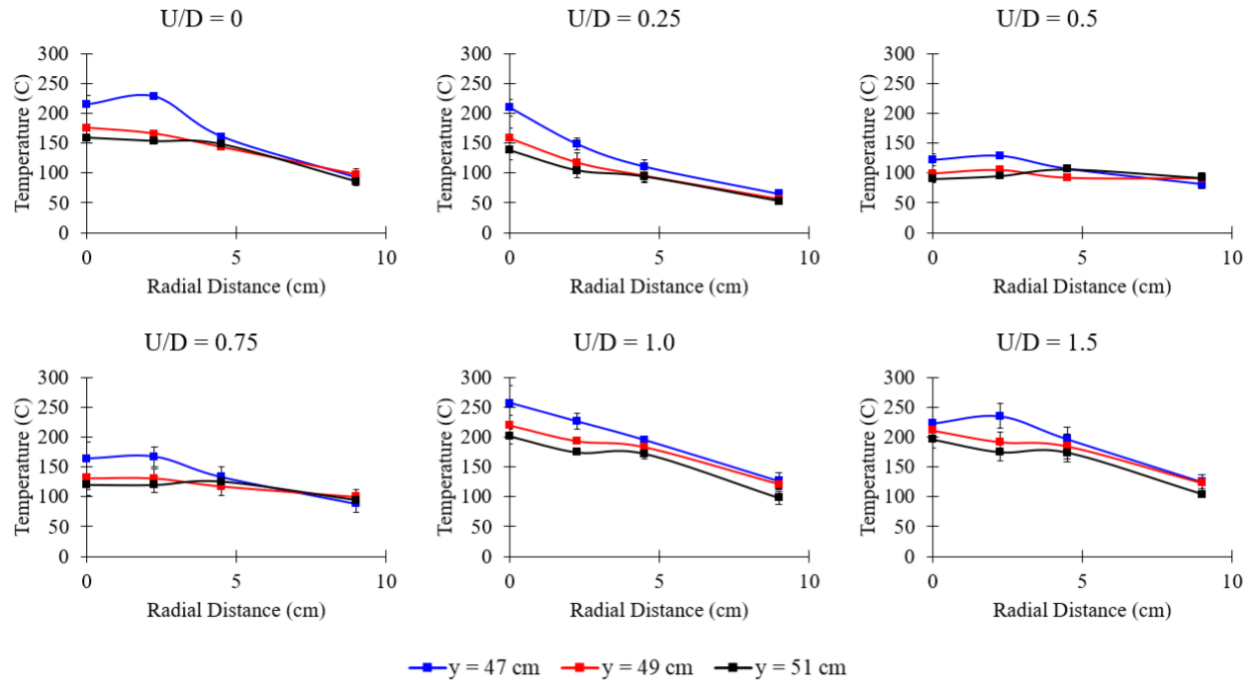


Figure 3-5 Radial temperature profiles at z -locations of 47, 49 and 51 cm measured from exit of the glass tube for varying ullages and for 10 g/min fuel flow.

These temperatures are only in the plume region, and an increase in temperature can either be attributed to an increased flame temperature or a reduction in the amount of cooler ambient air entrained. The claim that stage III flames show enhanced burning assumes that additional air is not being entrained but rather the flame is hotter. This claim is supported by the work in the next section.

3.2.2 Air Entrainment Correlation

Furthermore, an air entrainment correlation for pit fires was desired to determine if both more air was being drawn into the flame and increased premixing. Flame pulsation frequency is necessary to air entrainment, and pit flames exhibit two types of pulsation. The lateral oscillation (flapping) is only seen in fires where an ullage (U) exists, so this frequency was used in the entrainment correlation. The correlation is semi-empirical and combines experimental data with a parameter

derived through dimensional analysis. The variables selected for the analysis are the heat release rate (\dot{Q}), density (ρ), heat capacity (c_p), the Stefan-Boltzman radiation constant (σ), the flapping frequency (f), the volumetric mass entrainment rate (\dot{m}_{ent}'''), the ambient temperature (T_∞) and the gravitational constant (g). Table 2 shows the variables and their dimensions. Taking the dimensions from Table 2 as a matrix and reducing it to the row-echelon form gives Table 3.

Table 2 - Variables and dimensions for air entrainment analysis.

	\dot{Q}	ρc_p	σ	U	f	\dot{m}_{ent}'''	T_∞	g
	a1	a2	a3	a4	a5	a6	a7	a8
F (N)	1	1	1	0	0	1	0	0
L (m)	1	-2	-1	1	0	-4	0	1
T (s)	-1	0	-1	0	-1	1	0	-2
Θ (K)	0	1	-4	0	0	0	1	0

Table 3 - A reduced row-echelon form of Table 3.

	\dot{Q}	ρc_p	σ	U	f	\dot{m}_{ent}'''	T_∞	g
	a1	a2	a3	a4	a5	a6	a7	a8
F (N)	1	0	0	0	5/4	-3/2	1/4	5/2
L (m)	0	1	0	0	-1	2	0	-2
T (s)	0	0	1	0	-1/4	1/2	-1/4	1/2
Θ (K)	0	0	0	1	-7/2	2	-1/2	-6

The reduced matrix gives the following equations, which are unified and then grouped:

$$a1 = -\frac{5}{4}a5 + \frac{3}{2}a6 - \frac{1}{4}a7 - \frac{5}{2}a8 ,$$

$$a2 = a5 - 2a6 + 2a8 ,$$

$$a3 = \frac{1}{4}a5 - \frac{1}{2}a6 + \frac{1}{4}a7 - \frac{1}{2}a8 ,$$

$$a4 = \frac{7}{2}a5 - 2a6 + \frac{1}{2}a7 + 6a8 ,$$

$$F^0 L^0 T^0 \theta^0$$

$$\stackrel{\text{def}}{=} \dot{Q} \left(-\frac{5}{4}a5 + \frac{3}{2}a6 - \frac{1}{4}a7 - \frac{5}{2}a8 \right) \rho c_p^{(a5-2a6+2a8)} \sigma \left(\frac{1}{4}a5 - \frac{1}{2}a6 + \frac{1}{4}a7 - \frac{1}{2}a8 \right) U^{\left(\frac{7}{2}a5 - 2a6 + \frac{1}{2}a7 + 6a8 \right)} f^{a5} m_{ent}'''^{a6} T_{\infty}^{a7} g^{a8} ,$$

$$F^0 L^0 T^0 \theta^0 \stackrel{\text{def}}{=} \left(\frac{\rho c_p \sigma^{\frac{1}{4}} U^{\frac{7}{2}} f}{\dot{Q}^{\frac{5}{4}}} \right)^{a5} \left(\frac{\dot{Q}^{\frac{3}{2}} m_{ent}'''}{(\rho c_p)^2 \sigma^{\frac{1}{2}} U^2} \right)^{a6} \left(\frac{T_{\infty} \sigma^{\frac{1}{4}} U^{\frac{1}{2}}}{\dot{Q}^{\frac{1}{4}}} \right)^{a7} \left(\frac{g (\rho c_p)^2 U^6}{\dot{Q}^{-\frac{5}{2}} \sigma^{-\frac{1}{2}}} \right)^{a8}$$

[3-1]

Then neglecting the last two terms, ambient temperature variation and gravity variation, radiation effects, and assuming density and heat capacity are constant, gives the following relationship:

$$\frac{U^{\frac{7}{2}} f}{\dot{Q}^{\frac{5}{4}}} \propto \frac{\dot{Q}^{\frac{3}{2}} m_{ent}'''}{U^2} \quad [3-2]$$

Which is then rearranged to give the volumetric air entrainment as a function of the following parameter consisting of ullage, pulsation frequency, and heat release rate:

$$m_{ent}''' \propto \frac{U^{\frac{11}{2}} f}{\dot{Q}^{\frac{11}{4}}} \quad [3-3]$$

This parameter is then used with the experimental data to produce the following correlation:

$$m_{ent}''' = 1.6 \left(\frac{U^{5.5} f}{\dot{Q}^{2.75}} \right)^{-0.16} . \quad [3-4]$$

Figure 3-6 shows the goodness of fit of the correlation for small-scale pit fires at three mass flow rates. This equation gives the air entrained into the pit cavity not the plume. The lowest fuel rate has the worst fit to the correlation because hydrocarbon fuels typically burn in the range of 4 – 6 g/min [62], so 2 g/min is a low value to have entrainment based solely on \dot{Q} , which neglects radiative heat feedback and thus the model under predicts the experimental entrainment.

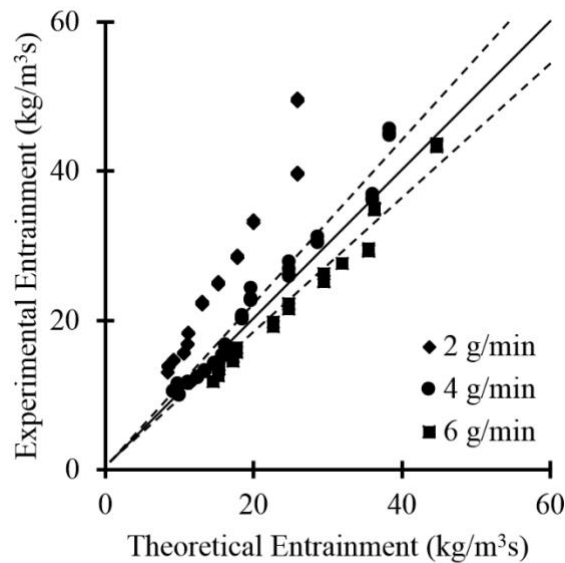


Figure 3-6 - Experimental versus theoretical entrainment rate for a square pit fire with dotted lines represented +/- 10% error.

The experimentally measured air entrainment rate (Figure 3-7) is seen to be a function of ullage and fuel mass flow rate, with deeper ullages having higher entrainment as the more air flow is needed to ensure air penetrates the cavity and higher fuel flow having less entrainment as the fire is less efficient. **However, the trends of increasing ullage leading to increased entrainment and increasing heat release rate leading to less entrainment are not reflected in the semi-empirical**

equation despite the good fit. The dimensional analysis does lead to a relationship that would match the trends seen in the experimental data. This indicates that the coefficients found from fitting the experimental data are likely to be inaccurate despite the agreement seen in Figure 3-6. This discrepancy is attributed the simplicity of the dimensional analysis which neglects radiative effects and assumes a constant density plume. A more detailed analysis and a larger set of experimental data is needed to create a general pit-fire entrainment model.

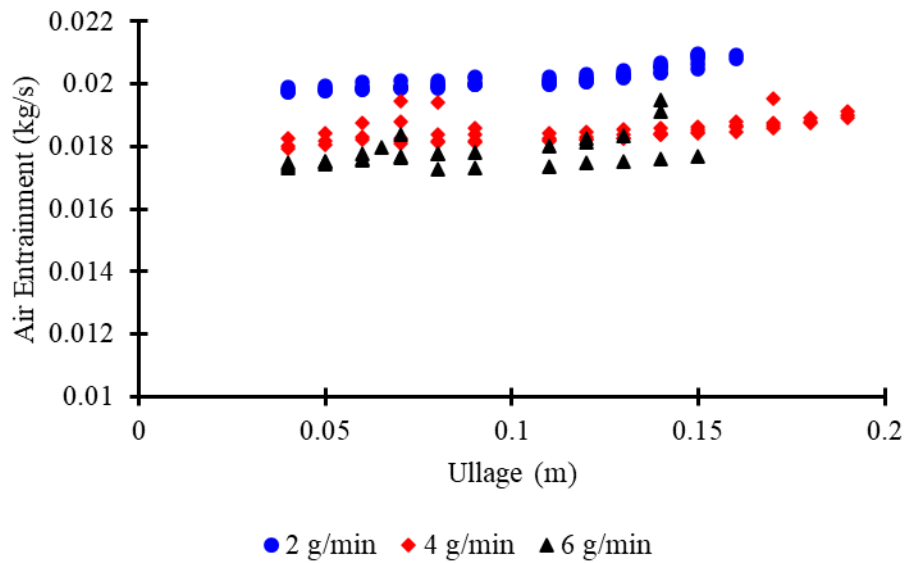


Figure 3-7 - Air entrainment as a function of ullage

A simple dimensional analysis can give the following relationship between plume temperature and air entrainment, $T_{plume} \sim \frac{\dot{Q}}{c_p \dot{m}_{ent}}$, which suggests that an increase in air entrainment should lead to a decrease in average plume temperature and given that Figure 3-7 shows that entrainment increases with increasing ullage this supports the trend seen for ullage to diameter ratios greater than 0.5. Additionally, as the heat release rate increases (e.g. increase fuel rate for a gas burner) the average plume temperature should increase which matches the trend seen in

Figure 3-8 regardless of ullage. This also supports the conclusion that the increase in plume temperature for stage III flames is due to an increase in flame temperature not a reduction in air entrainment compared to the other stages.

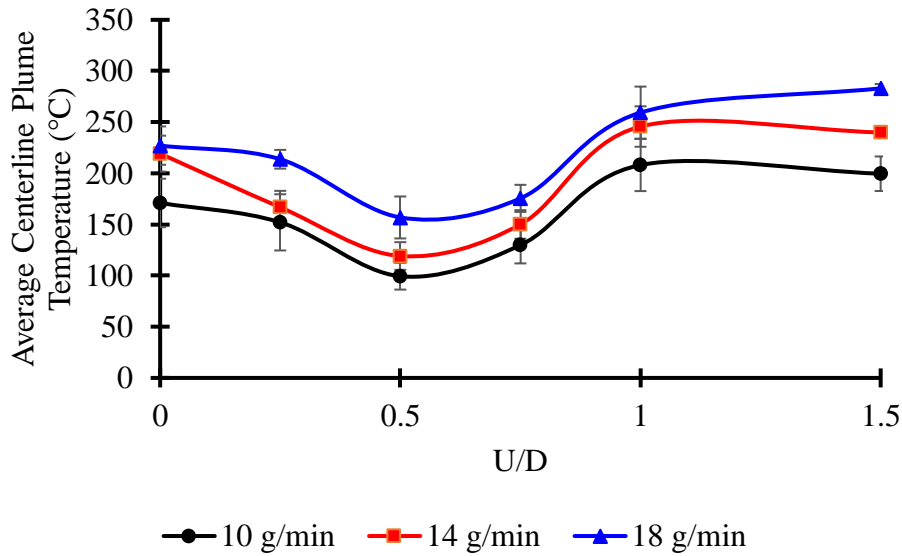


Figure 3-8 – Average centerline plume temperature as a function of ullage for 10, 14, 18 g/min methane

3.2.3 Carbon Monoxide and Carbon Dioxide Production

Given the strong relationship between air entrainment, flame pulsation, and combustion efficiency, Figure 3-9 shows the experimental relationship between pulsation frequency (f), ullage, and carbon monoxide/carbon dioxide ratio at a fuel flow rate of 6 g/min. In the range of ullages between 0.05 m to 0.1 m, the value of f is seen to be consistently lower than other ullages. Still, the air entrainment rate does not increase in this region, and the CO/CO₂ ratio, representing the inefficiency of combustion, is observed to be lower. The enhanced combustion is thus attributed to enhanced premixing, not increased air entrainment. This finding is essential as enhanced premixing leads to more complete combustion (rather than more combustion overall due to more air entrainment) and reduces the number of hazardous combustion products produced by the fire.

Thus, using an optimal ullage in a burn pit can burn waste faster, as shown by higher plume temperatures, and generate fewer hazardous emissions.

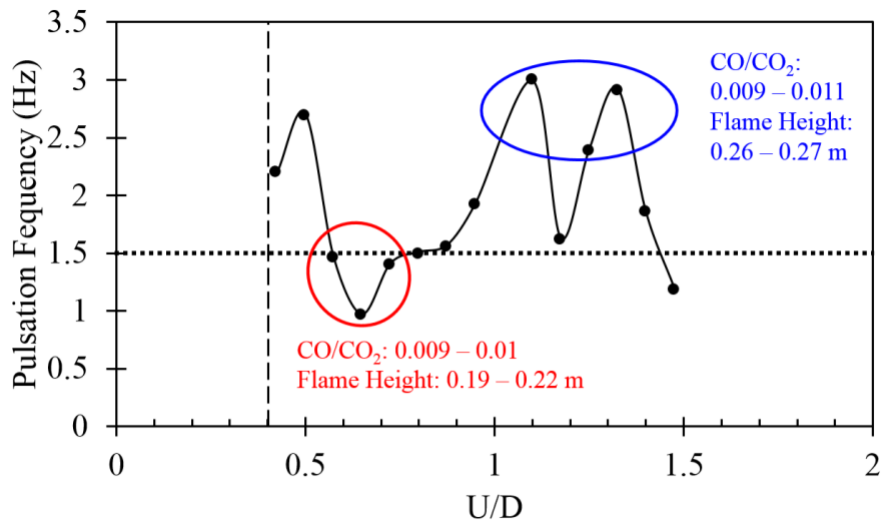


Figure 3-9 - Flapping frequency as a function of ullage with flame emissions, demonstrating a region of enhanced burning for a fuel flow rate of 6 g/min. CO/CO₂ measured using a Servomex Gas Analyzer of smoke extracted at 40 cm above the pit.

These two small-scale experimental studies found that for certain ullages, burning is enhanced, as shown by increased plume temperatures and reduced emissions. This enhancement is attributed to altered airflow, which increases premixing, and this altered airflow due to ullage is responsible for the four stages of flame behavior. The specific ullage where burning is enhanced depends on the mass-loss rate (fuel flow rate for the gas burner) and the fire's diameter. The gas burner allowed for the mass-loss rate to be decoupled from the airflow, but as the end goal is solid-waste fires, experiments with condensed phase fuels are desired. Additionally, larger-scale experiments are desired to determine if the enhancements seen at the small scale persist at scales closer to those seen in burn pits.

3.2.4 Oxygen Penetration and Parameter Characterization

The major parameters that dictate the flame dynamics in pit burning are: (1) ullage, (2) diameter of the burner, and (3) mass transfer of fuel and oxygen. Identification of the effect of the aforementioned parameters will assist in developing a physical insight into the pit burning problem. For a theoretical analysis, consider a cylindrical burner of diameter D at an ullage U (Fig. 3-9), as shown on an r - z plane for a non-reacting mass transfer analysis. The fuel convects from the fuel inlet at $z = 0$ and air is entrained axially and radially into the pit. The air entrainment and mixing strategies would vary with the ullage. A scaling analysis is considered in this study which would assist in analyzing the time scales for the fuel and oxygen mass transfer.

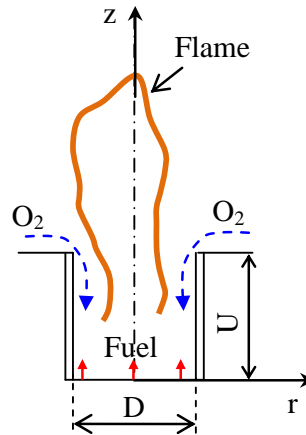


Figure 3-9 - Schematic of a circular burner of diameter D at an ullage U

The unsteady species conservation equation for fuel (F) is shown in equation (23). The scaling parameters for each of the terms are portrayed in equation [3-5], where Y , u , and \wp represent the mass fraction, average fuel velocity and binary mass diffusivity.

$$\frac{\partial Y_F}{\partial t} + \frac{\partial(u_F Y_F)}{\partial z} = \wp_{F,O_2} \frac{1}{r} \frac{\partial^2(r Y_F)}{\partial r^2} + \wp_{F,O_2} \frac{\partial^2 Y_F}{\partial z^2} \quad [3-5]$$

$$\sim \frac{1}{\tau_F} \quad \sim \frac{u_F}{U} \quad \sim \wp_{F,O_2} \frac{4}{D^2} \quad \sim \wp_{F,O_2} \frac{1}{U^2} \quad [3-6]$$

The ullage (U) and the boundary layer thickness (δ) have been used as the scaling dimension in the axial and the radial direction, respectively. The time scales for advection and diffusion of the fuel are shown in equation [3-7].

$$\tau_F \sim \left[\frac{U}{u_F} \right] \quad \tau_F \sim \left[\frac{\delta^2}{\rho_{F,O_2}} \right] \quad \tau_F \sim \left[\frac{U^2}{\rho_{F,O_2}} \right]$$

(advection of fuel) (radial diffusion of fuel) (axial diffusion of fuel) [3-7]

Similarly for oxygen (O_2), the species conservation equation is shown in equation [3-8] with the scaling as portrayed in equation [3-9]. Oxygen entrainment occurs from the sides of the pit and the scale for oxygen entrainment in the radial direction is considered to be the thickness of the boundary layer as formed by the convecting fuel. The time scales for diffusion of the oxygen are shown in equation [3-10].

$$\frac{\partial Y_{O_2}}{\partial t} = D_{O_2,F} \frac{1}{r} \frac{\partial^2 (r Y_{O_2})}{\partial r^2} + D_{O_2,F} \frac{\partial^2 Y_{O_2}}{\partial z^2} \quad [3-8]$$

$$\sim \frac{1}{\tau_0} \quad \sim D_{O_2,F} \left[\frac{1}{\delta} \frac{\delta}{\delta^2} \right] \quad \sim D_{O_2,F} \left[\frac{1}{U^2} \right] \quad [3-9]$$

$$\tau_O \sim \left[\frac{\delta^2}{D_{O_2,F}} \right] \quad \tau_O \sim \left[\frac{U^2}{D_{O_2,F}} \right]$$

(radial diffusion of O_2) (axial diffusion of O_2) [3-10]

For developing flow in the pit, fuel diffuses radially in the boundary layer in the time scale

$\tau_{F,D} \sim \delta_z^2 / \rho_{F,O_2}$, where δ_z is the boundary layer thickness, which is a function of z as evaluated

using equation [3-11]. In equation [3-11], ν is the kinematic viscosity of fuel. For known fuel

flow rate \dot{m} , u can be calculated as $\frac{\dot{m}}{\rho_F (\pi D^2 / 4)}$. The boundary layer thickness has a maximum

value of $D/2$ for the cylindrical burner.

$$\delta_z = \frac{5z}{\sqrt{\text{Re}_z}} = 5z \sqrt{\frac{u_F}{u_F z}} = 5 \sqrt{\frac{u_F z}{u_F}} \quad [3-11]$$

Oxygen diffuses radially near the rim of the pit and the time scale for radial diffusion of oxygen is evaluated as $\tau_{O_2,D} = \delta_U^2 / \varphi_{O_2,F}$, considering the boundary layer thickness at $z = U$ [3-12].

$$\tau_{O_2,D} \sim 25 \frac{u_F}{\varphi_{O_2,F}} \frac{U}{u_F} \sim 25(\text{Sc}) \frac{U}{u_F} \quad [3-12]$$

Here, Sc is the Schmidt number of the fuel considering $\varphi_{O_2,F} = \varphi_{F,O_2}$. The boundary layer thickness at the burner rim increases with an increase in ullage as shown in Fig. 3-9(a). This shows that oxygen can diffuse more towards the axis of the burner for deeper ullage cases. The time for radial diffusion of oxygen also increases based on the boundary layer thickness at the burner rim as shown in Fig. 3-9(b). Moreover, the time for diffusion reduces with an increase in fuel inlet velocity as the boundary layer thickness decreases.

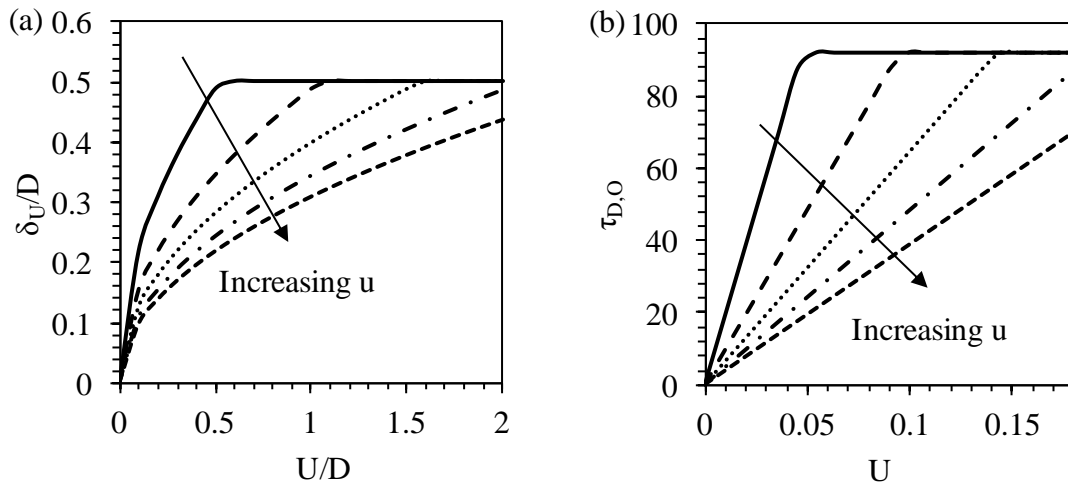


Figure 3-10 - Representative variation of (a) boundary layer thickness at $z = U$, and (b) radial diffusion time scale of oxygen with ullage and fuel inlet velocity

Further, the flame width (L_W) as shown in Fig. 3-10(a) can be defined as,

$$L_W \sim D - 2\delta_U \Rightarrow \frac{L_W}{D} \sim 1 - \frac{2\delta_U}{D} \quad [3-13]$$

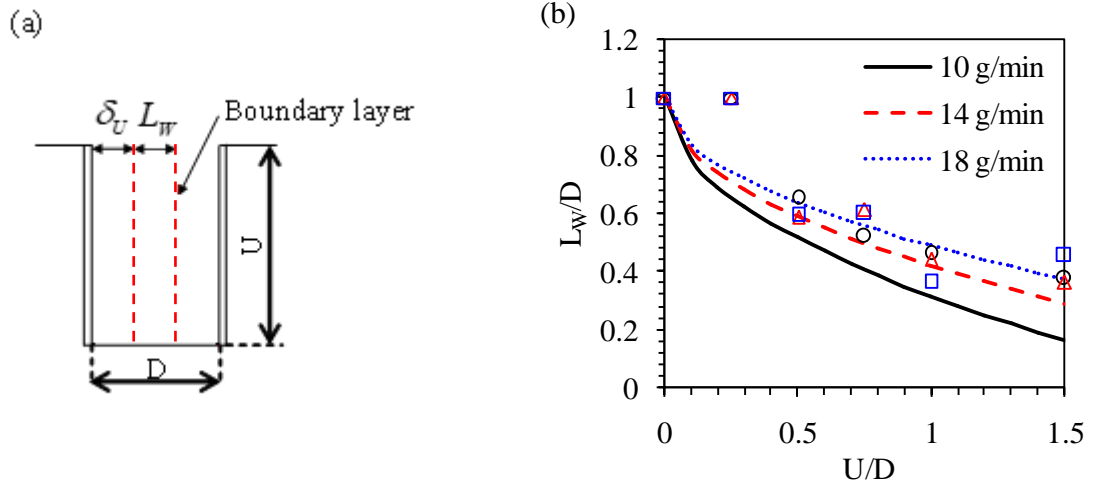


Figure 3-11 - Schematic showing boundary layer formation and flame width, (b) variation of flame width with ullage for different fuel flow rates (symbols represent experimental values, lines represent the predicted values)

Fig. 3-10(b) shows the variation of flame width as a function of non-dimensional ullage for different fuel flow rates. It is seen that the flame width reduces as ullage increases. This is due to the higher boundary layer thickness at the rim ($z = U$) for deeper ullages (Fig. 3-9a). The predicted flame width is seen to be in close comparison with the experimental flame width as obtained from the flame photographs.

The time scale for fuel advection can be evaluated as $\tau_{F,A} \sim (U/u_F)$, as shown in equation [3-14].

In this time scale, oxygen diffuses axially to a distance of L_{O_2} , which is determined by equation [3-13].

$$\tau_{F,A} \sim \left[\frac{L_{O_2}^2}{\rho_{O_2,F}} \right] \Rightarrow L_{O_2} \sim \sqrt{\tau_{F,A} \times \rho_{O_2,F}} \Rightarrow L_{O_2} \sim \sqrt{\frac{U}{u} \rho_{O_2,F}} \quad [3-14]$$

Fig. 3-11 (a) portrays the variation of this length scale, defined as oxygen penetration depth, as a function of ullage. It is observed that the diffusion length increases with ullage. However, the length non-dimensionalized with ullage depth is seen to decrease with the ullage as shown in Fig. 3-11(b), portraying that as ullage increases, the oxygen diffusion as compared to the ullage depth decreases. It is also seen that with an increase in the fuel velocity, the length to which oxygen diffuses decreases even further due to enhanced fuel convection.

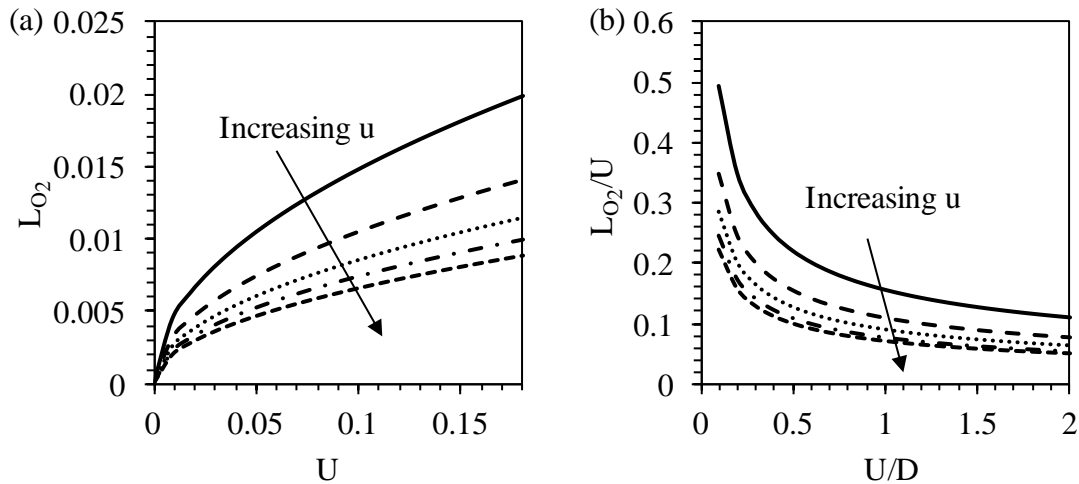


Figure 3-12 - Representative variation of (a) dimensional, and (b) non-dimensional axial diffusion scale of oxygen with ullage and fuel inlet velocity

Fig. 3-12 shows the variation of non-dimensionalized oxygen penetration depth with the ullage of the pit. The variation is also shown for different flow rates. The trend for this axial diffusion length is seen to be similar as compared to the experiment. Equation [3-14] has been scaled using a factor of 2.2 to match the experimental results.

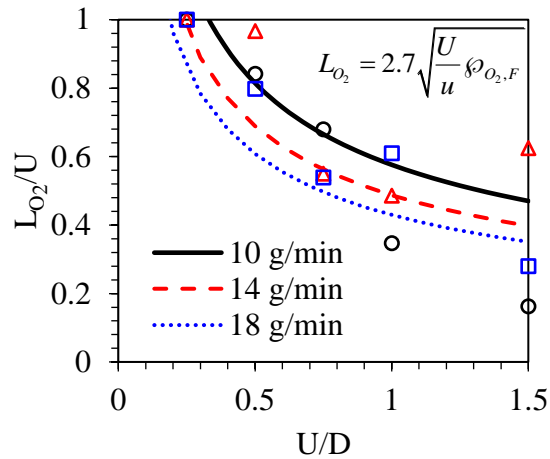


Figure 3-13 - Variation of non-dimensional oxygen penetration with ullage

The fuel and oxygen diffusion in the pit affects the flame shape and flame base location. For a small value of U/D (Fig. 3-13a), the normal diffusion flame is seen with the air entraining into the pit from the sides. As the ullage increases, air entrains deeper into the pit, and partial premixing can occur within the pit (Fig. 3-11b). As L_{O_2}/U reduces with ullage as shown in Fig. 3-13 (b), the flame base can shift slightly away from the fuel base. Moreover, the flame base width could decrease due to the boundary layer effects and radial diffusion of oxygen into the pit. At a much deeper ullage of U_3 (Fig. 3-13c), air entrains near the burner rim, and the partial premixing zone can shift further away from the fuel inlet.

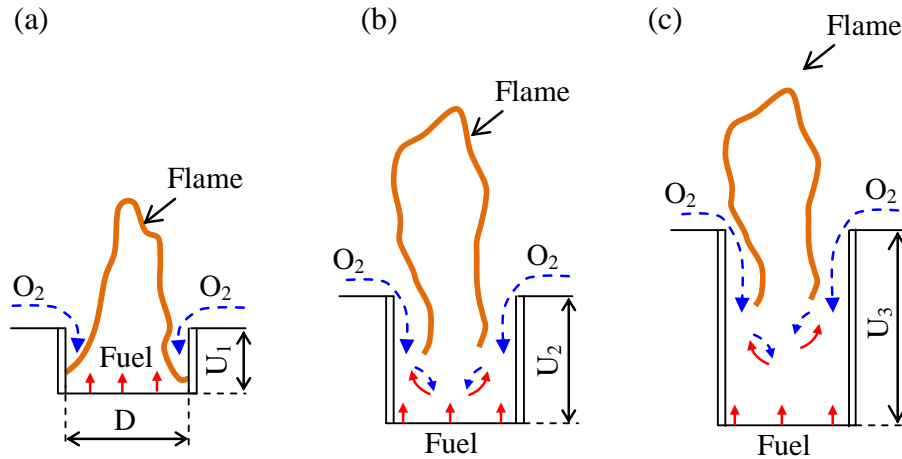


Figure 3-14 - Schematic of the flame behavior at ullage (a) U_1 , (b) U_2 , and (c) U_3 [$U_1 < U_2 < U_3$]

3.3 Particle Imaging Experiments

Particle tracking (P.T.) is a method for visualizing flows and obtaining instantaneous velocity measurements. Tracer particles are introduced to the flow (called seeding), and they are sufficiently small and have small enough momentum to faithfully follow the fluid flow dynamics. The fluid is illuminated, usually with a planar laser, to visualize the particles, and their movement is recorded, usually with a high-speed camera. P.T. with a planar laser allows for two-dimensional velocity measurements. The accuracy of the velocity calculations relies on the seed particles' ability to follow the flow and introduce the particles in such a way that the fluid flow patterns are not disturbed. A balance between small particles that flow better and larger particles that reflect lighter and are easier to track is needed when determining the appropriate particle size.

Additionally, the particles should not chemically interact with the fluid being measured. Ceramics, such as aluminum oxide, are the usual choice for seeding particles in flames or high-temperature flows. However, they can be difficult to disperse into flows as the electrostatic effect can lead to clumps forming [67]. For a gas flow, such as a flame, the seeding particles should be introduced in a stable concentration with a spatially uniform distribution while not altering the

existing flow pattern. As Melling [67] points out, swirling flows are challenging to seed appropriately. The vortex core is challenging to locate, and the core has lower fluid density and thus lower particle density.

Particle imaging velocimetry (PIV), particularly stereoscopic PIV for large-scale areas such as doorways, is used to analyze the airflow around a fire. Bidirectional flows are present in the cavity: fresh air is entrained into the reaction front and smoke leaves the reaction area. Past methods for characterizing fire flows were thermocouples and bi-directional pressure probes. Still, their expense and size limit the amount used to characterize a given space. Two-dimensional PIV has been used to characterize the air entrainment into a fire whirl, a phenomenon of similar nature (i.e., altered flame shape due to altered airflow) to that which we are investigating here [68].

3.3.1 Objective

Previous work on fires in the presence of an ullage has identified a novel flame behavior. The flame tip opening into two distinct flames and then closing into a single flame occurs with a quantifiable frequency [30], [55]. This behavior's mechanism is posited as altered airflow patterns induced by a significant ullage in these papers. To confirm and further investigate the airflow patterns for a "pit" fire with a certain ullage, PIV was set up with a small-scale pool fire. A pool fire rather than a gas burner was used to limit the airflow's fuel velocity. Methanol was selected as it has a low soot yield, and the laser sheet can illuminate the soot rather than the tracing particles, making the velocity measurements more uncertain. This experiment was done in collaboration with Dr. Jackie Sung's combustion diagnostics lab at the University of Connecticut, as they have a great wealth of knowledge regarding PIV with fire. These experiments' objective is to obtain a qualitative and quantitative understanding of the changes to the air entrainment pattern for a pool

fire caused by the presence of an ullage. It has been posited that the ullage introduces turbulence in the entrained air and leads to vortices forming in the pit cavity [30], and these vortices pull the flame apart into the twin peak structure.

3.3.2 Methodology

Ethanol was chosen as the fuel because it is a low soot fuel and has a blue flame that will not interact significantly with the laser sheet. An 8 cm by 8 cm square pool was selected because a circular pool would cause diffraction of the laser sheet and distort the results. Ullages of 6, 4, and 2 cm were tested. The main hurdle in the setup was introducing the seeding particles to disturb the delicate flame structure, disperse a relatively uniform concentration, and limit the number of clumps introduced to the flame. It was finally decided to use a vibrating mesh sifter positioned 10 cm above the flame (this height was limited by the size of the vent hood the pool was in). Ideally, the seeding particles would be introduced further above the flame to allow for a more uniform distribution within the plume and reduce disturbances to the plume structure. A Nd:Yag laser was used, and the sheet was located at the midplane of the pit. A high-speed camera at 2000 fps was used to record the laser's interaction with the seeding particles. The images use a yellow-blue spectrum with the seeding particles showing up as yellow on a blue background, with denser concentrations of particles showing up as a brighter yellow.

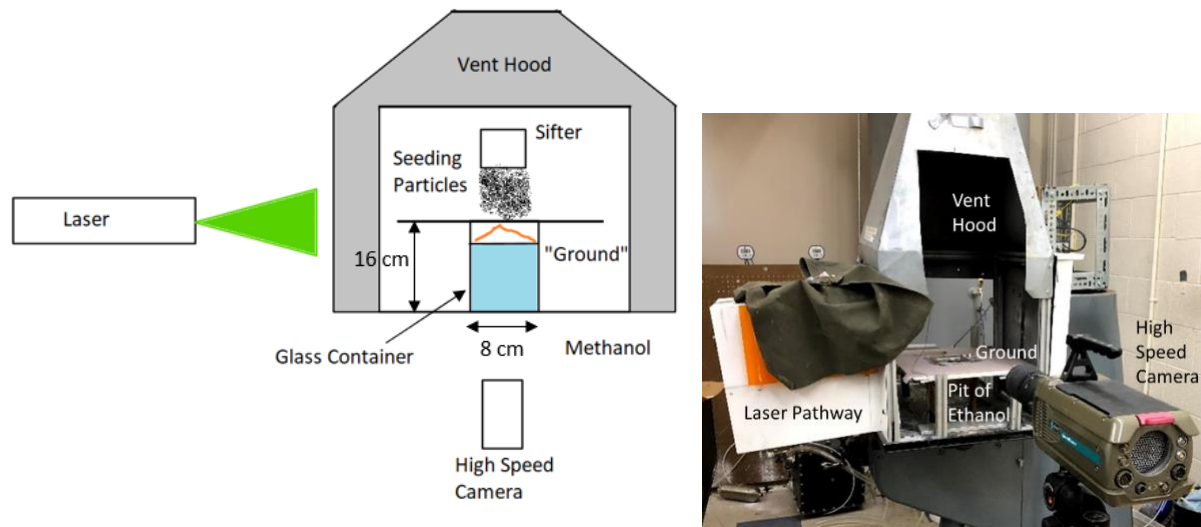


Figure 3-15 - Experimental setup diagram (left) and photo (right)

Four stages of flame behavior are described in this thesis's introduction, but a brief recap will be given here. Stage I flames (for $U/D = 0$ to 0.25) are a standard flame with the ground around the fuel that has been shown to alter airflow into the flame [26] but not alter flame behavior. Stage II flames (for $U/D = 0.5$ to 0.75) have a sufficient ullage for the airflow into the pit to affect the flame behavior. The pit edge causes the shear boundary layer to increase and interact with more than just the flame's outermost parts. These changes to the airflow alter the flame behavior, causing the flame to open into the twin peaks and closes into a single peak with a specific frequency. As the flame tip opens, the flame base narrows as the twin peaks reduce the amount of airflow into the pit, creating low oxygen regions in the pit. Then as the twin peaks close, the flame base widens. This behavior is attributed to increased Kelvin-Helmholtz instabilities from airflow into the pit and reduced radial airflow, causing air to be axially entrained, introducing more Rayleigh-Taylor instabilities. The flame still exhibits puffing behavior, with a different frequency to the flapping

behavior. Stage III flames ($U/D = 1.0$) are at still deeper ullages. The airflow into the pit is insufficient to fully penetrate the burner surface, causing the flame base to oscillate its anchoring to the burner. Therefore, in addition to the flame base narrowing and widening in the lateral direction, the flame base also moves vertically in the pit. The twin-peak structure with its flapping behavior and the puffing behavior are both still seen. The lifted-off flame doesn't draw air as deep into the pit as the attached flame, reducing premixing, leading to lower plume temperatures. Finally, at stage IV ($U/D = 1.5$), airflow into the pit is too weak to allow combustion in the bottom of the pit, causing the flame to completely detach from the burner surface and anchor near the top of the pit. The flame still has flapping and puffing behavior.

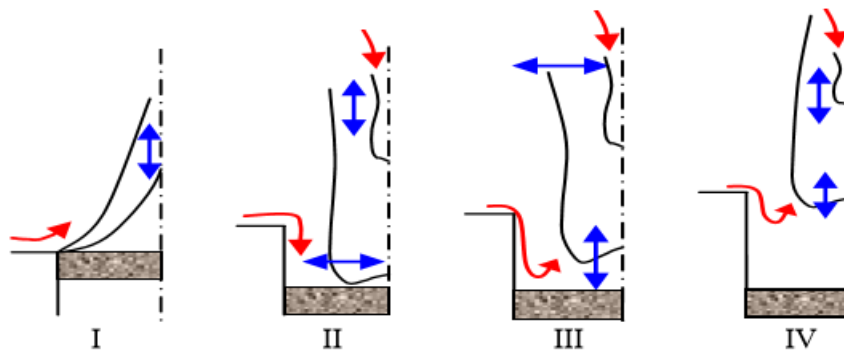


Figure 3-16 - The theorized relationship between ullage and flame behavior (red arrows signify airflow and blue arrows signify flame movement)

3.3.3 Results

We see recirculation zones forming at the pit's sides and moving towards the center, decaying with a sample vortex in Figure 3-17. This matches the periodic nature of the twin peak formation, with the vortex at the edge pulling the flame into the two peaks, and then as the vortex decays and moves inwards to the centerline, it pushes the two peaks back together. This concurs with the hypothesized airflow patterns. The U-shaped flame seen for gaseous flames in previous

experiments was not seen for these experiments. However, some of the theorized air flow patterns (see Figure 3-16) were seen for stages I and II.

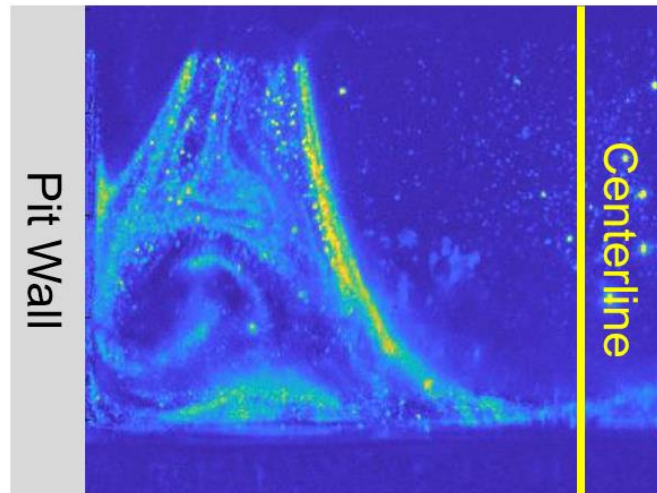


Figure 3-17 - Sample recirculation vortex formed next to the cavity wall

First, a 2 cm ullage ($U/D = 0.25$) did show the puffing generally seen for a pool fire, and the airflows are seen (Figure 3-17) reflect that typically seen for pool fires. There are radial flows into the flame that then become vertical as buoyancy takes over.

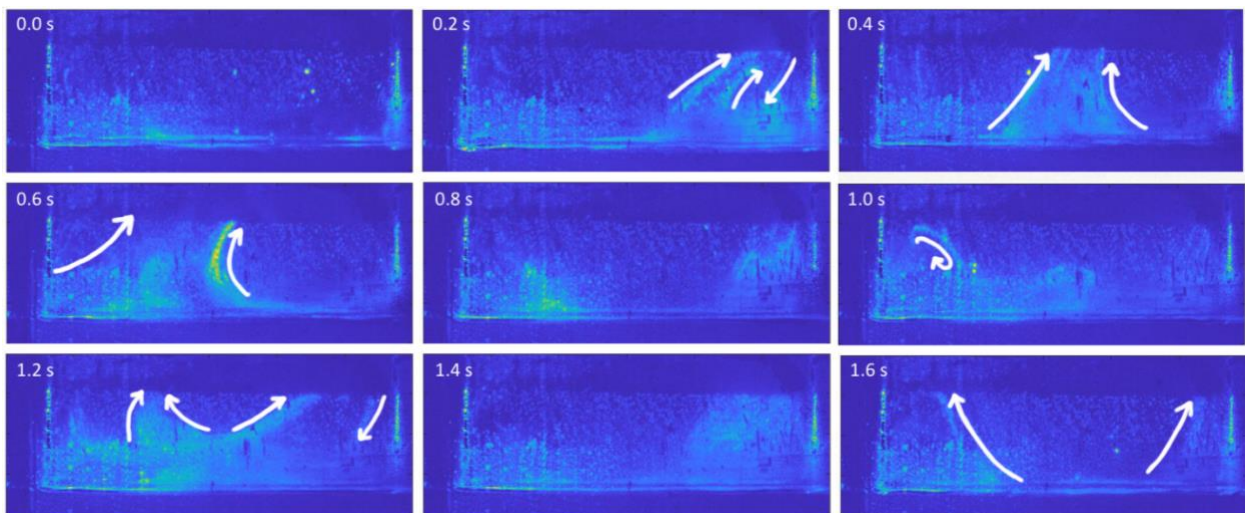


Figure 3-18 - $U = 2$ cm ($U/D = 0.25$), stage II flames, with airflows highlighted by white arrows

Second, a 4 cm ullage ($U/D = 0.5R$) did not show the U-shaped flame seen in the gaseous flames, but the theorized recirculation zones that cause the U-shape were seen in the seeding field. One reason for the lack of a U-shaped flame is that the ethanol is too pale to be seen, and the U-shape may be present but not visible to the naked eye.

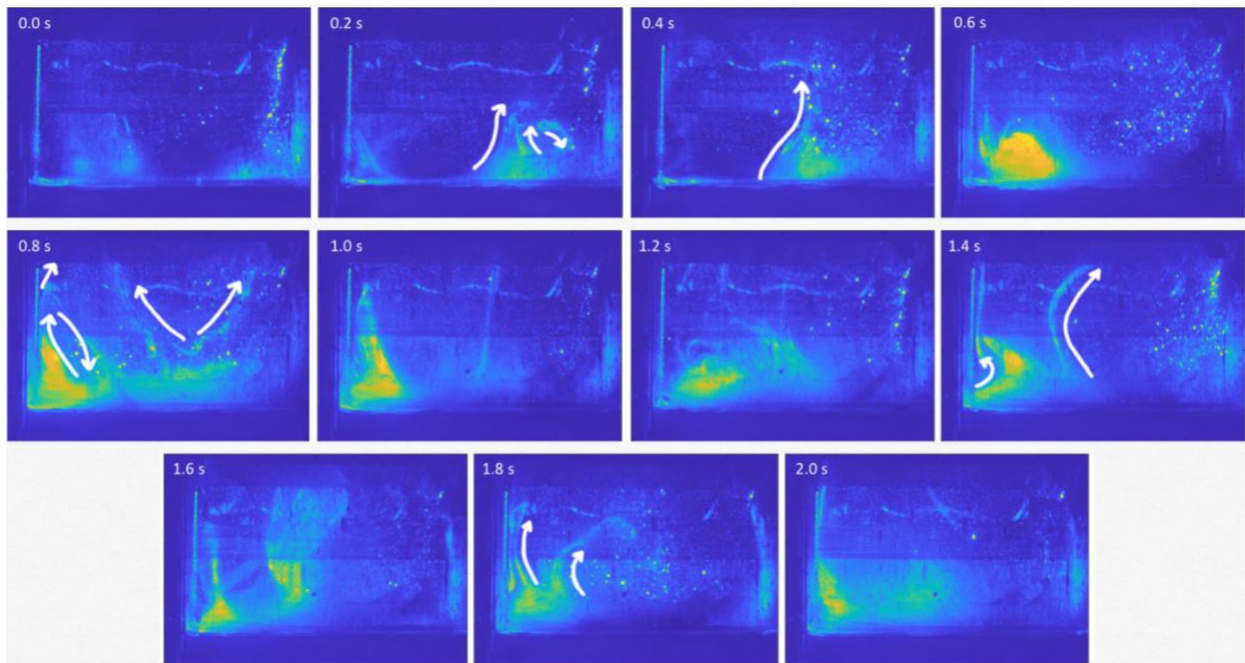


Figure 3-19 - $U = 4$ cm ($U/D = 0.5$), stage II flames, with airflows highlighted by white arrows

Finally, at a 6 cm ullage ($U/D = 0.75$), recirculation zones are also seen but the ability of the seeding particles to reach the base of the flame is worsened.

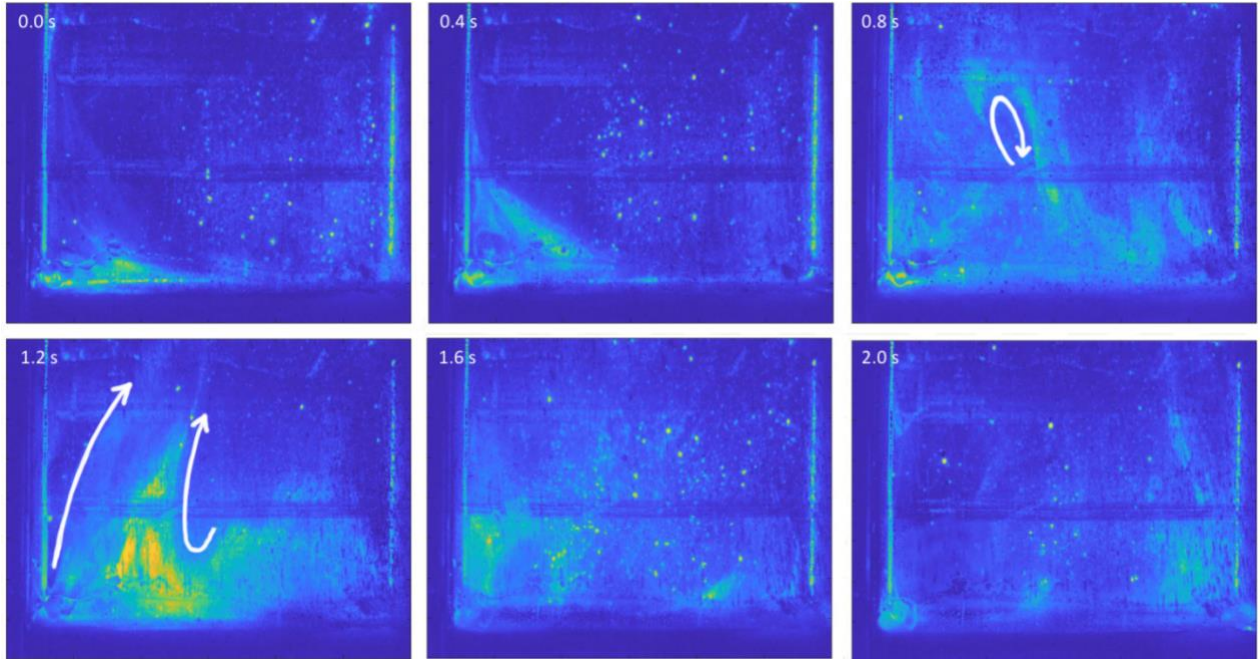


Figure 3-20 - $U = 6 \text{ cm}$ ($U/D = 0.75$), stage IV, with airflows highlighted by white arrows

At $U/D = 0.5$, a vortex is seen forming next to the pit wall and then moving towards the center while becoming less coherent (Figure 3-20). This supports the theorized airflow seen for stage III flames.

3.3.4 Discussion

Issues arose with the selected seeding method (mesh sifter). It did not consistently provide a uniform seeding concentration over the whole area of interest, and some clumps did pass through the mesh and disrupt the airflow (Figure 3-21). Due to these two factors, it was decided that a quantitative analysis of the velocity field was not possible with a sufficient degree of certainty. Instead, snapshots from the videos were used to describe the air flow patterns occurring at different ullages qualitatively.

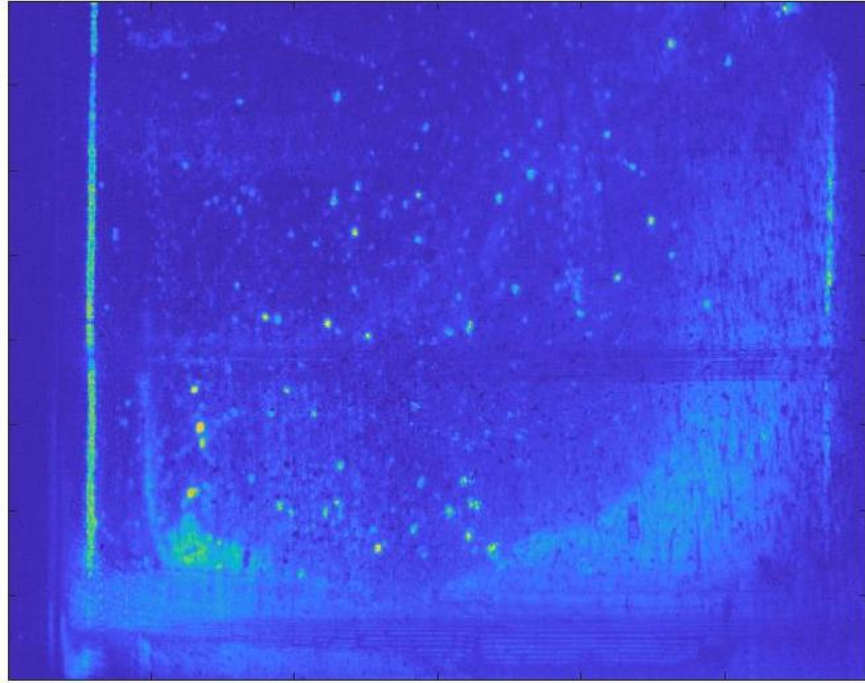


Figure 3-21 - Clumps of seeding particles in the field of view

4 Mass Loss Rates for Pit Fires

The end application of this thesis is the development of an optimal pit shape for use in open-air waste fires, as such it is vital that experiments be conducted at the scale of such waste fires. Literature on these fires reveals that they range from the 0.5 meter scale (a single-family burn-pit for example) to several meters (a burn-pit for a whole U.S. military base). Additionally, these waste fires burn a variety of solid waste from biomass (food scraps, agricultural waste) to fabric (waste uniforms) to plastics, thus experiments with solid waste need to be conducted. However, given the difficulty in determining the effects on the fire of both a shift to solid fuel and a larger scale, it was decided to first increase the size of the fire while using a liquid fuel (which has been examined in Chapter 3 and in literature, and shows similar behavior to that seen for gas fires). This chapter discusses experiments conducted in a circular pit with a 0.57 m diameter and burning kerosene (intended for heating usage) fuel.

4.1 Experimental Setup

At the meso-scale, experiments with constant ullage were performed to capture the effects of a wide range of ullage to diameter ratios. Existing experiments on pit fires with a constant ullage only address small-scale fires (2.5 cm and 5 cm diameter from Shi et al.[28], or 5 to 20 cm from Kuang et al.[29]). The only large-scale studies (100 cm and 150 cm from Shi et al.[27]) don't have a constant ullage (the ullage increases as fuel burns off), preventing the determination of a precise optimum ullage. This experiment seeks to address this gap in the existing body of knowledge. Therefore, tests with a constantly replenishing pool of kerosene, a 57 cm diameter circular pit, were performed with plume temperatures and mass loss rate measured and flame behavior captured by video recording.

Figure 4.1 shows the experimental setup, which consists of the “pit”, the constantly-replenishing fuel setup, a thermocouple tree above the “pit”, and a ground around the “pit” opening. The pit is made of a 55-gallon steel drum (57.15 cm in diameter) as the drum is prefabricated, water-tight, and falls within the test cavity's desired geometry. This diameter was selected as a diameter of greater than 30 cm is required to have large-scale convective and radiative heat fluxes. When balancing available containers and the vent hood's limits, a diameter of greater than 55 cm (transitional flow regime but approaching turbulent and significant scale heat flux behavior) was deemed acceptable. The 55-gallon drum had a sufficient diameter and allowed ullages up to 1.25 times the diameter. A "ground" was constructed of gypsum board (122 cm by 122 cm) around the drum, with the near barrel parts being easily replaceable as it degrades during the burn. The barrel is insulated with 5 cm thick Kaowool to ensure adiabatic wall conditions. A constant ullage is maintained through a constantly replenishing pool system which consists of two communicating vessels filled with kerosene, a peristaltic pump that moves fuel from the supply vessel to the fuel tank. The fuel barrel located at the same height as the pit, connected at the bottom to the pit, and open to the atmosphere so ambient air pressure ensures the liquid level in the burn barrel is the same as that in the fuel barrel. The level in the fuel barrel is kept constant by continuously pumping kerosene into it with any excess above the desired fill level flowing back to the fuel barrel through the overflow opening. Direct videos are recorded at 60 frames per second using a DSLR camera for a straight-on view and a GoPro at 30 frames per second for an overhead view. Twenty-four K-type thermocouples (0.2 mm diameter) are arranged as an array in the plume region. An additional seven thermocouples are placed into the barrel, such that one thermocouple is below the kerosene, and one is at the kerosene level. Finally, a thermocouple located outside the barrel under the insulation is used to determine the fuel's radiative heating. Experiments are done

at ullages (U) from 14.25 to 57 cm, corresponding to 0.25 to 1 times the diameters. Data was collected for 2 minutes at three instances (trials) during the burn, after allowing the burn to reach a steady state (about 5 minutes after ignition). The plume temperature data is time-averaged for each trial and is averaged over three trials for each ullage. The frequency data is the average of three cycles in the 10 minutes of video recording for each ullage. Flame height is estimated by image processing using the diameter of the barrel as a reference. The 0D ullage case was attempted but ultimately discarded due to difficulties in maintaining the constant ullage without overflow in the system shown below, however it is assumed that the 0.25D case will be similar to the 0D case as seen in Chapter 3.

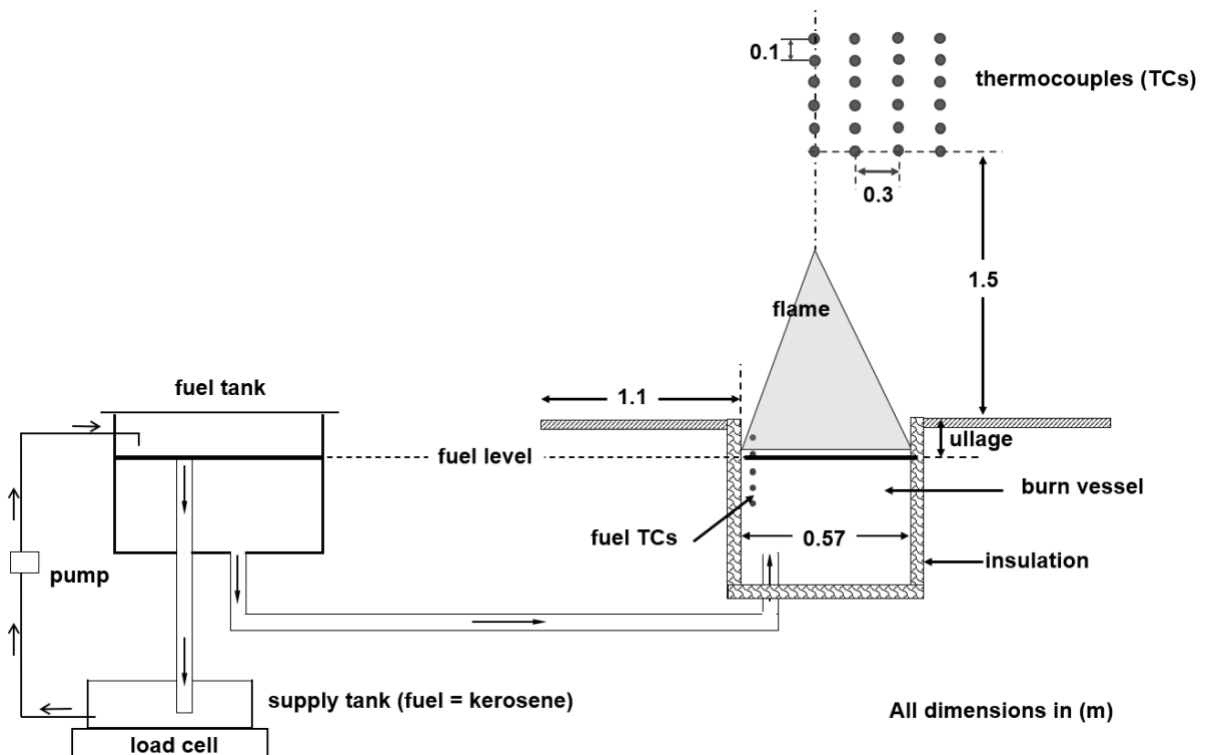


Figure 4-1 - Meso-scale kerosene pool fire setup

4.2 Results

The meso-scale experiments confirm the existence of an ullage to diameter ratio where the fire has enhanced burning, and that it is again in the Stage II region ($U/D \sim 0.5$ to 0.75) as was seen for the small-scale gas and methanol fires. Specifically, it is seen that a fire with an ullage to diameter ratio of $0.75D$ has a comparable mass loss rate to a pool fire, and an increased plume temperature compared to all other ullages. Together these results indicate that this ullage allows greater radiative heating of the fuel and increased oxygen penetration into the pit leading to enhanced combustion. While the nature of the pit material prevented an examination of the anchoring location of the fire, it is assumed to behave similarly to what is seen at the small-scale as it agrees with those trends in temperature profiles. This has positive implications for the larger goal of solid waste disposal with open-air pit fires, and that certain pit shapes can burn waste faster and, in this way, reduce the hazard to people by reducing the exposure time.

4.2.1 Mass Loss Rate

A variety of literature exists for liquid pit fires at the small-scale (up to a 20 cm diameter) and this data shows that at ullages greater than $0.5D$ the mass loss is comparable or greater than that of the $0D$ ullage case. The mass flux data from these experiments are compared to small-scale work on the effects of ullage on flame behavior done by Shi et al. [28] with methanol and Kung et al. [29] with heptane in Figure 4-2.

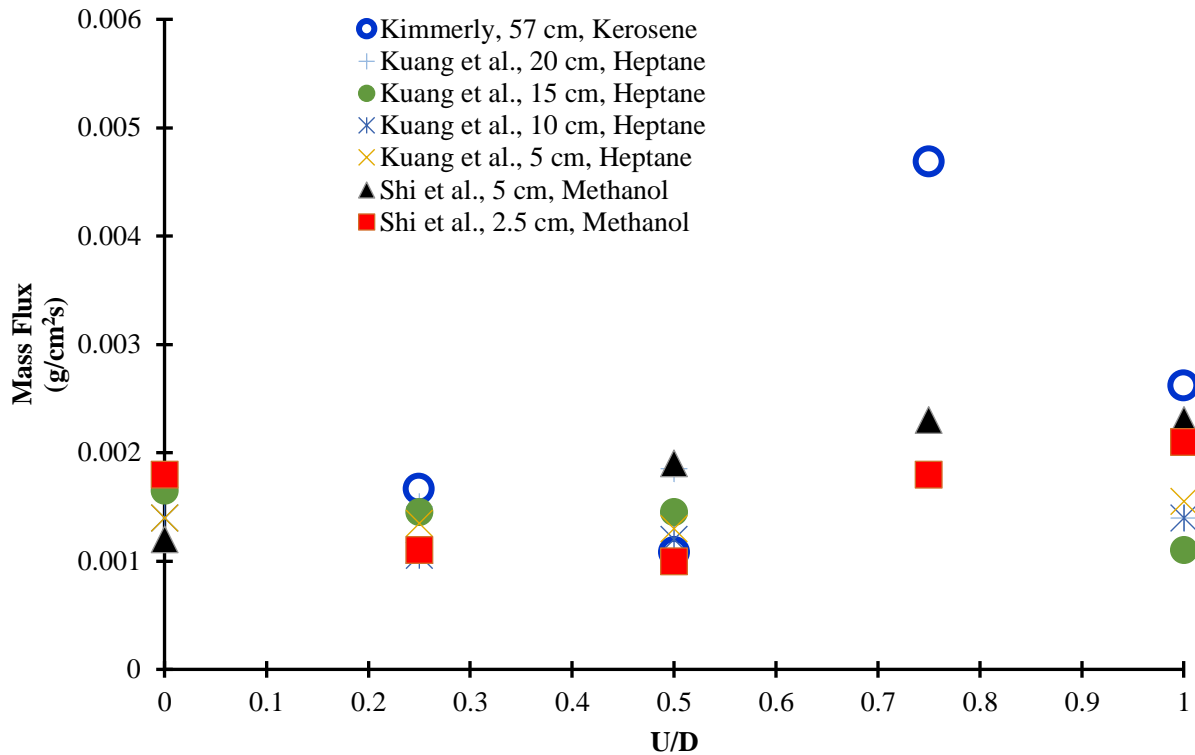


Figure 4-2 - Mass flux rates for meso-scale and small-scale pool fires in pit geometries with varying ullage.

The mass flux values in Figure 4-2 is converted to burning rate in mm/min and compared to the values from Drysdale [69] for tractor kerosene at a range of diameters in Figure 4-3. There is some difference in values that is expected because the Drysdale data is from tractor kerosene while the meso-scale data is from heating kerosene and they each have different additives. The 0.75D ullage is falls on the curve from the Drysdale data, but the 0.25D ullage is below the 0D curve. The flame height is found from the video and a defined pixel to m ratio, specifically this is the flame height above the ground as the anchoring location within the pit cannot be verified from the video. Then when comparing the flame height data from Drysdale in Figure 4-4, the 0D ullage case aligns with that found in Drysdale but the 0.75D ullage case has a smaller flame

height despite the same mass flux. This difference can be attributed to an altered flame shape like that seen in Figures 1-3 and 1-4, so a cylindrical shaped flame that is wider but shorter than that seen for a pool fire. This flame shape is due to the increased oxygen penetration into the pit at higher ullages (like seen in Chapter 3 for small-scale fires) which leads to more premixing and thus reduced flame necking. From both the burning rate and the non-dimensional flame height, we can see that increase the ullage leads to a decrease in flame height but increasing ullage causes a decrease in burning rate until the critical ullage of $0.75D$ is reached where there is a sharp increase in burning rate followed by a decrease in burning rate at $1D$. These two results combine to describe a flame that is vertically shorter but is wider giving a cylindrical shape that has a larger reaction surface area and thus consumes more fuel.

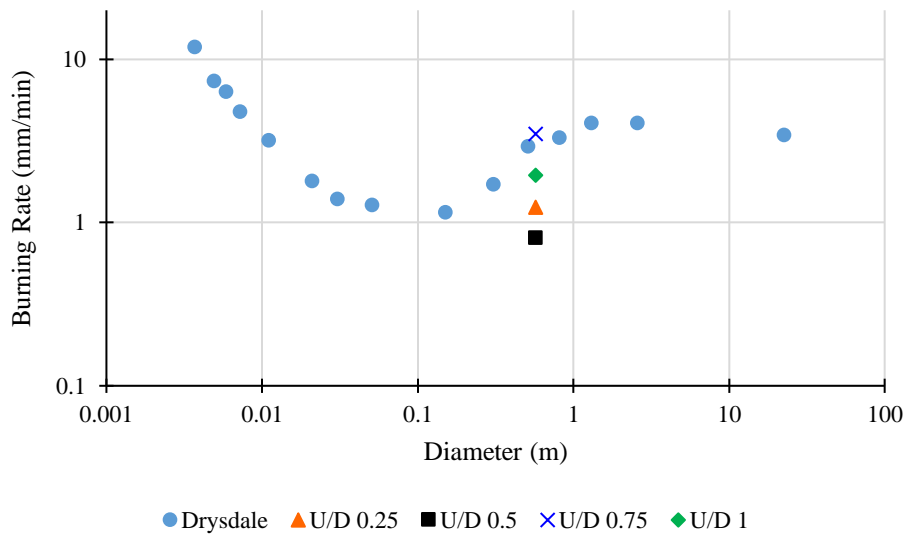


Figure 4-3 Burning rate data from Drysdale [69] with ullage cases from Figure 4-2.

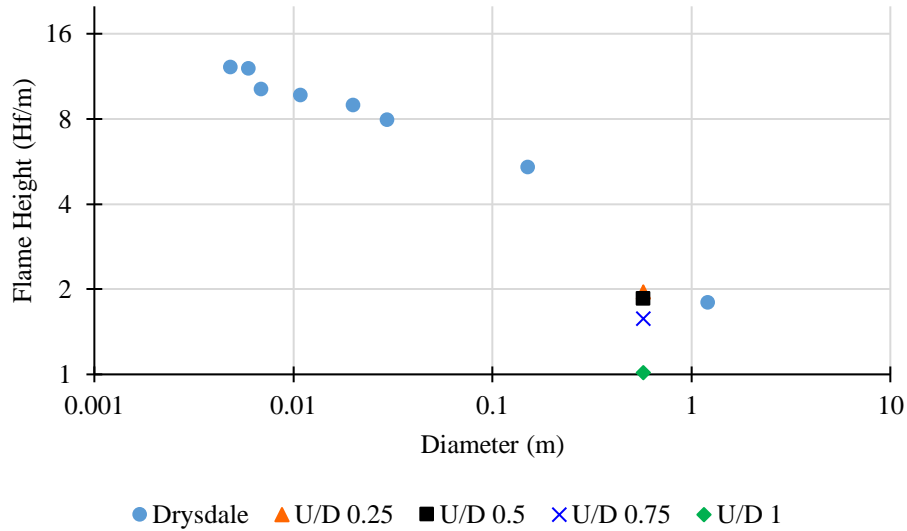


Figure 4-4 Non-dimensionalized flame height data from Drysdale [69] with meso-scale ullage cases.

4.2.2 Flame Height

Shi et al. examined flame behavior for methanol pool fires with ullages of 0.25D, 0.5D, and 1D (top Figure 4-5). They found that the flame tip opened-up along the centerline and closed in a cycle starting at 0.25D ullage. For the other two cases, vortex shedding, and flame oscillation features are clearly observed and indicate enhanced premixing. Since the burner is not transparent, the flame anchoring location could not be experimentally determined. The vertical line in the photograph at $t = 50$ ms is equal to the diameter of the burner. For the 0.25D case, the maximum flame height equals the burner diameter and the maximum flame height for the 0.5D and 1D cases significantly increases.

When comparing Shi et al.'s results to that of the meso-scale kerosene fires, the flame tip opening is not seen, and the average flame height decreases as the ullage increases. This difference in behavior between the small-scale and meso-scale is due to the onset of turbulence at the larger

diameter. This increased turbulence when combined with the increased partial premixing leads to the wide cylindrical flames that Shi et al. saw in their meso-scale experiments.

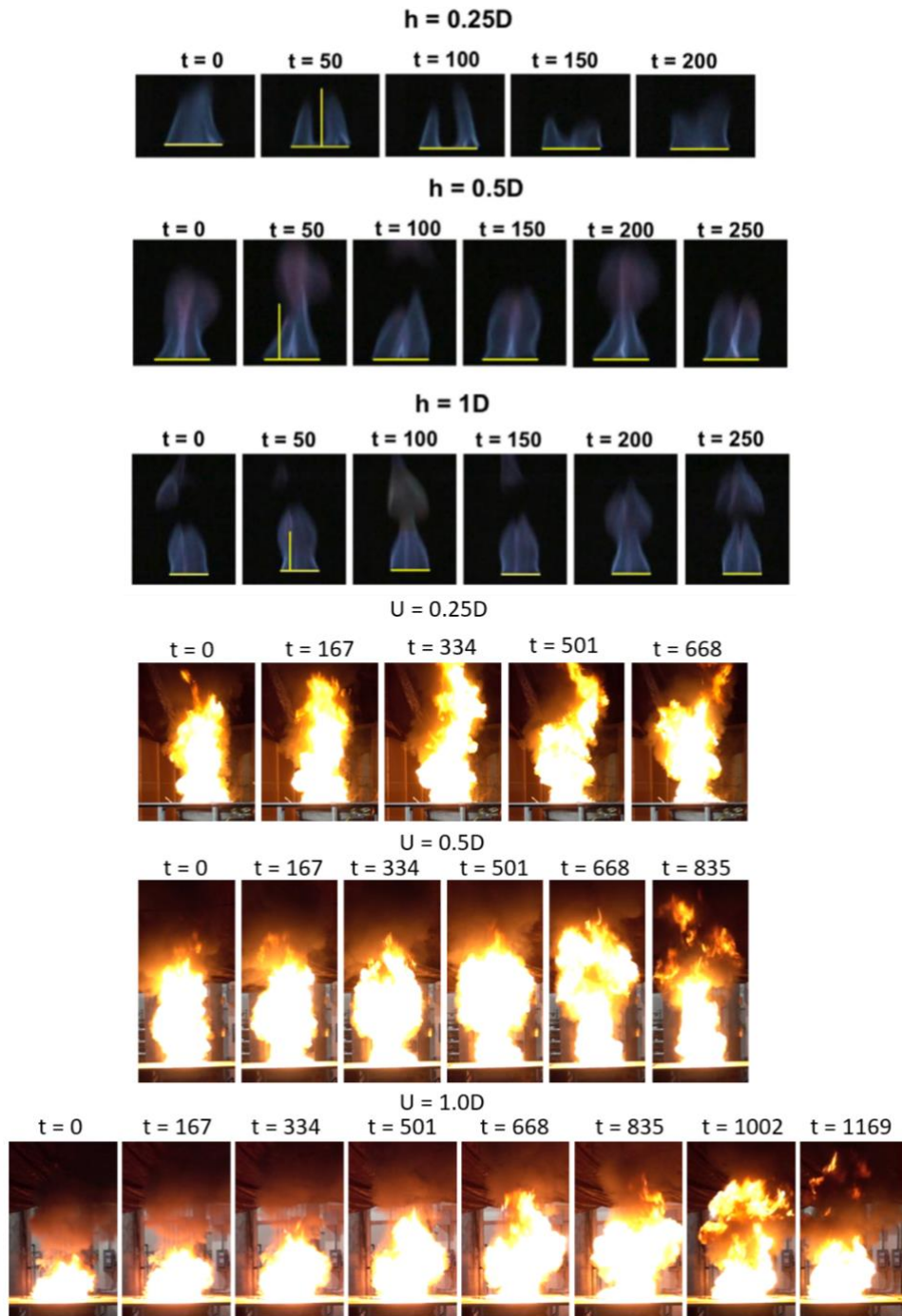


Figure 4-5 – Flame heights over time for small-scale (times in milliseconds) [28] and meso-scale (times in seconds) pool fires in pit geometries with varying ullage.

4.2.3 Centerline and Radial Temperature Profiles

The plume temperature profiles are examined both on the centerline and radially like they were for the small-scale experiments. The thermocouple tree is located 1.5 m above the ground/opening of the pit for all ullages tested. The tree, see Figure 4-6, consists of four thermocouples with a 0.3 m spacing at three elevations (1.6, 1.8 and 2 m from the ground) for radial measurements, and six thermocouples with 0.1 m spacing for the centerline measurements. Additionally, there are six thermocouples with 1 cm spacing located inside the pit such that lowest thermocouple is in the kerosene, the next lowest is at the liquid level, and the remaining four thermocouples are in the space above the liquid level.

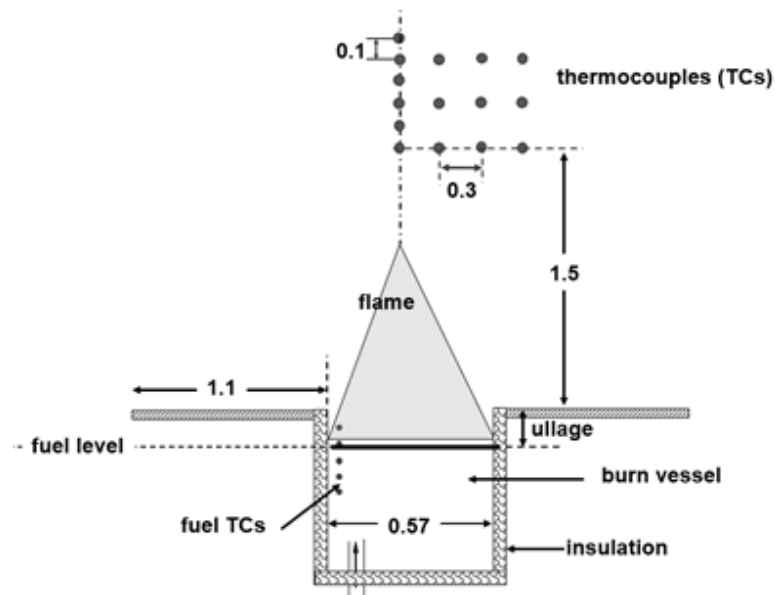


Figure 4-6 Thermocouple tree location in reference to the pit

For the centerline plume temperatures, a similar trend to that seen at the small-scale is seen here, with increasing ullage leading to an increase in temperature until a certain ullage is reached and then increasing ullage leads to a decrease in temperature. For the small-scale, increasing ullage led to decreasing temperatures until a certain ullage is reached and then increasing ullage leads to increasing temperature. The switch in behavior occurs for $U/D = 0.75$

for both small-scale and meso-scale. This difference in behavior between the small-scale and meso-scale is attributed to the shift from a gaseous fuel to a liquid fuel (and the increasing ullage allowing radiative heat in the pit to evaporate the fuel more quickly as more of the pit wall is exposed to the flame), and the transition to turbulent flames from laminar flames at the meso-scale.

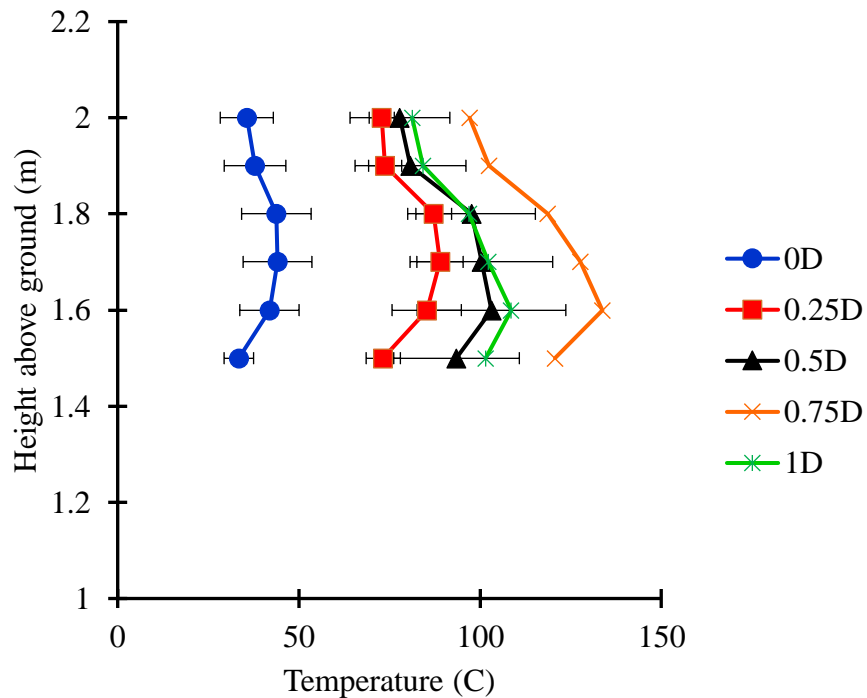


Figure 4-7 Centerline plume temperatures for meso-scale (57.3 cm diameter) kerosene pool fires.

When the radial temperature profiles are considered, the same trend seen for the centerline is seen here. Additionally, the plume has a less Gaussian profile at $U/D = 0.75$, with higher temperatures near the centerline. A higher plume temperature reflects more efficient combustion, indicating that an ullage of 0.75 times the diameter enhances the burning.

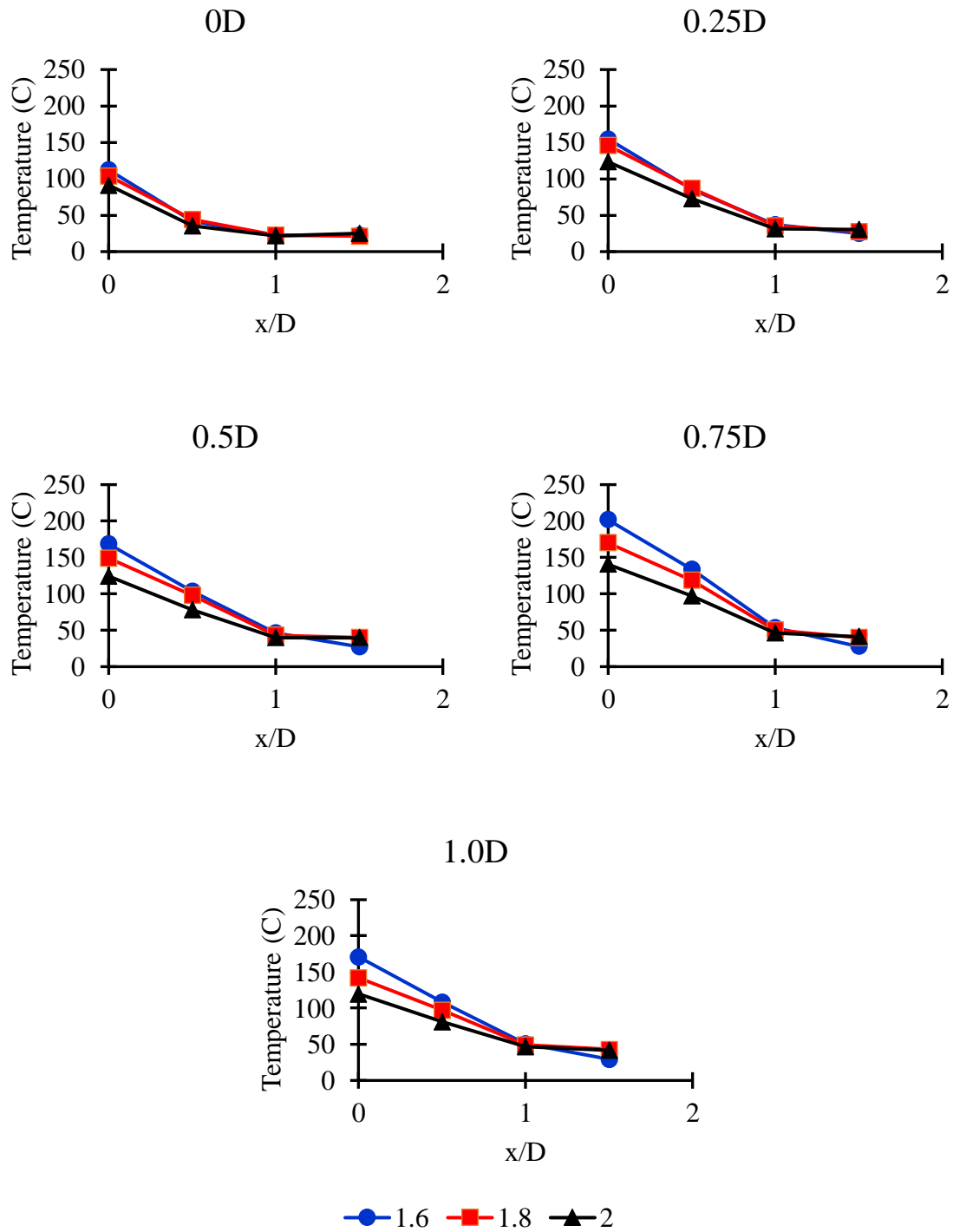


Figure 4-8 Radial plume temperatures for meso-scale experiments at 1.6, 1.8, and 2.0 meters above the “ground” for several ullages.

As was previously discussed in the small-scale experiments, an increase in average plume temperature at a certain ullage can be due to either an increased flame temperature or a decrease in air entrainment. It was shown that the increase seen at the small-scale was due to an increase in flame temperature which is an indicator of increased combustion efficiency. This is also seen at the meso-scale where the increase in mass loss rate occurs when the increase in plume temperatures does, indicating that at an ullage of $0.75D$ burning is enhanced leading to increased mass loss and increased flame temperatures. The increased slope of the radial profile can also be linked to an increase in flame temperature with an increase in air entrainment, the combination leading to a higher centerline temperature with cooler radial temperatures due to radial air entrainment into the plume.

4.2.4 Flame Height

The flame height is considered to see if similar trends exist to that seen at the small-scale. The average flame height was found from analyzing the videos of each fire with some image processing code in MATLAB. They are then compared to Heskestad's [70] flame height correlation, using the measured heat flux, for the centerline plume temperatures. Despite the difference in mass flux which in turn leads to the variation in the calculated flame heights, the measured flame height is very consistent for all the ullages. This could be because the measured flame height doesn't account for how much flame is inside the cavity and as such can't be seen on the film or because the presence of an ullage leads to less variation in flame height than expected by changes in mass flux. However, the consistent flame height implies that any increase in plume temperature is not due to the flame being closer to the thermocouple tree but a hotter flame. The difference between the Heskestad correlation and the observed values at $0.75D$ is due the reduced flame necking and thus different flame shape from that assumed by Heskestad.

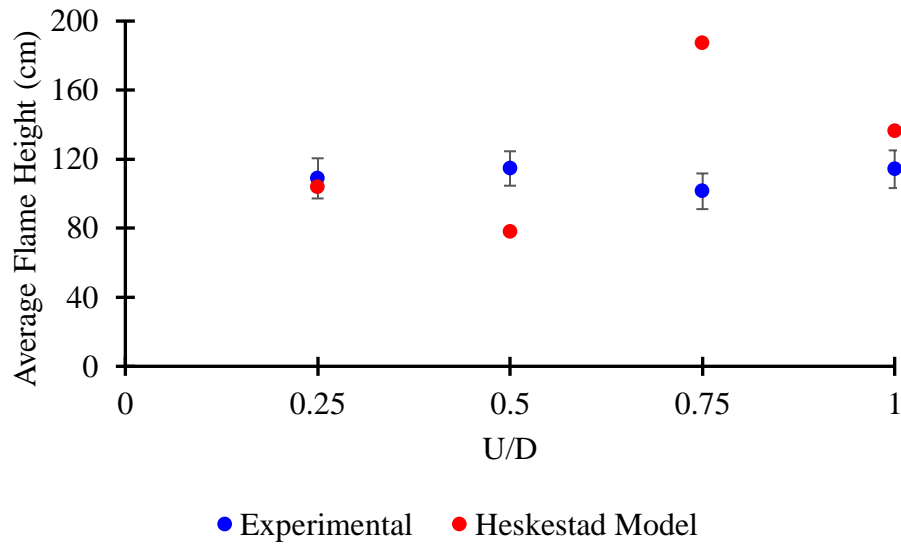


Figure 4-9 Flame height for ullage

4.3 Comparison to 1-D model

The average temperature in the plume is compared to the average temperature from the model in figure 4-8 and the trend is similar but shows different ullages for the maximum temperature. In the experimental work, the temperature increases from 0.25D to 0.75D before decreasing at 1D, where as the model shows the highest average temperature at 0.5D with a decrease after this.

This offset between the model and the experimental data can be attributed to the simplified radiation model and the assumptions of the mass flux equation in the model. The mass flux equation assumes a fixed radiative fraction of the heat release rate, and a constant view factor between the fuel and the flame. It does not account for the radiative feedback from the pit walls to the fuel which did occur in the experiment because the steel drum got hot enough to glow red. Figure 4-10 shows that the model always over predicts the average temperature and shows an increase in temperature at 0.5D while the experiments show this increase at 0.75D. However, the model does capture the trend so it can be used for the design of future experiments.

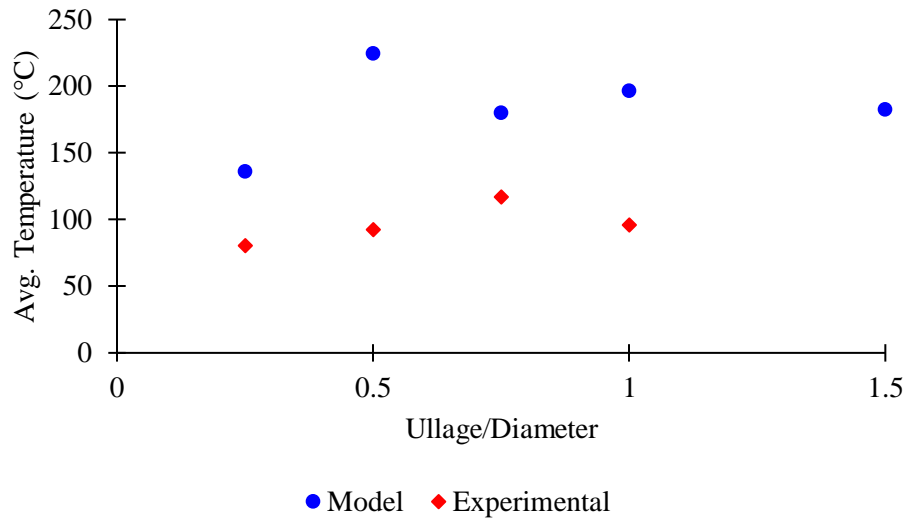


Figure 4-10 Average Pit Temperature for Meso Scale Experiments and Modelling

5 Conclusions and Future Work

The original motivation for this thesis was to explore simple ways to enhance burning that can be applied to the issue of open-air waste fires in impoverished or remote areas where most approaches are not feasible. A search of the existing literature reveals the use of burn pits as a common fire control method for waste fires and the influence of ullage of fire behavior offers a way to enhance burning. Further investigation into the specific effects of ullage on fire behavior was needed.

First, several small-scale experiments were conducted on gas diffusion fires, and the mechanics behind the flame shape and anchoring location seen at certain ullages is elucidated. Notably, four stages of flame behavior as a function of ullage to diameter ratio were defined and supported with experimental evidence. Stage II flames demonstrated enhanced burning with

reduced CO to CO₂ production. From these experiments, it appears that certain ullage to diameter ratios do lead to enhanced burning and an optimal pit geometry exists at the small-scale.

However, a small gas fire is not a large burn pit so further work with condensed fuels and at a larger scale was needed. This led to the development of a meso-scale ($1\text{ m} > \text{diameter} > 50\text{ cm}$) experiment with a liquid fuel. The twin-peak flame shape did not appear at the meso-scale, but enhancements were still seen, indicating that while the altered air flow might not be strong enough to change the flame shape it was sufficient to introduce more oxygen into the cavity at certain ullages. Most notably, in a 57 cm diameter cavity an ullage to diameter ratio has the same mass flux of fuel as a pool fire; therefore, a burn pit of this geometry would provide thermal protection and fire control without reducing the efficiency of the fire. These results support the hypothesis that certain ullage to diameter ratios enhance burning and that there exists an optimal burn pit shape.

Finally, a one-zone model was developed to allow a parameter study to be conducted and guide the design of future experiments. This is necessary given the time and cost investment necessary for large-scale testing ($\text{diameter} \geq 1\text{ m}$). The one-zone model was then compared to the experimental results to determine its usefulness.

For the small-scale experiments, the 9 cm diameter circular pit results are used. The model's temperature profiles and pressure profiles are used to compare against the plume temperature and frequency trends across a range of ullage to diameter ratios. Figure 5-1 compares the pit temperatures for a 9 cm diameter to the experimental results for a gas flow rate of 10 g/min.

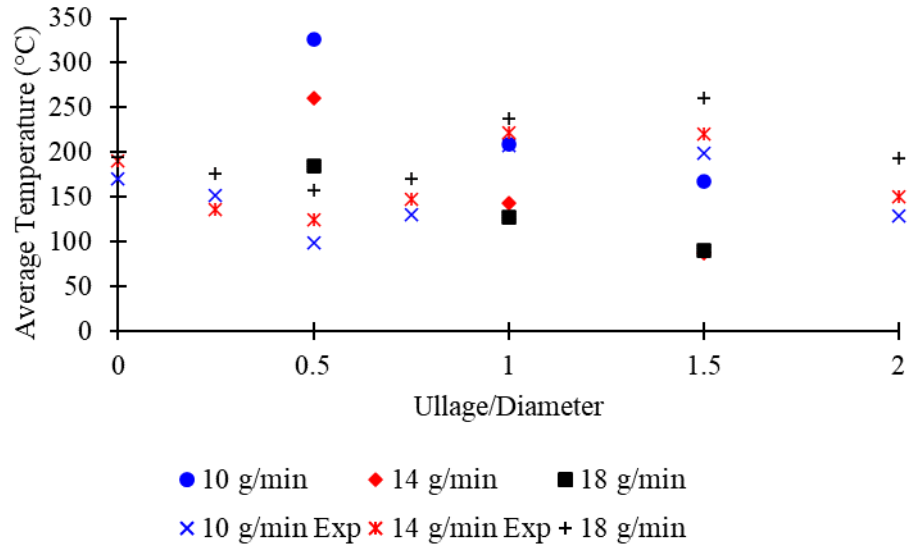


Figure 5-1 – Comparison of model and experimental temperature results for a 9 cm diameter methane pit fire

We see a similar trend of increasing ullage and decreasing temperatures. Still, unlike the experimental results, we do not see a reversal of this trend (i.e., increasing ullage and increasing temperature) after 0.5D. Additionally, the frequency is determined by examining pressure at the top of the pit and noticing the peaks and lows. The model mimics the flame's pulsation using conditionals on the flow into the pit and a critical oxygen limit.

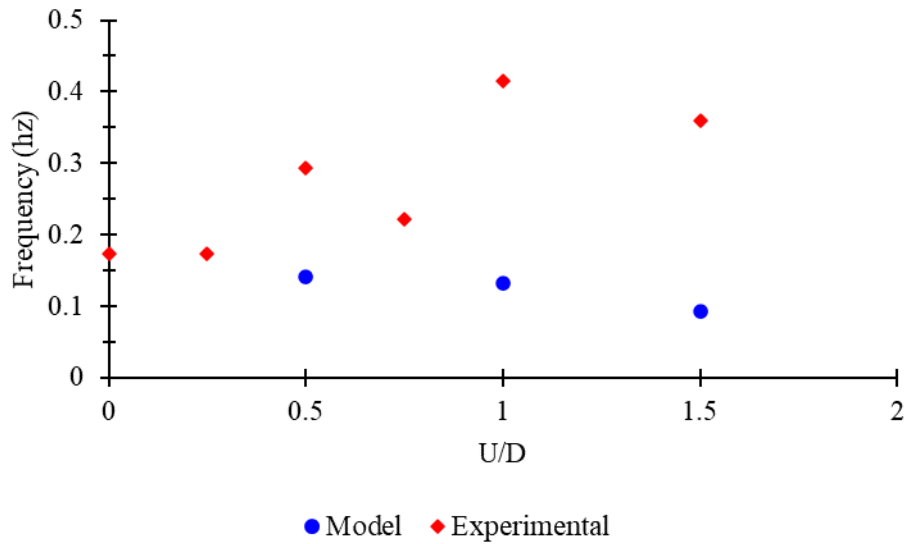


Figure 5-2 – Comparison of model and experimental results frequency results for a 9 cm diameter 10 g/min methane pit fire

The one-zone model was found to be a good starting point for modeling the altered air flow in pit fires, but more work is needed to refine its accuracy if it is to be a useful tool in designing future experiments.

Overall, this thesis provides further investigation into the effects of ullage on fires and indicates that an ullage to diameter ratio of 0.75 has a burning rate equivalent to that of a pool fire while offering increased thermal protection when compared to the pool fire. This has good implications for the development of a simple open-air pit fire for solid waste disposal that reduces the hazards inherent in these fires. While it is acknowledged that this pit geometry which enhances burning is highly simplified, for instance holes in soil rarely have perfectly smooth walls, the idea that altering the shape of a burn pit can lead to burning the same amount of waste faster is a powerful one. A simple pit shape cannot be misused, in that it can't make the fire more hazardous, and it isn't a tool that can be repurposed. This issue of repurposing safety technology is clearly illustrated by the EPA's "clean cookstove" project. In this work, the EPA developed an advanced

cookstove that greatly reduced the hazardous emissions typically associated with open flame cooking fires in impoverished homes. However, despite the clear benefits to personal health offered by adopting this new technology the actual widespread adoption of these devices is quite low [71]. Several factors contribute to this limited usage, namely ability and motivation. It takes time to learn how to use any new technology and if the time commitment is seen to be too high this will discourage adoption. Additionally, the benefits of a “cleaner” cookstove are very long-term and thus difficult to grasp for some. If an individual has more pressing short-term needs that the new cookstove could address, for instance selling it for scrap metal and using the profits to purchase needed food, then they are likely to prioritize these short-term benefits over the long-term health benefits. In this way, simply changing a burn pit shape is a better starting solution than developing some small-scale incinerator technology which could be repurposed to address other concerns the user might have. The altered geometry requires very little new knowledge to implement and requires no additional materials which could be repurposed by users. Furthermore, the altered pit shape offers both short- and long-term benefits. In the short term, the altered shape allows more fuel to be burnt faster allowing the user to devote that time to other tasks. In the long term, by burning the same amount of waste faster the total exposure time to the smoke from these fires is reduced and thus offers long-term health benefits by reducing total personal exposure. To put it simply, the quantity of harmful products might not be reduced but the individual is exposed to less of them over time.

Another study of “clean” cookstove adoption by Lindgren [72] emphasizes that poverty is the largest obstacle, specifically the people who need this new technology the most are often also those least able to afford the monetary investment of purchasing this technology. In this way, an

altered pit shape is an excellent remedy to the burn pit issue because it requires no cost to implement. However, Lindgren points out that even when the cost of cookstoves is removed adoption of the new technology still remains low, and thus understanding the specific context and behaviors that you are seeking to change is essential. This is another appeal of the altered pit shape; it is immensely flexible in its implementation. If there is not enough space to dig a larger pit then the amount of fuel placed in the pit can be altered instead, or vice versa, to achieve the desired depth to diameter ratio. To summarize an optimum ullage to diameter ratio provides a simple, low-information, and low-cost method that is highly flexible to address different contexts while still offering an enhanced fire for waste disposal.

Further work is needed to determine if the enhancements seen with liquid fuels holds true for solid fuels and if the enhancements seen at a 57 cm diameter hold true at diameters > 1 m. Future work would consist of larger-scale (> 1 m) liquid fires to determine if the mass loss at $0.75D$ ullages remains comparable to pool fires. Then the fuel should be transitioned to solid fuels, starting with a homogenous fuel (e.g., PMMA, wood, polyurethane foam) and then finally moving to mixed solid fuels which mimic the types of fuels that would be in an open-air solid waste fire or burn pit. It is likely that certain fuel types (e.g. biomass, plastics, human waste) will show enhanced burning in different pit shapes and fill ratios. This would allow users to customize their pit based on the main solid waste type they are burning, and this can accommodate the seasonality of waste type (e.g. biomass from agricultural work). This is a further benefit of the flexibility of the altered pit shape solution. Additional work should be done to better understand the anchoring location and the flow field (with velocity measurements) around the pit and inside the pit. This data will help refine the understanding of heat transfer within the pit and how the thermally insulative and radiative properties of different wall materials affect the fire behavior. This can then

be used to tailor the pit design to specific soil types for different global regions. Finally, more work is needed to understand the chemistry behind the reduction in CO production for stage II flames, and to determine if this reduction is significant and if the reduction in emissions is comparable to that achieved by reducing exposure time. Even if the reduction in emission quantity is not enough to significantly impact long-term health outcomes, it can still have significant impacts on environmental impacts. Finally, additional pit shapes (e.g., elongated rectangular pit) should be explored at the large scale where the flames are fully turbulent. This investigation of different general shapes is also critical to understand the effects that the wide variety of pit shapes seen in the field (from non-straight walls, to trenches on US Army bases, to non-circular or irregularly shaped holes). This variation is also a fact of differing soil textures that can impact the ability to make different pit shapes. It is likely that a different ullage to diameter ratio offers enhancement for each pit shape, but perhaps overarching categories exist that can group several shapes together. The ultimate result of this research would be a set of pit shapes and fill levels that allow more solid waste to be burned in a shorter time, users would be advised to dig their pits as in general shapes (round, longer than wide etc.) and then told what ratio of the pit to fill up with fuel/waste. Then they would be advised to try and keep the pit filled with fuel as it burns by pushing additional fuel into it. It would be explained to users that not only do these alterations burn their waste faster but in doing so improves their long-term health by reducing the exposure time. This information is easily passed on through word of mouth and simple ratios are much easier to gauge than precise measurements, so no additional tools are needed to implement the new pit shape.

In conclusion, it is hoped that this research will be the foundation of a simple set of pit shapes and fill ratios that can be tailored to the type of waste being burned (e.g. biomass, plastics, human waste, etc.), the available space for the pit, and the soil type (e.g. looser, sandier, etc.).

Open air pit fires offer a simple method for disposing of solid waste, while allowing people to confine the fire to one desired location and be protected from the heat. By optimizing the pit shape and fill ratio (ullage to diameter), more waste can be burned in a shorter time which reduces the exposure time of people to the hazardous smoke. Additionally, this optimal shape might reduce the quantity of hazardous emissions which will reduce the environmental impact of this waste disposal method. It is hoped that this simple, low cost, low infrastructure, and easily spread concept will help those who rely on open air fires to dispose of their solid waste.

References

- [1] S. Pyne, *Fire A Brief History*. University of Washington Press, 2001.
- [2] R. C. Porter, *The Economics of Waste*. New York: Routledge, 2002. doi: 10.4324/9781936331543.

- [3] S. Strasser, *Waste and want: A social history of trash*. Macmillan, 2000.
- [4] I. A. Al-Khatib *et al.*, “Trends and problems of solid waste management in developing countries: A case study in seven Palestinian districts,” *Waste Management*, vol. 27, no. 12, pp. 1910–1919, Jan. 2007, doi: 10.1016/j.wasman.2006.11.006.
- [5] N. Seltenrich, “Incineration Versus Recycling: In Europe, A Debate Over Trash,” *Yale E360*, pp. 1–7, 2013.
- [6] C. Wiedinmyer, R. J. Yokelson, and B. K. Gullett, “Global Emissions of Trace Gases, Particulate Matter, and Hazardous Air Pollutants from Open Burning of Domestic Waste,” *Environmental Science and Technology*, vol. 48, pp. 9523–9350, 2014.
- [7] B. E. Bassey, M. O. Benka-Coker, and H. S. Aluyi, “Characterization and management of solid medical wastes in the Federal Capital Territory, Abuja Nigeria,” *African Health Sciences*, vol. 6, no. 1, pp. 59–63, 2006, doi: 10.5555/afhs.2006.6.1.58.
- [8] J. Aurell, B. K. Gullett, and D. Yamamoto, “Emissions from Open Burning of Simulated Military Waste from Forward Operating Bases,” *Environmental Science & Technology*, vol. 46, no. 20, pp. 11004–11012, Oct. 2012, doi: 10.1021/es303131k.
- [9] B. K. Gullett, W. P. Linak, A. Touati, S. J. Wasson, S. Gatica, and C. J. King, “Characterization of air emissions and residual ash from open burning of electronic wastes during simulated rudimentary recycling operations,” *Journal of Material Cycles and Waste Management*, vol. 9, no. 1, pp. 69–79, Mar. 2007, doi: 10.1007/s10163-006-0161-x.
- [10] M. Bjerregaard and H. Meekings, “Domestic and Refugee Camp Waste Management Collection and Disposal,” *Oxfam*, 2008.

- [11] P. M. Lemieux, C. C. Lutes, and D. A. Santoianni, "Emissions of organic air toxics from open burning: a comprehensive review," *Progress in Energy and Combustion Science*, vol. 30, no. 1, pp. 1–32, Jan. 2004, doi: 10.1016/j.pecs.2003.08.001.
- [12] B. K. Gullett, P. M. Lemieux, C. C. Lutes, C. K. Winterrowd, and D. L. Winters, "Emissions of PCDD/F from uncontrolled, domestic waste burning," *Chemosphere*, vol. 43, no. 4–7, pp. 721–725, May 2001, doi: 10.1016/S0045-6535(00)00425-2.
- [13] A. Hodzic, C. Wiedinmyer, D. Salcedo, and J. L. Jimenez, "Impact of Trash Burning on Air Quality in Mexico City," 2012, doi: 10.1021/es203954r.
- [14] S. Weichenthal *et al.*, "The impact of a landfill fire on ambient air quality in the north: A case study in Iqaluit, Canada," *Environmental Research*, vol. 142, pp. 46–50, Oct. 2015, doi: 10.1016/J.ENVRES.2015.06.018.
- [15] A. Singh Nagpure, A. Ramaswami, and A. Russell, "Characterizing the Spatial and Temporal Patterns of Open Burning of Municipal Solid Waste (MSW) in Indian Cities", doi: 10.1021/acs.est.5b03243.
- [16] A. Rim-Rukeh, "An Assessment of the Contribution of Municipal Solid Waste Dump Sites Fire to Atmospheric Pollution," *Open Journal of Air Pollution*, vol. 3, pp. 53–60, 2014, doi: 10.4236/ojap.2014.33006.
- [17] L. Lundin, B. Gullett, W. F. Carroll, A. Touati, S. Marklund, and H. Fiedler, "The effect of developing nations' municipal waste composition on PCDD/PCDF emissions from open burning," *Atmospheric Environment*, vol. 79, pp. 433–441, 2013, doi: 10.1016/j.atmosenv.2013.06.040.

- [18] T. Zhang *et al.*, “Emissions of unintentional persistent organic pollutants from open burning of municipal solid waste from developing countries,” *Chemosphere*, vol. 84, no. 7, pp. 994–1001, Aug. 2011, doi: 10.1016/j.chemosphere.2011.04.070.
- [19] P. M. Lemieux, C. C. Lutes, J. A. Abbott, and K. M. Aldous, “Emissions of Polychlorinated Dibenzo-p-dioxins and Polychlorinated Dibenzofurans from the Open Burning of Household Waste in Barrels,” 2000, doi: 10.1021/ES990465T.
- [20] L. W. Tian, D. Lucas, S. L. Fischer, S. C. Lee, and C. P. Koshland, “Particle and gas emissions from a simulated fire pit,” *Environmental Science & Technology*, vol. 42, no. 7, pp. 2503–2508, 2008.
- [21] B. D. Woodall, D. P. Yamamoto, B. K. Gullett, and A. Touati, “Emissions from Small-Scale Burns of Simulated Deployed U.S. Military Waste,” *Environmental Science & Technology*, vol. 46, pp. 10997–11003, 2012.
- [22] D. M. Demarini, P. M. Lemieux, J. V Ryan, L. R. Brooks, and R. W. Williams, “Mutagenicity and Chemical Analysis of Emissions from the Open Burning of Scrap Rubber Tires,” 1994.
- [23] B. D. Woodall, D. P. Yamamoto, B. K. Gullett, and A. Touati, “Emissions from Small-Scale Burns of Simulated Deployed U.S. Military Waste”, doi: 10.1021/es3021556.
- [24] K. W. Blasch, J. E. Kolivosky, and J. M. Heller, “Environmental Air Sampling Near Burn Pit and Incinerator Operations at Bagram Airfield , Afghanistan,” *Journal of Environmental Medicine*, vol. 58, no. 8S, 2016, doi: 10.1097/JOM.0000000000000792.
- [25] E. J. T. Levin *et al.*, “Biomass burning smoke aerosol properties measured during Fire Laboratory at Missoula Experiments (FLAME),” *Journal of Geophysical Research Atmospheres*, vol. 115, no. 18, pp. 1–15, 2010, doi: 10.1029/2009JD013601.

- [26] N. Wu, G. Kolb, and J. L. Torero, "Piloted Ignition of a Slick of Oil on a Water Sublayer: The Effect of Weathering," in *27th International Symposium on Combustion*, 1998, pp. 2783–2790.
- [27] X. Shi *et al.*, "Influence of ullage to cavity size ratio on in-situ burning of oil spills in ice-infested water," *Cold Regions Science and Technology*, vol. 140, pp. 5–13, Aug. 2017, doi: 10.1016/J.COLDREGIONS.2017.04.010.
- [28] X. Shi, A. K. Sahu, S. Nair, V. Raghavan, and A. S. Rangwala, "Effect of ullage on burning behavior of small-scale pool fires in a cavity," *Proceedings of the Combustion Institute*, vol. 36, no. 2, pp. 3113–3120, 2017, doi: 10.1016/j.proci.2016.06.123.
- [29] C. Kuang, L. Hu, X. Zhang, Y. Lin, and L. W. Kostiuk, "An experimental study on the burning rates of n-heptane pool fires with various lip heights in cross flow," *Combustion and Flame*, vol. 201, pp. 93–103, 2019, doi: 10.1016/j.combustflame.2018.12.011.
- [30] B. Z. Dlugogorski and M. Wilson, "Effect of Ullage on Properties of Small-Scale Pool Fires," *Developments in Chemical Engineering and Mineral Processing*, vol. 8, no. 1–2, pp. 149–166, May 2000, doi: 10.1002/apj.5500080110.
- [31] E. S. Artemenko and V. I. Blinov, "Burning of liquids in vessels with change of level," *Combustion, Explosion, and Shock Waves*, vol. 4, no. 1, pp. 69–75, 1968, doi: 10.1007/BF00843071.
- [32] Z. Gao, S. Lin, J. Ji, and M. Li, "An experimental study on combustion performance and flame spread characteristics over liquid diesel and ethanol-diesel blended fuel," *Energy*, vol. 170, pp. 349–355, 2019, doi: 10.1016/j.energy.2018.12.130.

- [33] C. Liu, L. Ding, M. Jangi, J. Ji, L. Yu, and H. Wan, "Experimental study of the effect of ullage height on flame characteristics of pool fires," *Combustion and Flame*, vol. 216, pp. 245–255, 2020, doi: 10.1016/j.combustflame.2020.03.009.
- [34] D. D. Drysdale, A. J. R. Macmillan, and D. Shilitto, "The King's Cross fire: Experimental verification of the 'Trench effect,'" *Fire Safety Journal*, vol. 18, no. 1, pp. 75–82, Jan. 1992, doi: 10.1016/0379-7112(92)90048-H.
- [35] X. Shi, P. W. Bellino, A. Simeoni, and A. S. Rangwala, "Experimental study of burning behavior of large-scale crude oil fires in ice cavities," *Fire Safety Journal*, vol. 79, pp. 91–99, Jan. 2016, doi: 10.1016/J.FIRESAF.2015.11.007.
- [36] F. Gori and S. Corasaniti, "Theoretical prediction of the soil thermal conductivity at moderately high temperatures," *Journal of Heat Transfer*, vol. 124, no. 6, pp. 1001–1008, 2002, doi: 10.1115/1.1513573.
- [37] Y. Utiskul, J. G. Quintiere, A. S. Rangwala, B. A. Ringwelski, K. Wakatsuki, and T. Naruse, "Compartment fire phenomena under limited ventilation," *Fire Safety Journal*, vol. 40, no. 4, pp. 367–390, Jun. 2005, doi: 10.1016/j.firesaf.2005.02.002.
- [38] Q. Z. He, C. H. Li, S. X. Lu, and S. S. Huang, "Experimental study of pool fire burning behaviors in ceiling vented ship cabins," in *Procedia Engineering*, 2014, vol. 71, pp. 462–469. doi: 10.1016/j.proeng.2014.04.066.
- [39] W. K. Chow and Y. Gao, "Oscillating behaviour of fire-induced air flow through a ceiling vent," *Applied Thermal Engineering*, vol. 29, no. 16, pp. 3289–3298, Nov. 2009, doi: 10.1016/j.applthermaleng.2009.05.001.
- [40] C.-F. Than and B. J. Savelonis, "Modeling Fire Behavior in an Enclosure with a Ceiling Vent," 1993.

- [41] X. Chen and S. X. Lu, "On the Analysis of Flame Pulsation and Fire Induced Vent Flow Oscillatory Behaviors in Confined Enclosures with Horizontal Openings," 2018. doi: 10.1016/j.proeng.2017.12.131.
- [42] L. Kerrison, E. R. Galea, and M. K. Patel, "A Two-dimensional Numerical Investigation of the Oscillatory Flow Behaviour in Rectangular Fire Compartments with a Single Horizontal Ceiling Vent," *Fire Safety Journal*, 1998, doi: 10.1016/S0379-7112(97)00042-8.
- [43] V. Kimmerly and A. S. Rangwala, "Laboratory-scale investigation of air entrainment in burn pits used for waste disposal," *Fuel*, 2020.
- [44] G. Magnus, "Tests on combustion velocity of liquid fuels and temperature distribution in flames and beneath surface of the burning liquid," in *First International Symposium on the Use of Models in Fire Research*, 1961, pp. 76–90.
- [45] D. D. Drysdale, A. J. R. Macmillan, and D. Shilitto, "The King's Cross Fire: Experimental Verification of the 'Trench Effect,'" *Fire Safety Journal*, vol. 18, pp. 75–82, 1992.
- [46] B. M. Cetegen and T. A. Ahmed, "Experiments on the periodic instability of buoyant plumes and pool fires," *Combustion and Flame*, vol. 93, no. 1–2, pp. 157–184, Apr. 1993, doi: 10.1016/0010-2180(93)90090-P.
- [47] A. Hamins, J. C. Yang, and T. Kashiwagi, "An experimental investigation of the pulsation frequency of flames," *Symposium (International) on Combustion*, vol. 24, no. 1, pp. 1695–1702, Jan. 1992, doi: 10.1016/S0082-0784(06)80198-0.
- [48] E. J. Weckman and A. Sobiesiak, "The oscillatory behaviour of medium-scale pool fires," *Symposium (International) on Combustion*, vol. 22, no. 1, pp. 1299–1310, Jan. 1989, doi: 10.1016/S0082-0784(89)80141-9.

- [49] W. M. G. Malalasekera, H. K. Versteeg, and K. Gilchrist, "A review of research and an experimental study on the pulsation of buoyant diffusion flames and pool fires," *Fire and Materials*, vol. 20, no. 6, pp. 261–271, 1996, doi: 10.1002/(SICI)1099-1018(199611)20:6<261::AID-FAM578>3.0.CO;2-M.
- [50] S. Ishizuka, "An experimental study on the opening of laminar diffusion flame tips," *Symposium (International) on Combustion*, vol. 19, no. 1, pp. 319–326, 1982, doi: 10.1016/S0082-0784(82)80203-8.
- [51] D. L. Urban, Z. G. Yuan, P. B. Sunderland, K. C. Lin, Z. Dai, and G. M. Faeth, "Smoke-point properties of non-buoyant round laminar jet diffusion flames," *Proceedings of the Combustion Institute*, vol. 28, no. 2, pp. 1965–1972, 2000, doi: 10.1016/s0082-0784(00)80602-5.
- [52] S. Ishizuka and Y. Sakai, "Structure and tip-opening of laminar diffusion flames," *Symposium (International) on Combustion*, vol. 21, no. 1, pp. 1821–1828, 1988, doi: 10.1016/S0082-0784(88)80416-8.
- [53] M. Mizomoto, Y. Asaka, S. Ikai, and C. K. Law, "Effects of preferential diffusion on the burning intensity of curved flames," *Symposium (International) on Combustion*, vol. 20, no. 1, pp. 1933–1939, 1985, doi: 10.1016/S0082-0784(85)80692-5.
- [54] Y. Mizobuchi, T. Nambu, and T. Takeno, "Numerical study of tip opening of hydrogen/air Bunsen flame," *Proceedings of the Combustion Institute*, vol. 37, no. 2, pp. 1775–1781, 2019, doi: 10.1016/j.proci.2018.05.025.
- [55] X. Shi, A. Kumar Sahu, S. Nair, V. Raghavan, and A. S. Rangwala, "Effect of ullage on burning behavior of small-scale pool fires in a cavity," *Proceedings of the Combustion Institute*, vol. 36, pp. 3113–3120, 2016, doi: 10.1016/j.proci.2016.06.123.

- [56] B. Ponizy, A. Claverie, and B. Veyssi re, “Tulip flame - the mechanism of flame front inversion,” *Combustion and Flame*, vol. 161, no. 12, pp. 3051–3062, 2014, doi: 10.1016/j.combustflame.2014.06.001.
- [57] C. Clanet and G. Searby, “On the ‘Tulip flame’ phenomenon,” *Combustion and Flame*, vol. 105, no. 1–2, pp. 225–238, 1996, doi: 10.1016/0010-2180(95)00195-6.
- [58] A. Hariharan and I. Wichman, “Premixed tulip shaped flames in a rectangular combustion chamber,” *8th US National Combustion Meeting 2013*, vol. 3, pp. 2056–2063, 2013.
- [59] U. Swami, A. Ambekar, D. Gondge, S. Sreedhara, and A. Chowdhury, “Burn rate characterization of desensitized isopropyl nitrate blends,” *Combustion and Flame*, vol. 190, no. May 2019, pp. 454–466, 2018, doi: 10.1016/j.combustflame.2017.11.026.
- [60] Y. Zhang, M. Kim, P. B. Sunderland, J. G. Quintiere, and J. de Ris, “A burner to emulate condensed phase fuels,” *Experimental Thermal and Fluid Science*, vol. 73, pp. 87–93, 2016, doi: 10.1016/j.expthermflusci.2015.09.025.
- [61] T. Tanaka, “SFPE Handbook of Fire Protection Engineering,” 5th ed., M. J. Hurley, D. Gottuk, J. R. Hall Jr., K. Harada, E. Kuligowski, M. Puchovsky, J. L. Torero, J. M. Watts Jr., and C. Wieczorek, Eds. Springer Science+Business, 2016, pp. 455–485.
- [62] J. G. Quintiere, *Fundamentals of fire phenomena*. University of Maryland, Department of Fire Protection Engineering., 2006.
- [63] J. G. Quintiere and A. S. Rangwala, “A theory for flame extinction based on flame temperature,” *Fire and Materials*, vol. 28, no. 5, pp. 387–402, 2004, doi: 10.1002/fam.835.
- [64] J. G. Quintiere, *Principles of FIRE BEHAVIOR*, 2nd ed. Boca Raton: CRC Press, 2016. doi: 10.1201/9781315369655.

- [65] E. E. Zukoski, T. Kubota, and B. Cetegen, “Entrainment in fire plumes,” *Fire Safety Journal*, vol. 3, no. 3, pp. 107–121, Feb. 1981, doi: 10.1016/0379-7112(81)90037-0.
- [66] B. M. Cetegen, E. E. Zukoski, and T. Kubota, “Entrainment and Flame Geometry of Fire Plumes,” Gaithersburg, MD, 1982.
- [67] A. Melling, “Tracer particles and seeding for particle image velocimetry,” *Measurement Science and Technology*, vol. 8, no. 12, pp. 1406–1416, 1997, doi: 10.1088/0957-0233/8/12/005.
- [68] M. I. Hassan, K. Kuwana, K. Saito, and F. Wang, “Flow structure of a fixed-frame type fire whirl,” *Fire Safety Science*, pp. 951–962, 2005, doi: 10.3801/IAFSS.FSS.8-951.
- [69] D. Drysdale, *An Introduction to Fire Dynamics*. John Wiley & Sons, 2011.
- [70] G. Heskestad, “Engineering relations for fire plumes,” *Fire Safety Journal*, vol. 7, no. 1, pp. 25–32, Jan. 1984, doi: 10.1016/0379-7112(84)90005-5.
- [71] M. Jürisoo, F. Lambe, and M. Osborne, “Beyond buying: The application of service design methodology to understand adoption of clean cookstoves in Kenya and Zambia,” *Energy Research & Social Science*, vol. 39, pp. 164–176, May 2018, doi: 10.1016/j.erss.2017.11.023.
- [72] S. A. Lindgren, “Clean cooking for all? A critical review of behavior, stakeholder engagement, and adoption for the global diffusion of improved cookstoves,” *Energy Research & Social Science*, vol. 68, p. 101539, Oct. 2020, doi: 10.1016/j.erss.2020.101539.

Annex A – Model Code Gas Burner

```
In[1]:= $TextStyle = {FontFamily -> "Times", FontSize -> 14};
```

Model 1.0: Pit fire with gaseous fuel – No coupling between mass transfer and heat transfer

```
In[87]:= Clear[t]

Hcox = 13 000;          (*Heat of Combustion of per kg of O2 consumed kJ/kg*)
omega = 1.4;
g = 9.81;              (*acceleration due to gravity m/s2*)
dout = 1.2;            (*density of air at Ambient Temp kg/m3 *)
Tout = 293;           (*Ambient Temp K *)
(*Tv=350;              (*Boiling point of heptane in K***)
Tf = 1300 + 273;
(*Flame temperature at extinction also called critical flame temperature*)
oxout = .233;          (*Ambient Oxygen concentration in g/g*)
cp = 1.0;              (*Specific heat of air kJ/kgK*)
cd = .66;              (*Orifice Discharge Coefficient*)
diameter = 0.09 (* Diameter of pit m*)
height = 1*diameter;  (* Height of pit m*)
(*CHANGE height to get different Ullage ratios*)

V = (diameter)^2 *  $\frac{\text{Pi}}{4}$  * height; (*Volume of Pit*)

As = Pi * diameter * height; (*Area of walls*)

A0 = (diameter)^2 *  $\frac{\text{Pi}}{4}$ ; (*Area of top vent m2*)

Af = (diameter)^2 *  $\frac{\text{Pi}}{4}$ ; (*Area of Fuel m2*)
```

```

F = .8;                (*A kind of view factor used when calculating Qe*)
deltaHc = 45;          (*Heat of combustion of fuel kJ/g*)
sigma = 5.67 * 10 ^(-11); (*Stefan Boltzmann constant kW/m2K4*)
mfree = 0.17 / Af      (*g/s m2*) (*Note experiments were for example at 10,
14 and 18 g/min = 0.17, 0.23 and 0.3 g/s of methane air flow *)
hc = 20;              (* Convective heat transfer coefficient W/m2 K*)
r = deltaHc * 1000 / Hcox; (* Stoichiometric Co eff *)
BF = 1; (*Blocking factor- basically = Ln(B+1)/B,
where B is the mass transfer number for the fuel*)
alpha = 0;

(*Step functions to set in-flow and out-flow conditions*)
step[a_] := If[a > 0., 1, 0]
ox[o_] := If[o ≤ 0, 0, 1]
air[c_] := If[c ≤ 0, 1, 0]

poto[d_] := If[d > 35, 0, 1]
(*this just sets an upper limit such that if mf cannot exceed an arbitrarily
chosen 35 g/s. It will not be used now but will be useful when mass
transfer is coupled to heat transfer for a liquid fuel in the pit*)

mdot[dpx_, Tx_] := A0 cd Sqrt[2 dout Abs[dpx]] (step[dpx] * Sqrt[Tout / Tx] - step[-dpx])
(*Solves for vent flow in and out of the top vent*)
dpt[t_] := dpb[t] + dout (1 - Tout / T[t]) g height (*pressure at the top of cavity
is a function of T[t] and pressure at the bottom of cavity (dpb[t]*)
Yox[t_] := Yox1[t] * T[t]
T[t_] := 1 / Tinv[t]
h[t_] := Sqrt[19.1 * .01 * 950 * 272 / (t + 1)] * 0.001 (*kW/m2K*)

mt[t_] := mdot[dpt[t], T[t]] (*kg/s*) (*mass flow through top vent *)
mb[t_] := alpha mdot[dpb[t], T[t]] (*kg/s*) (*mass flow through the bottom vent =
0 applicable for pit - set by making alpha = 0*)

mf[t_] := ((1 - Exp[-t/10])**mfree * (Yox[t]) / 0.233 (( F * sigma * T[t]^4) / L )) (*g/s m2*)

mfcrit[t_] := ((1 - Exp[-t/10])**mfree * (Yoxcrit[t]) / 0.233 (( F * sigma * T[t]^4) / L )) (*g/s m2*)

(*The (1 - Exp[-t/10]) is the rampup time. It maybe
needed if the model does not start smoothly. The F * sigma * T[t]^4 / L
is a radiative loss with F being a view factor.*)

```

```

Yoxcrit[t_] := 0.1294304768436963` - 0.00008230253288356285` T[t]
(* This is a limiting condition of oxygen vs. temperature in the pit. It reduces
the concentration of oxygen as the temperature of the pit increases. The
other way of doing this is solving the gas phase chemical reaction using
a one step reaction model using constants from Westbrook and Dryer. The
limiting reactant is oxygen which is solved for in the equations*)

```

```

x[t_] := step[Yoxcrit[t]] * Yoxcrit[t]
Qdot[t_] := ox[Yox[t] - x[t]] * potof[mf[t]] * mf[t] * deltaHc * Af +
  air[Yox[t]] * (-step[-dpb[t]] * Hcox * 0.233 * mb[t] - step[-dpt[t]] * Hcox * 0.233 * mt[t])
E3[t_] := (step[dpb[t]] * T[t] + step[-dpb[t]] Tout) mb[t] cp
E4[t_] := (step[dpt[t]] * T[t] + step[-dpt[t]] Tout) mt[t] cp

oxt[t_] := (step[dpt[t]] * Yox[t] + step[-dpt[t]] oxout) mt[t]
oxb[t_] := (step[dpb[t]] * Yox[t] + step[-dpb[t]] oxout) mb[t]

temprhs[t_] := (-mt[t] - mb[t] + mf[t] * 0.001 * Af) / (dout Tout V)
prhs[t_] := (Qdot[t] - h[t] As (T[t] - Tout) - E3[t] - E4[t]) (omega - 1) / V

```

```

oxrhs[t_] := (-Qdot[t] / Hcox - oxt[t] - oxb[t]) / (dout Tout V)
endtime = 600;

```

```

SetOptions[ListPlot, ImageSize -> 350, PlotStyle -> GrayLevel[0],
  Ticks -> {Automatic}, Frame -> False, GridLines -> None];

```

```

SetOptions[Plot, ImageSize -> 350,
  PlotStyle -> GrayLevel[0], Frame -> False, GridLines -> None];

```

```
Out[97]= 0.09
```

```
Out[106]= 26.7223
```

```

In[134]:= sol = NDSolve[{Tinv'[t] == temprhs[t], dpb'[t] == prhs[t],
  Yox1'[t] == oxrhs[t], Tinv[0] == 1/Tout, dpb[0] == 0, Yox1[0] == oxout/Tout},
  {Tinv, dpb, Yox1}, {t, 0, endtime}, MaxSteps -> 10000000,
  AccuracyGoal -> 2, Method -> {"DiscontinuityProcessing" -> False}]

```


Annex B – Model Code Liquid

```

ln[ ]:= Clear[t]

ln[ ]:= Hcox = 13000;      (*Heat of Combustion of per kg of O2 consumed kJ/kg*)
omega = 1.4;
g = 9.81;                (*acceleration due to gravity m/s2*)
dout = 1.2;              (*density of air at Ambient Temp kg/m3 *)
Tout = 293;             (*Ambient Temp K *)
Tv = 424;               (*Boiling point of kerosene in K*)
Tf = 1300 + 273;
(*Flame temperature at extinction also called critical flame temperature*)
oxout = .233;           (*Ambient Oxygen concentration in g/g*)
cp = 1.0;               (*Specific heat of air kJ/kgK*)
cd = .66;               (*Orifice Discharge Coefficient*)
diameter = 0.57 (* Diameter of pit m*)
height = 0.25 * diameter; (* Height of pit m*)
(*CHANGE height to get different Ullage ratios*)
V = (diameter)2 *  $\frac{\text{Pi}}{4}$  * height; (*Volume of Pit*)
As = Pi * diameter * height; (*Area of walls*)
A0 = (diameter)2 *  $\frac{\text{Pi}}{4}$ ; (*Area of top vent m2*)
Af = (diameter)2 *  $\frac{\text{Pi}}{4}$ ; (*Area of Fuel m2*)

F = .8;                 (*A kind of view factor used when calculating Qe*)
deltaHc = 43.2;         (*Heat of combustion of fuel kJ/g*)
sigma = 5.67 * 10(-11); (*Stefan Boltzmann constant kW/m2K4*)
(*mfree=0.17/Af*)      (*g/s m2*) (*Note experiments were for example at 10,
14 and 18 g/min = 0.17, 0.23 and 0.3 g/s of methane air flow *)
hc = 20;               (* Convective heat transfer coefficient W/m2 K*)
r = deltaHc * 1000 / Hcox; (* Stoichiometric Co eff *)
BF = 1; (*Blocking factor- basically = Ln(B+1)/B,
where B is the mass transfer number for the fuel*)
alpha = 0;

(*Step functions to set in-flow and out-flow conditions*)
step[a_] := If[a > 0., 1, 0]
ox[o_] := If[o ≤ 0, 0, 1]
air[c_] := If[c ≤ 0, 1, 0]
poto[d_] := If[d > 35, 0, 1] (*this just sets an upper limit such that if mf cannot
exceed an arbitrarily chosen 35 g/s. It will not be used now but will be useful
when mass transfer is coupled to heat transfer for a liquid fuel in the pit*)

```

```

mdot[dpx_, Tx_] := A0 cd Sqrt[2 dout Abs[dpx]] (step[dpx] Sqrt[Tout / Tx] - step[-dpx] )
(*Solves for vent flow in and out of the top vent*)
dpt[t_] := dpb[t] + dout (1 - Tout / T[t]) gheight (*pressure at the top of
cavity is a function of T[t] and pressure at the bottom of cavity (dpb[t]*)
Yox[t_] := Yox1[t] × T[t]
T[t_] := 1 / Tinv[t]
h[t_] := Sqrt[19.1 * .01 * 950 * 272 / (t + 1)] * 0.001 (*kW/m2K*)

mt[t_] := mdot[dpt[t], T[t]] (*kg/s*) (*mass flow through top vent *)
mb[t_] := alpha mdot[dpb[t], T[t]] (*kg/s*)
(*mass flow through the bottom vent = 0 applicable for pit - set by making alpha = 0*)

L[t_] := 251 + 2.01 * (TV - T[t])
(*B[t_] := (0.233*1000*(deltaHc/1.268) - 1.068*(TV-298)) / L[t]
Bcrit[t_] := (Yoxcrit[t]*1000*(deltaHc/1.268) - 1.068*(TV-298)) / L[t]*)
mfree :=
39 + (5 * (1.05 / (Exp[1.05] - 1))) * (deltaHc / 1.268) * (1 - 0.074) * (Yox[t] - 0.233)) / L[t]

mf[t_] := (1 - Exp[-t / 10]) * (mfree + (F * sigma * T[t]^4) / L[t]) (*g/s m2*)

mfcrit[t_] := (1 - Exp[-t / 10]) * (mfree + (F * sigma * T[t]^4) / L[t]) (*g/s m2*)

(*The (1-Exp[-t/10]) is the rampup time. It maybe
needed if the model does not start smoothly. The F*sigma*T[t]^4)/L
is a radiative loss with F being a view factor.*)

Yoxcrit[t_] := 0.1294304768436963` - 0.00008230253288356285` T[t]
(* This is a limiting condition of oxygen vs. temperature in the
pit. It reduces the concentration of oxygen as the temperature of the pit
increases. The other way of doing this is solving the gas phase chemical
reaction using a one step reaction model using constants from Westbrook and
Dryer. The limiting reactant is oxygen which is solved for in the equations*)

x[t_] := step[Yoxcrit[t]] × Yoxcrit[t]
Qdot[t_] := ox[Yox[t] - x[t]] * poto[mf[t]] * mf[t] * deltaHc * Af +
air[Yox[t]] * (-step[-dpb[t]] * Hcox * 0.233 * mb[t] - step[-dpt[t]] * Hcox * 0.233 * mt[t])
E3[t_] := (step[dpb[t]] × T[t] + step[-dpb[t]] Tout) mb[t] cp
E4[t_] := (step[dpt[t]] × T[t] + step[-dpt[t]] Tout) mt[t] cp

oxt[t_] := (step[dpt[t]] × Yox[t] + step[-dpt[t]] oxout) mt[t]
oxb[t_] := (step[dpb[t]] × Yox[t] + step[-dpb[t]] oxout) mb[t]

temprhs[t_] := (-mt[t] - mb[t] + mf[t] * 0.001 * Af) / (dout Tout V)
prhs[t_] := (Qdot[t] - h[t] As (T[t] - Tout) - E3[t] - E4[t]) (omega - 1) / V
oxrhs[t_] := (-Qdot[t] / Hcox - oxt[t] - oxb[t]) / (dout Tout V)
endtime = 600;

```

```
SetOptions[ListPlot, ImageSize → 350, PlotStyle → GrayLevel[0],  
  Ticks → {Automatic}, Frame → False, GridLines → None];
```

```
SetOptions[Plot, ImageSize → 350, PlotStyle → GrayLevel[0], Frame → False, GridLines → None];
```

Out[] = 0.57

```
in[ ] := sol = NDSolve[{Tinv'[t] == temprhs[t], dpb'[t] == prhs[t],  
  Yox1'[t] == oxrhs[t], Tinv[0] == 1 / Tout, dpb[0] == 0, Yox1[0] == oxout / Tout},  
  {Tinv, dpb, Yox1}, {t, 0, endtime}, MaxSteps → 10000000, AccuracyGoal → 2,  
  Method → {"DiscontinuityProcessing" → False}]
```

Greater: Invalid comparison with $-0.266053 - 0.223225 i$ attempted.

Greater: Invalid comparison with $0.266053 + 0.223225 i$ attempted.

Greater: Invalid comparison with $-0.266053 - 0.223225 i$ attempted.

General: Further output of Greater:nord will be suppressed during this calculation.

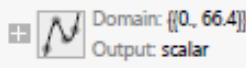

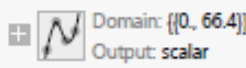
LessEqual: Invalid comparison with $-3.42839 \times 10^{-10} + 2.1056 \times 10^{-11} i$ attempted.

LessEqual: Invalid comparison with $-3.42839 \times 10^{-10} + 2.1056 \times 10^{-11} i$ attempted.

LessEqual: Invalid comparison with $-3.42839 \times 10^{-10} + 2.1056 \times 10^{-11} i$ attempted.

General: Further output of LessEqual:nord will be suppressed during this calculation.

NDSolve: The function value {«1»} is not a list of numbers with dimensions {3} at {t, dpb[t], Tinv[t], Yox1[t]} =
{66.5081, -0.81305 - 1.41539 i, 0.00121749 - 0.00333383 i, $-3.47205 \times 10^{-13} + 1.1686 \times 10^{-12} i$ }.

```
Out[ ] := {{Tinv → InterpolatingFunction[  
   Domain: {{0, 66.4}}  
  Output: scalar  
  Data not in notebook. Store now →  
  ],  
  dpb → InterpolatingFunction[  
   Domain: {{0, 66.4}}  
  Output: scalar  
  Data not in notebook. Store now →  
  ],  
  Yox1 → InterpolatingFunction[  
   Domain: {{0, 66.4}}  
  Output: scalar  
  Data not in notebook. Store now →  
  ] ]}}
```

```
in[ ] := endtime = 66.4
```

Out[] = 66.4

```
in[ ] := Export["025D_kero_Temp.xls", Table[Evaluate[(T[t] - 273) /. sol], {t, 0, endtime, 0.1}]];
Export["025D_kero_Yox.xls", Table[Evaluate[(Yox[t] * 100) /. sol], {t, 0, endtime, 0.1}]];
Export["025D_kero_PBot.xls", Table[Evaluate[dpb[t] /. sol], {t, 0, endtime, 0.1}]];
Export["025D_kero_Ptop.xls", Table[Evaluate[dpt[t] /. sol], {t, 0, endtime, 0.1}]];
Export["025D_kero_MassTop.xls", Table[Evaluate[mt[t] /. sol], {t, 0, endtime, 0.1}]];
Export["025D_kero_Qdot.xls", Table[Evaluate[Qdot[t] /. sol], {t, 0, endtime, 0.1}]];
```

... InterpolatingFunction: Input value {66.4} lies outside the range of data in the interpolating function. Extrapolation will be used.

... InterpolatingFunction: Input value {66.4} lies outside the range of data in the interpolating function. Extrapolation will be used.

... InterpolatingFunction: Input value {66.4} lies outside the range of data in the interpolating function. Extrapolation will be used.

... InterpolatingFunction: Input value {66.4} lies outside the range of data in the interpolating function. Extrapolation will be used.

... InterpolatingFunction: Input value {66.4} lies outside the range of data in the interpolating function. Extrapolation will be used.

... InterpolatingFunction: Input value {66.4} lies outside the range of data in the interpolating function. Extrapolation will be used.

... InterpolatingFunction: Input value {66.4} lies outside the range of data in the interpolating function. Extrapolation will be used.

... InterpolatingFunction: Input value {66.4} lies outside the range of data in the interpolating function. Extrapolation will be used.

... InterpolatingFunction: Input value {66.4} lies outside the range of data in the interpolating function. Extrapolation will be used.

... General: Further output of InterpolatingFunction::dmval will be suppressed during this calculation.

... InterpolatingFunction: Input value {66.4} lies outside the range of data in the interpolating function. Extrapolation will be used.

... InterpolatingFunction: Input value {66.4} lies outside the range of data in the interpolating function. Extrapolation will be used.

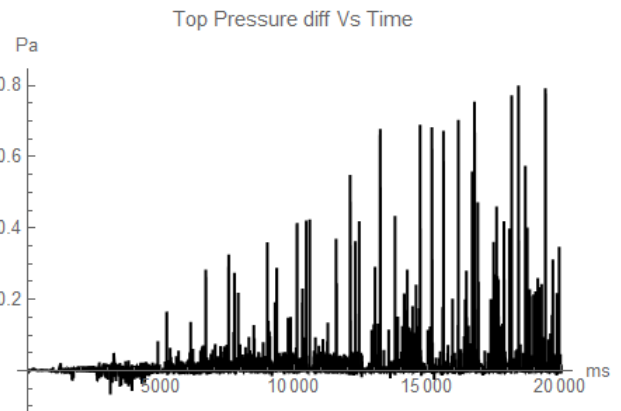
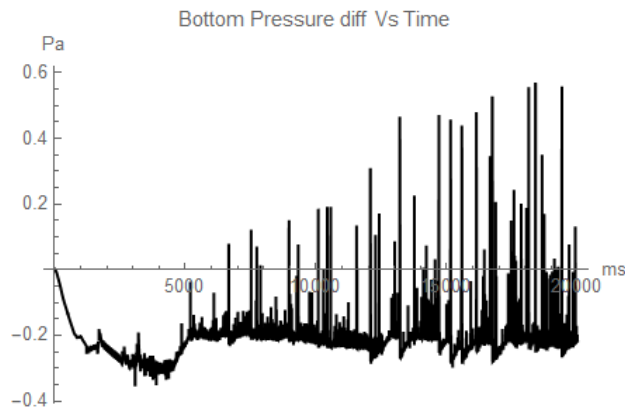
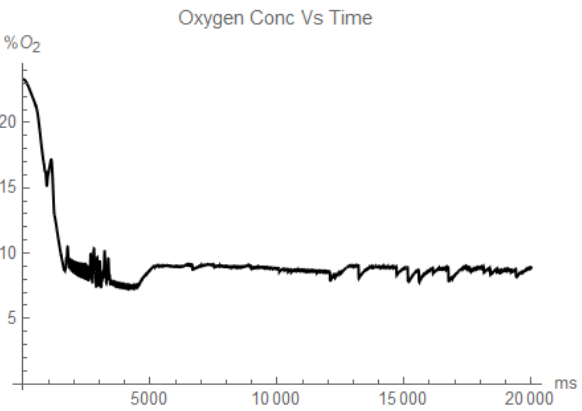
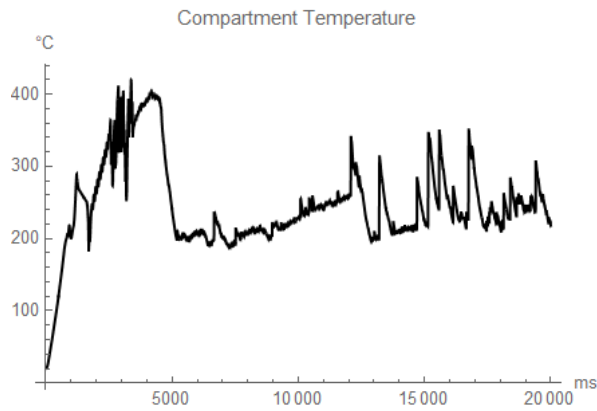
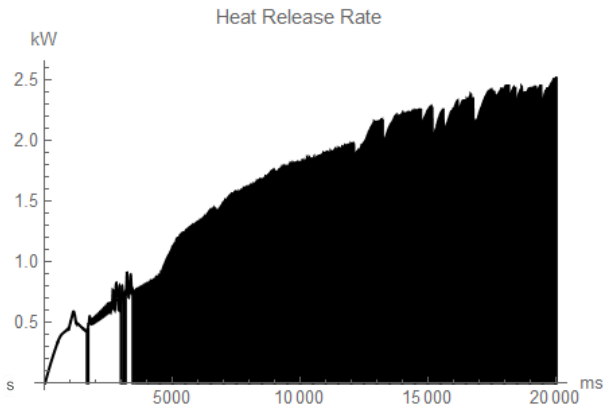
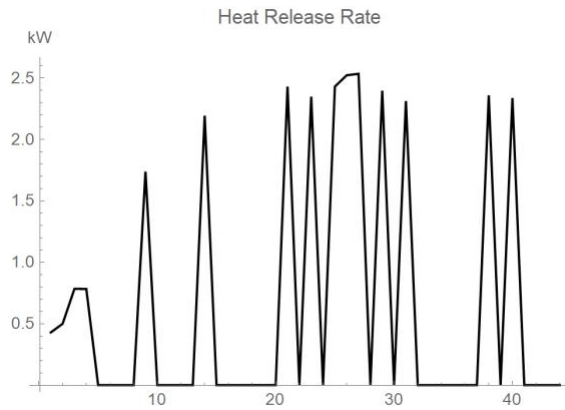
... InterpolatingFunction: Input value {66.4} lies outside the range of data in the interpolating function. Extrapolation will be used.

... General: Further output of InterpolatingFunction::dmval will be suppressed during this calculation.

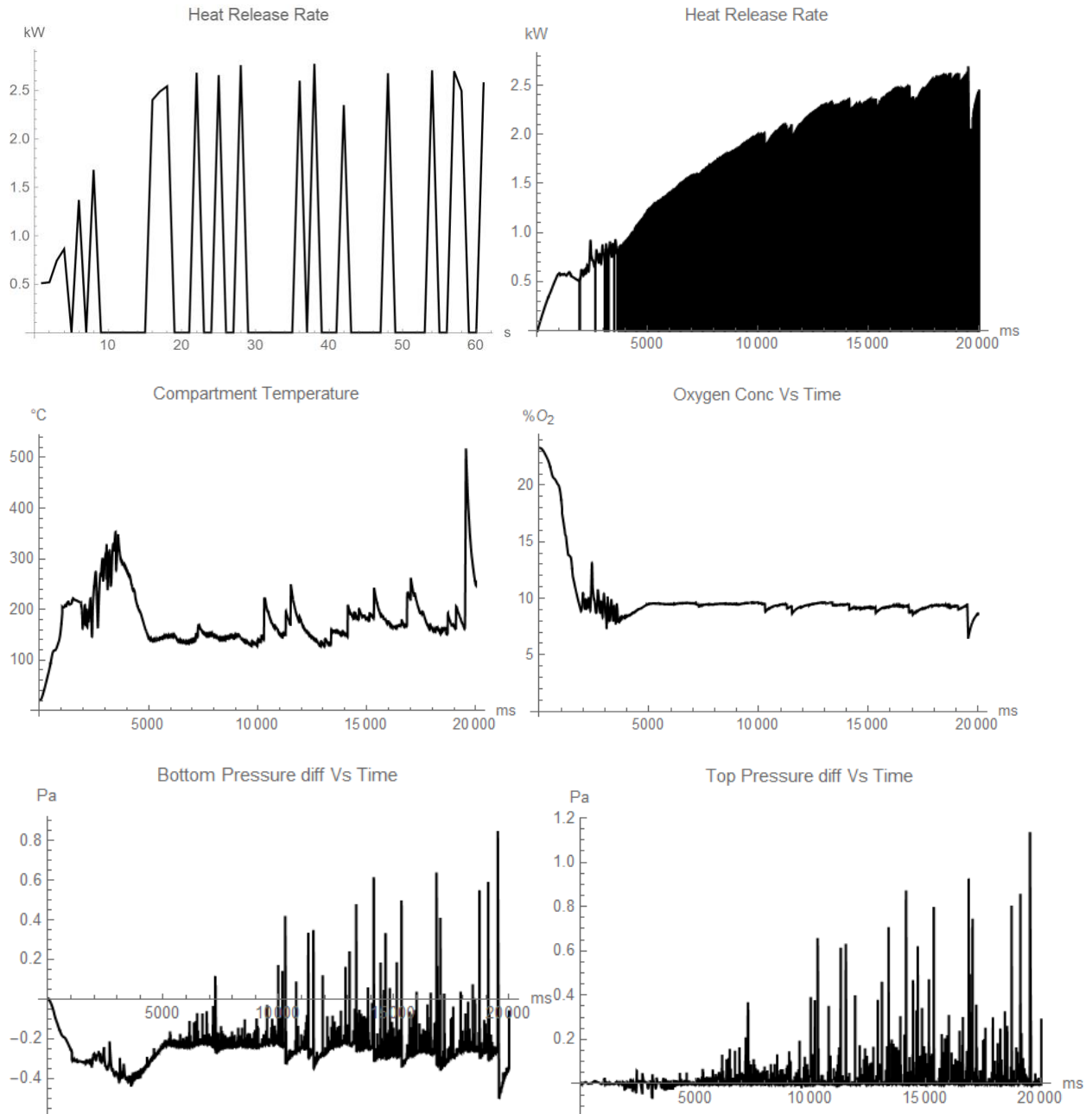
Annex C – Model Graphs

10 g/min

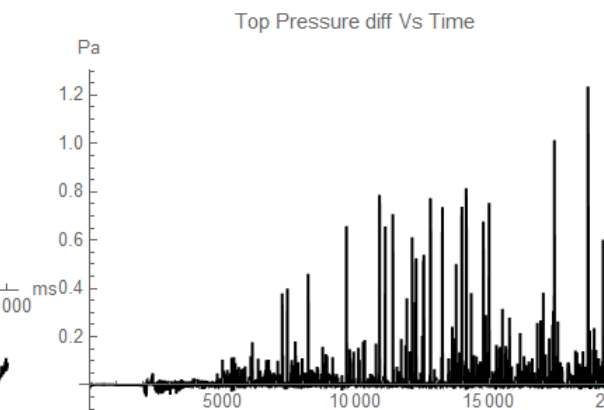
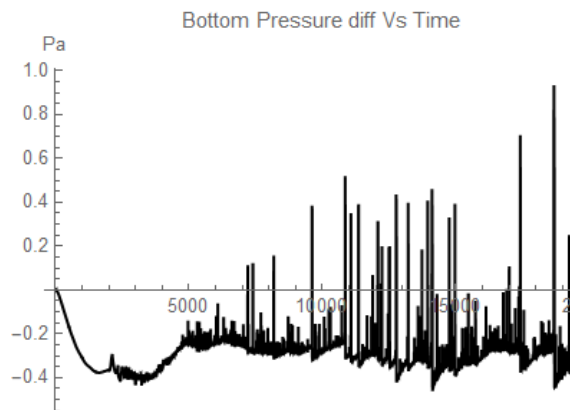
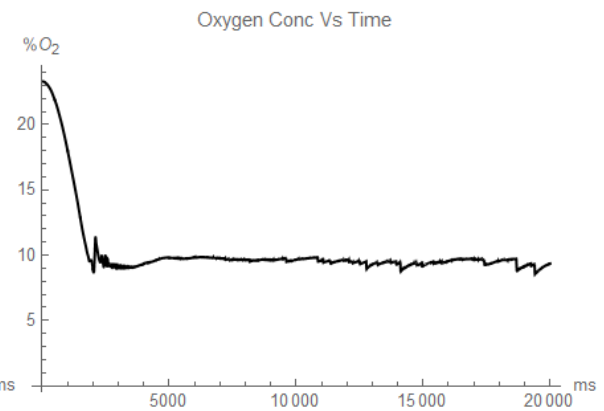
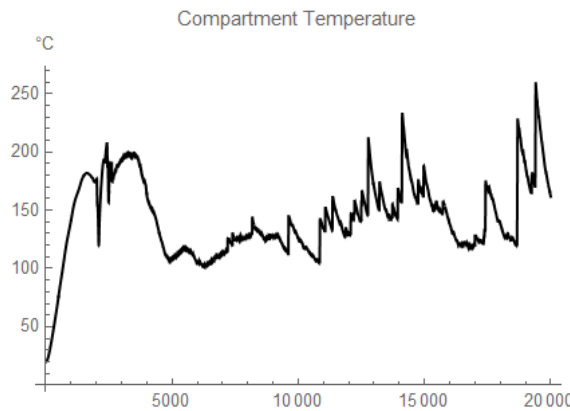
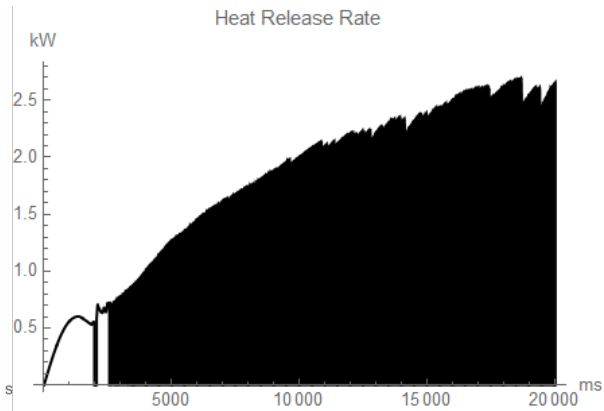
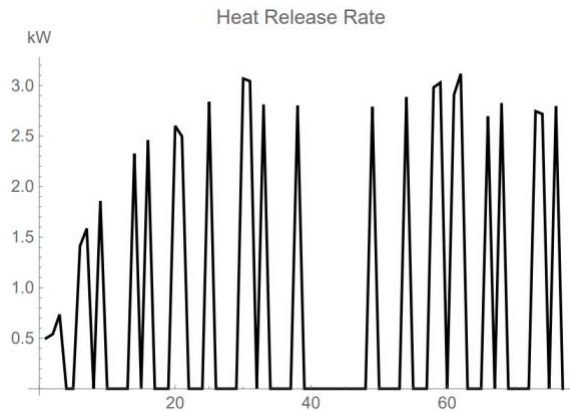
U/D = 0.5



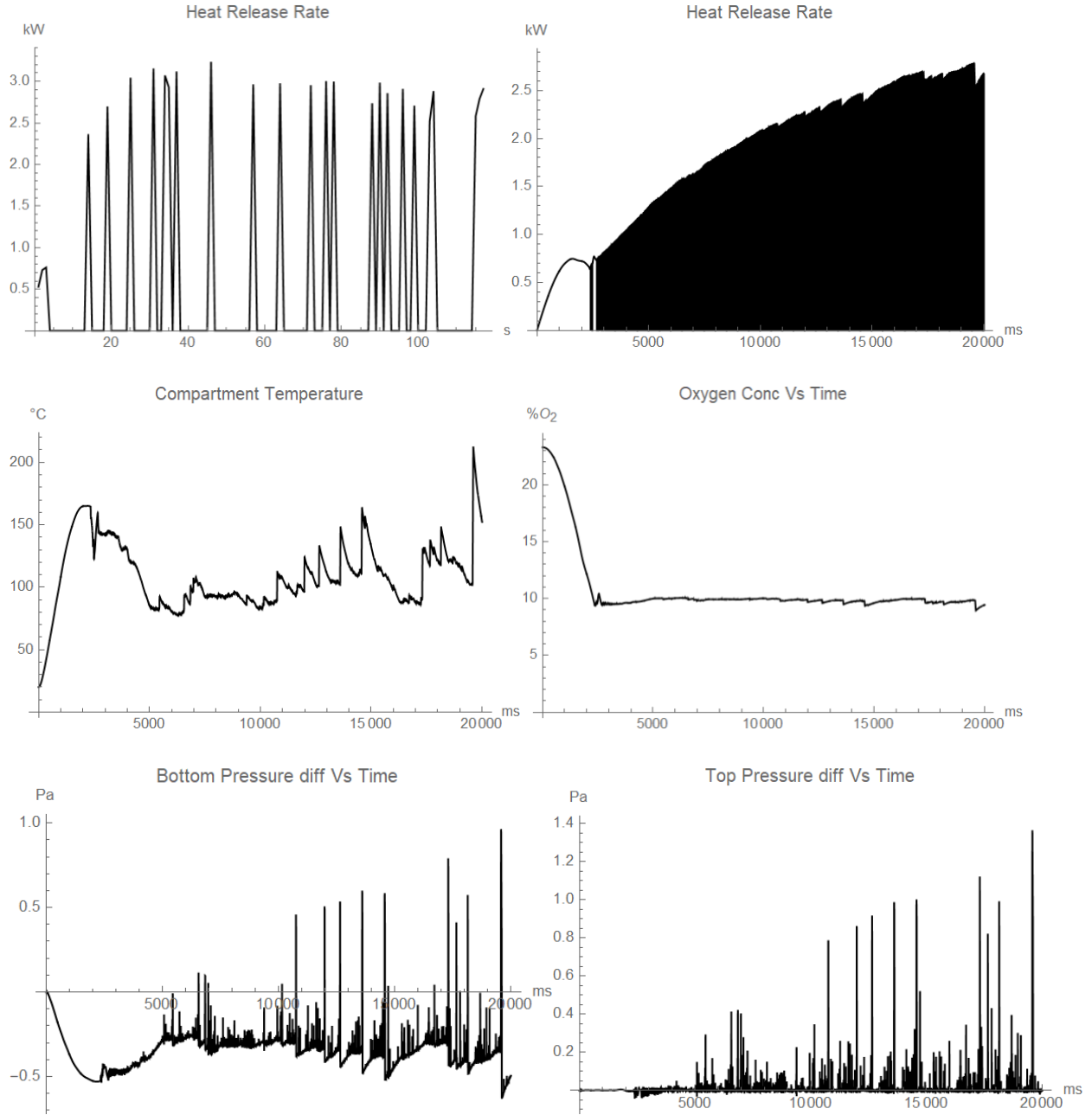
$U/D = 0.75$



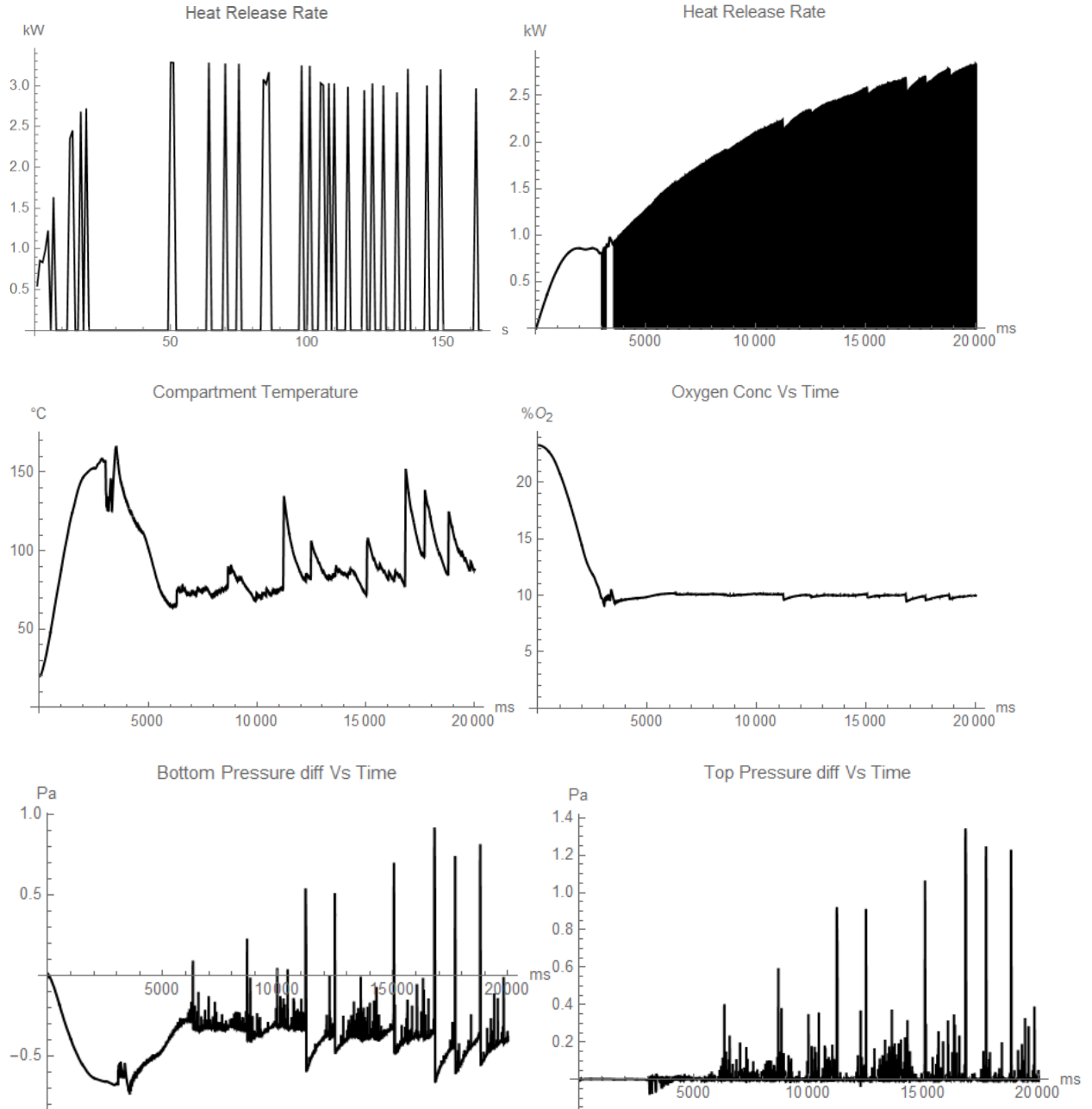
$U/D = 1.0$



$U/D = 1.5$

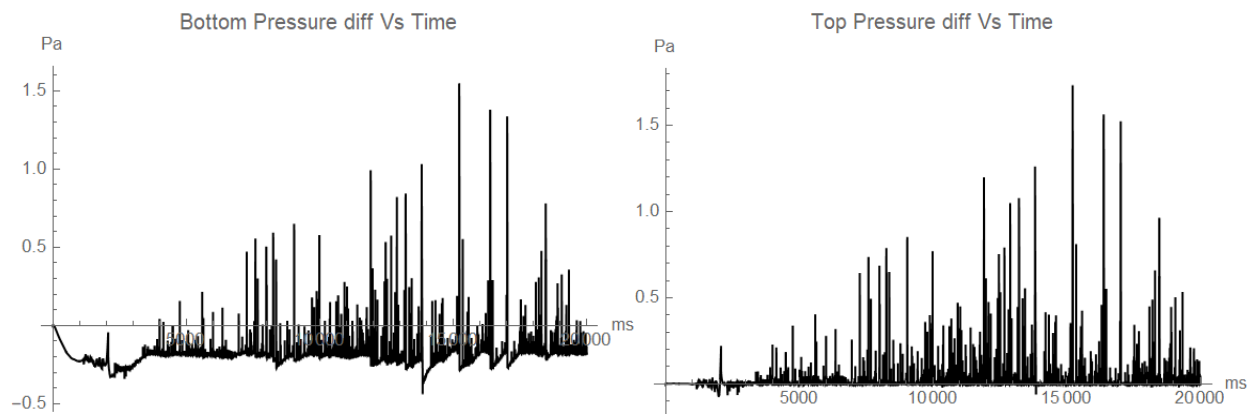
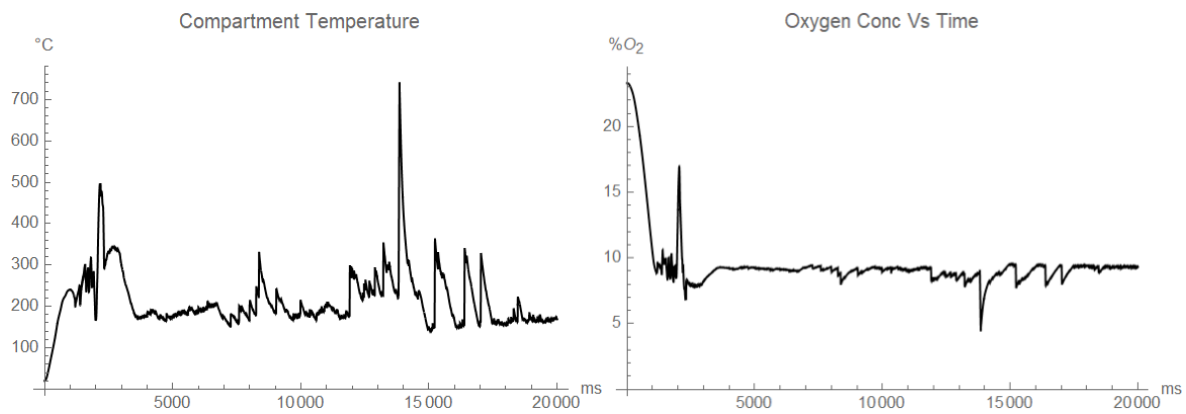
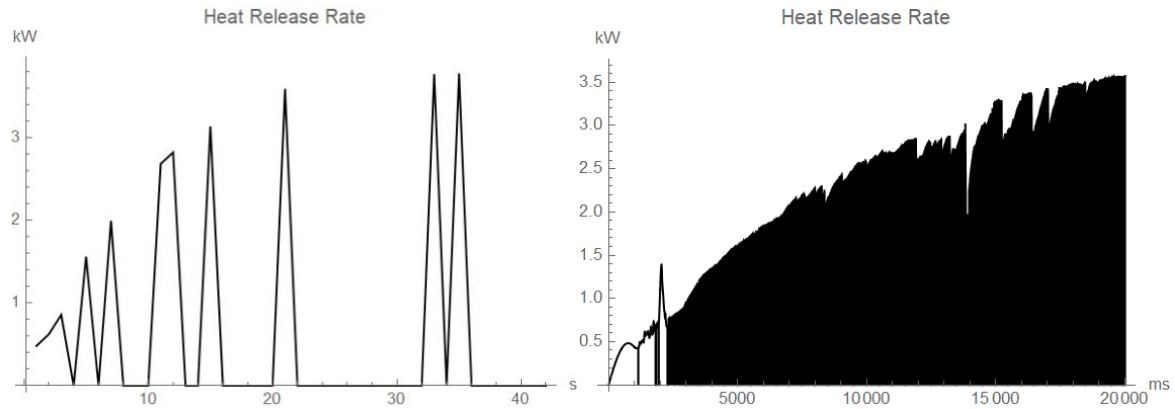


U/D = 2.0

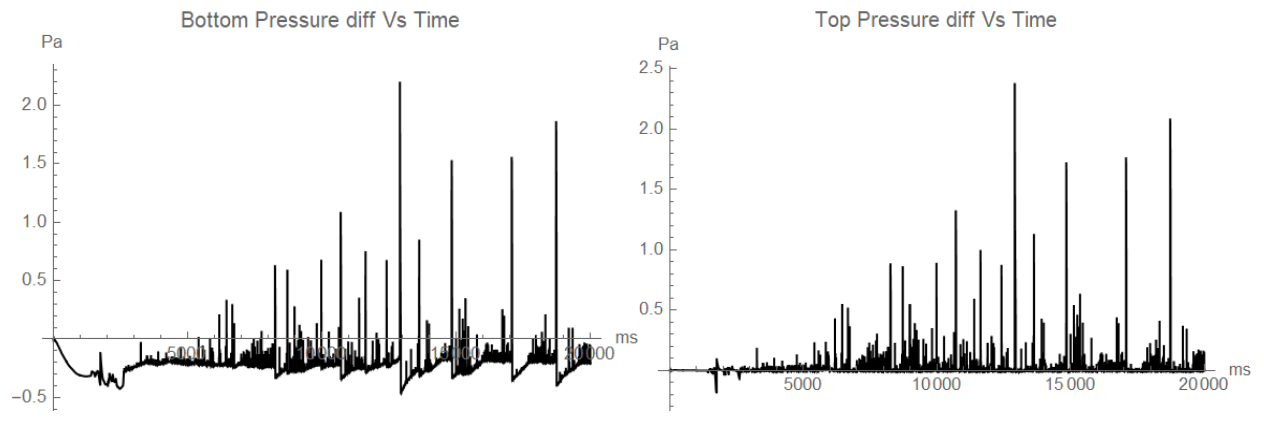
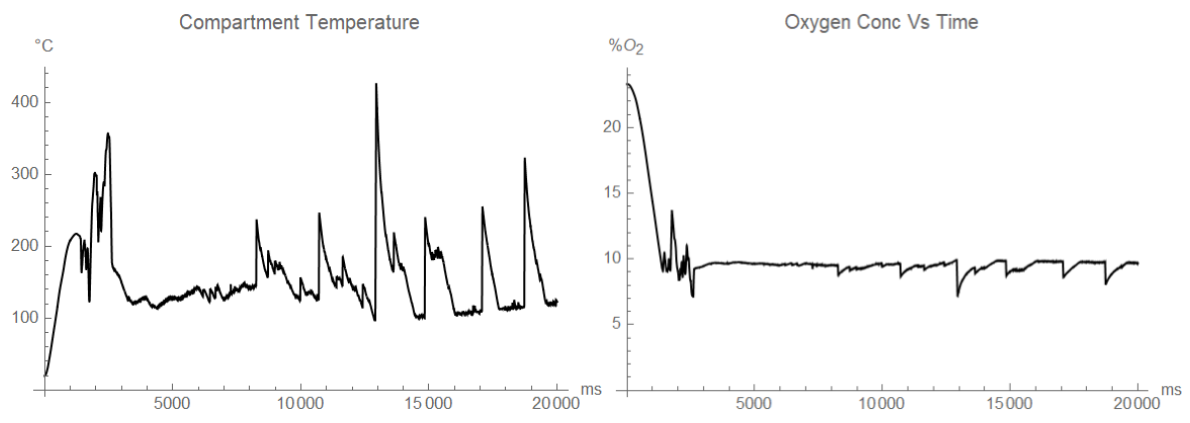
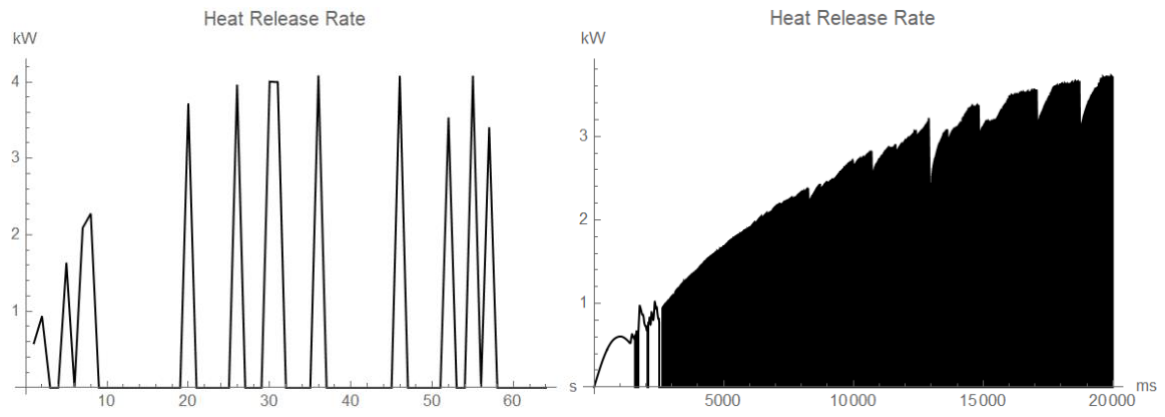


14 g/min

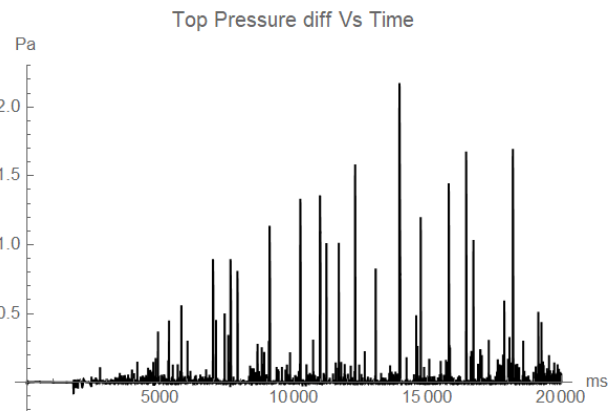
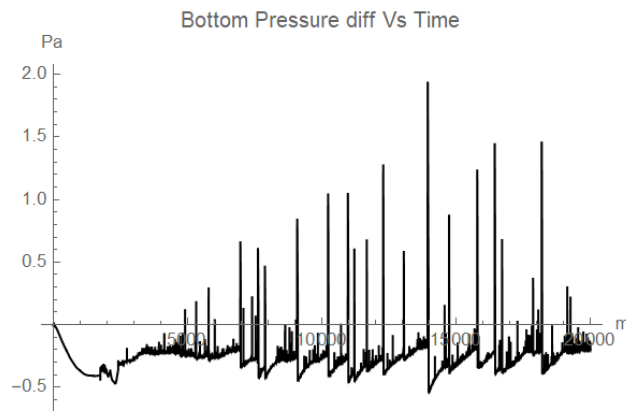
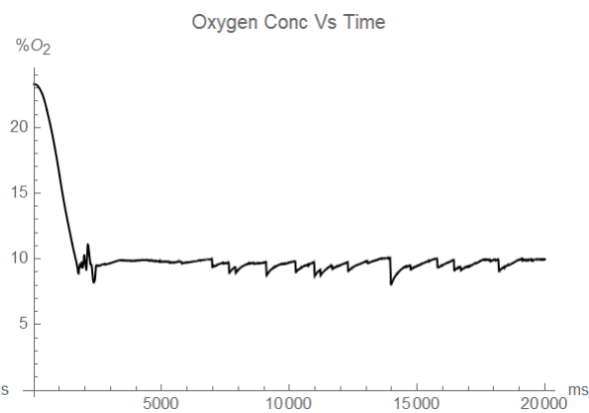
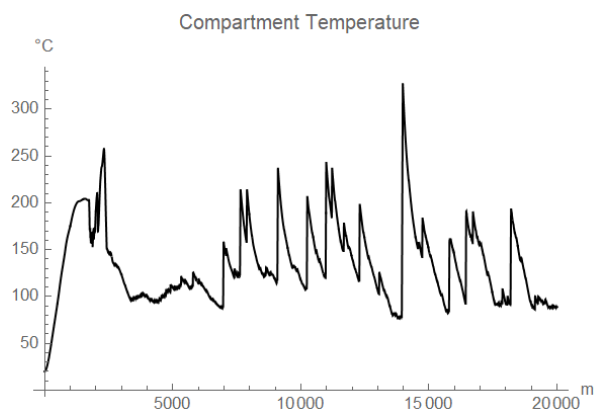
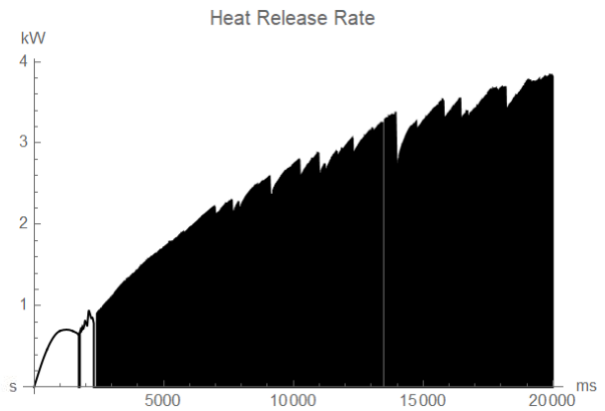
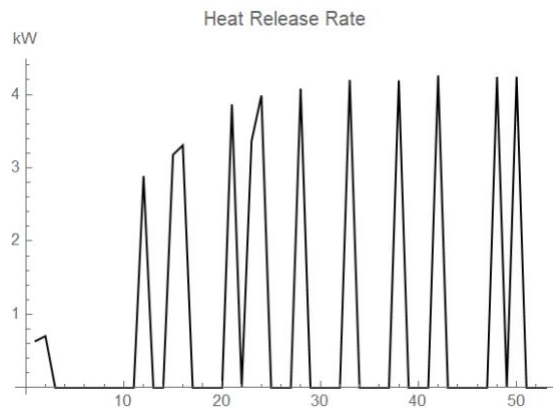
U/D = 0.5



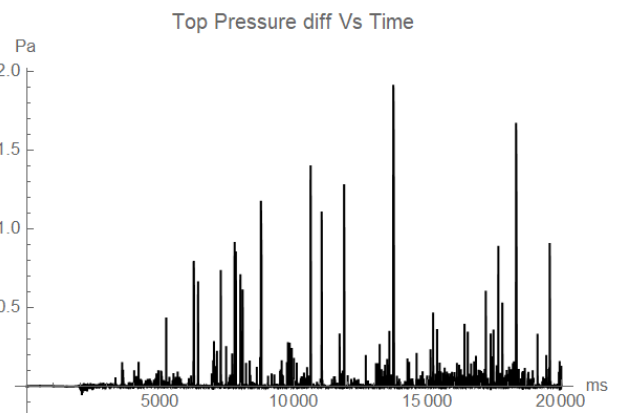
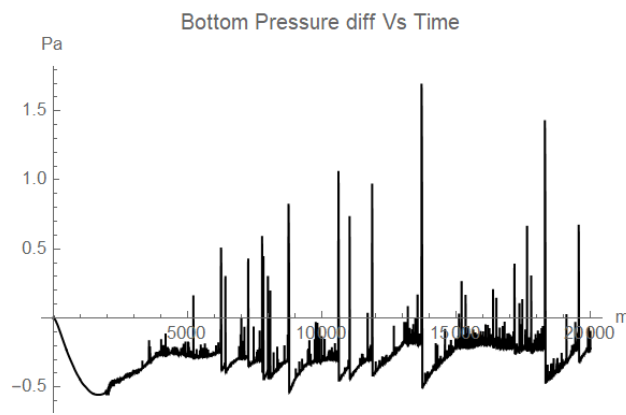
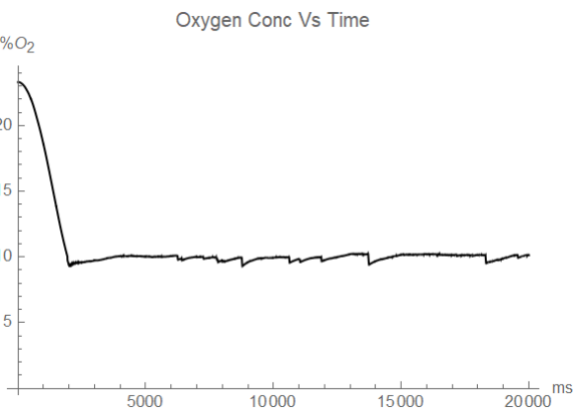
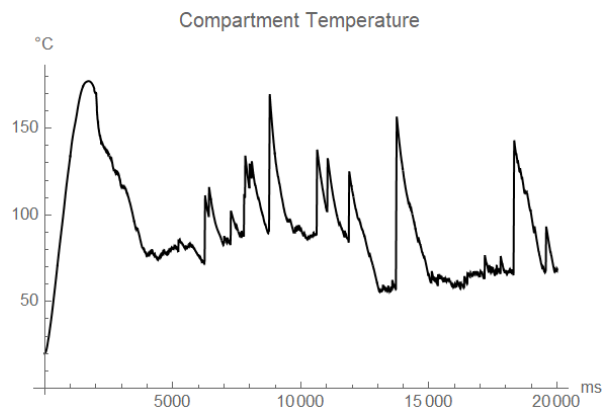
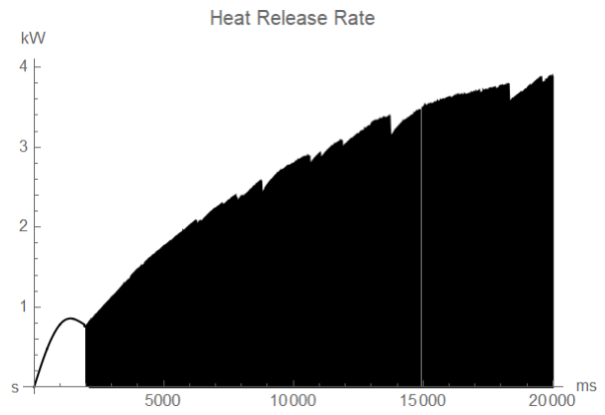
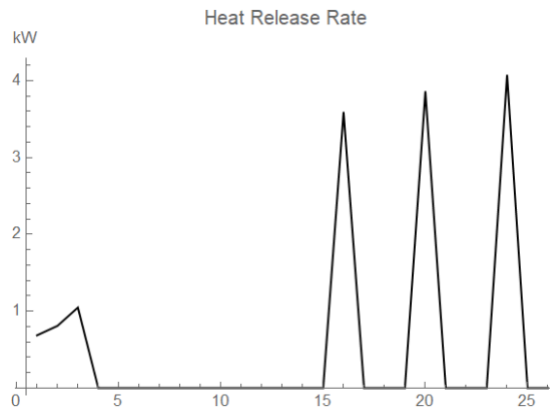
U/D = 0.75



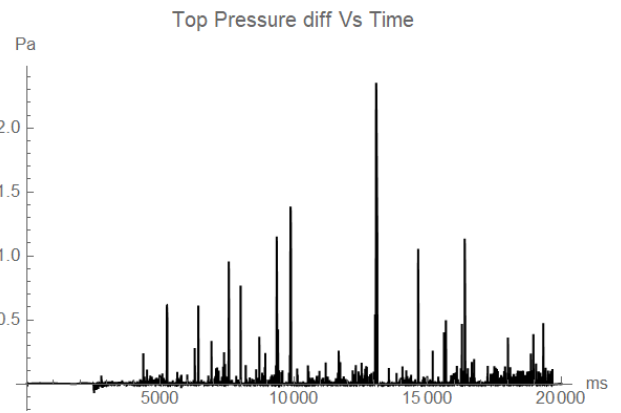
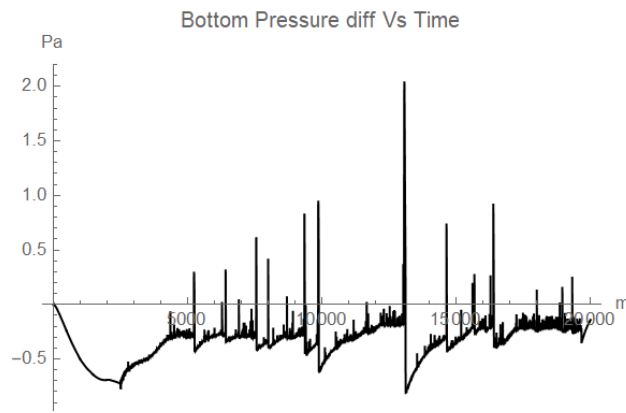
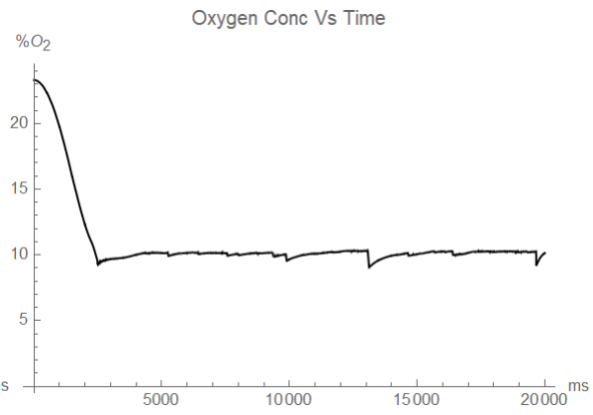
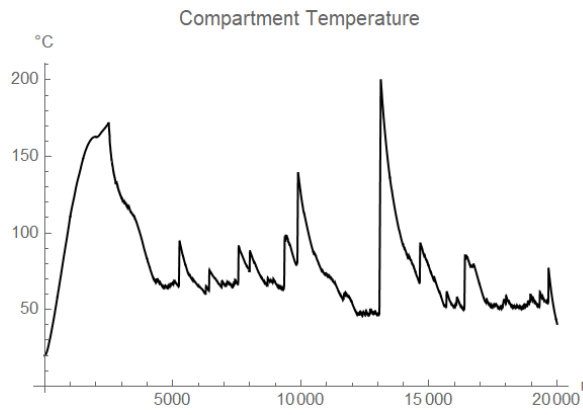
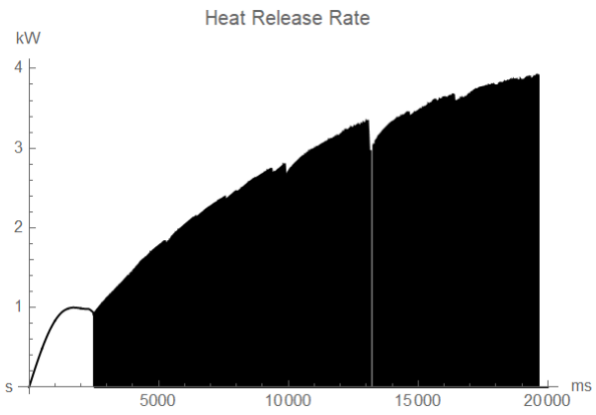
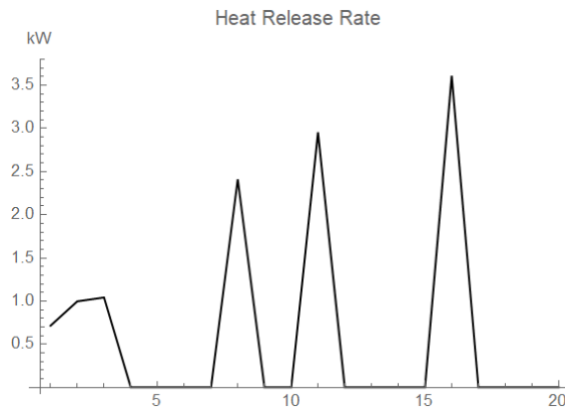
U/D = 1.0



$U/D = 1.5$

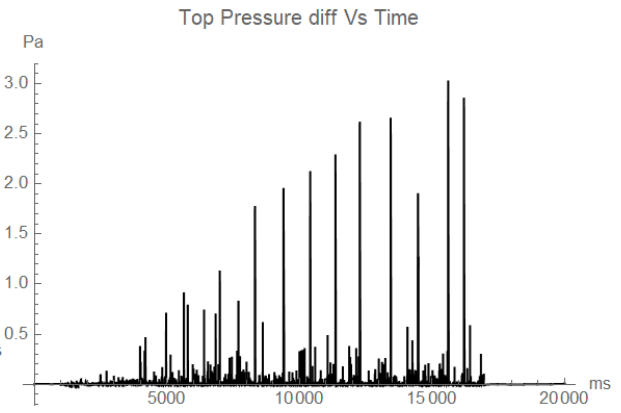
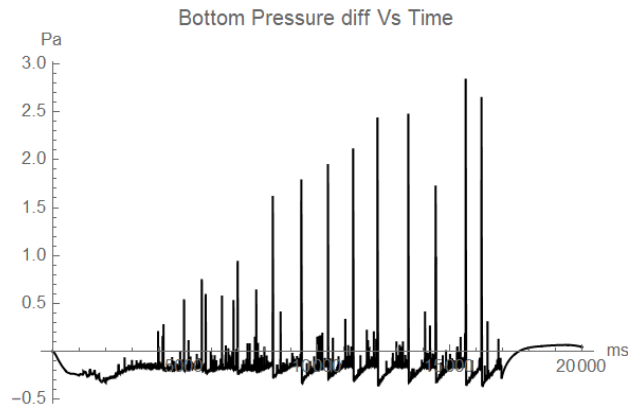
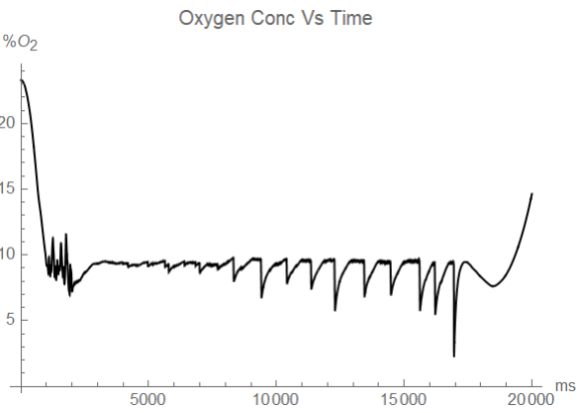
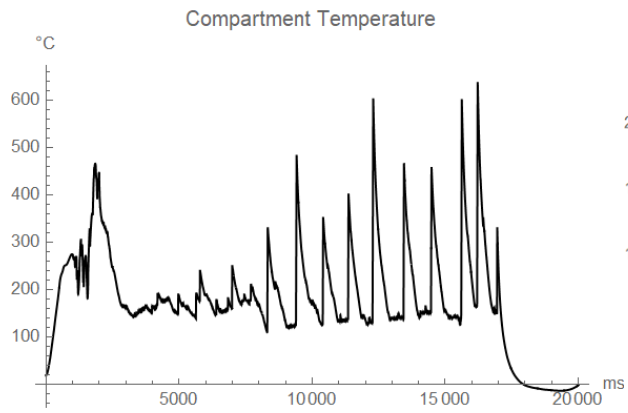
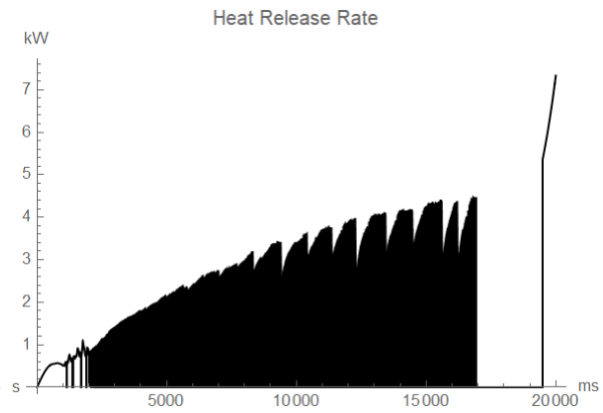
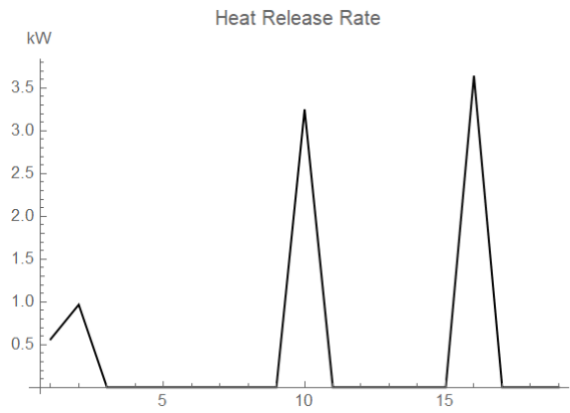


U/D = 2.0

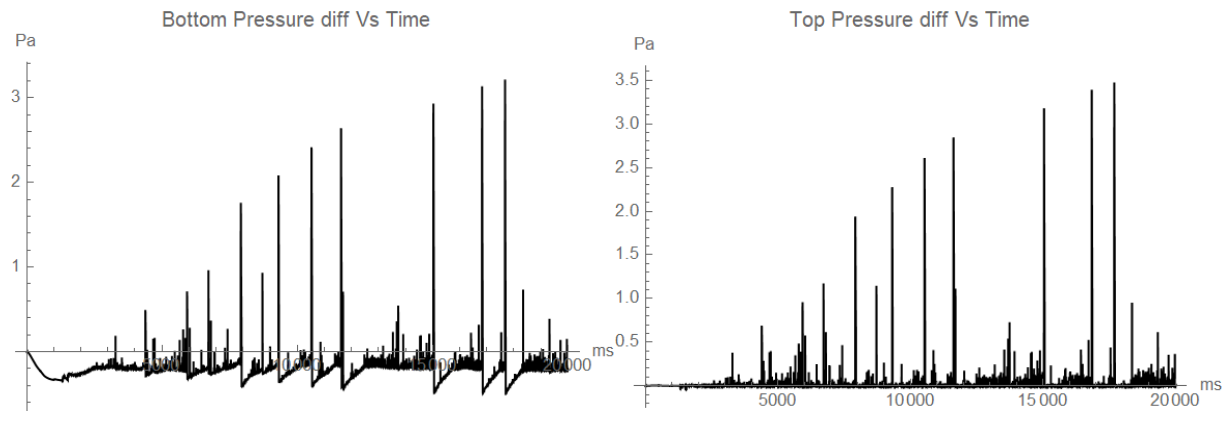
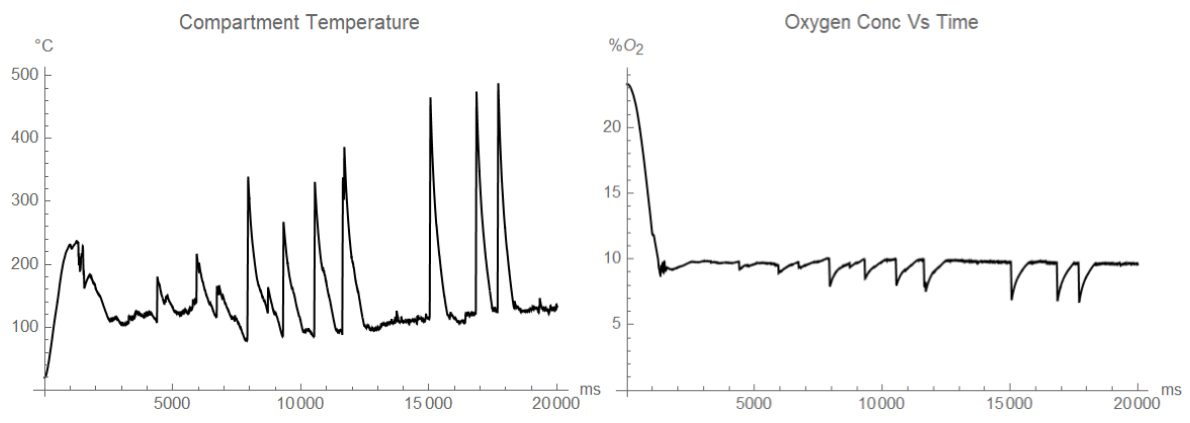
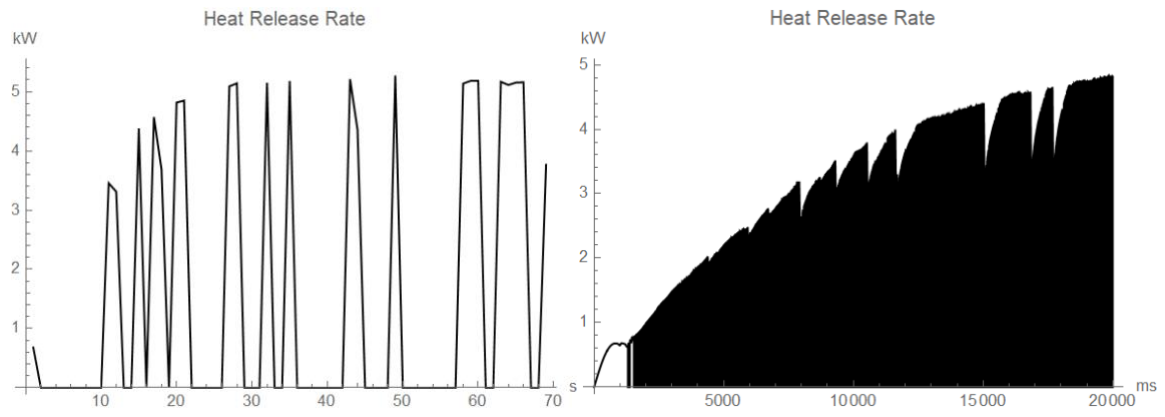


18 g/min

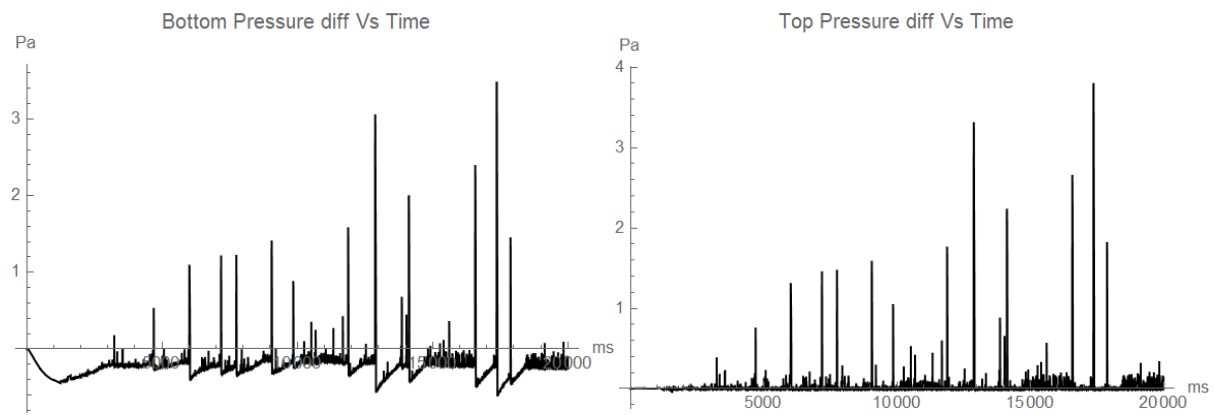
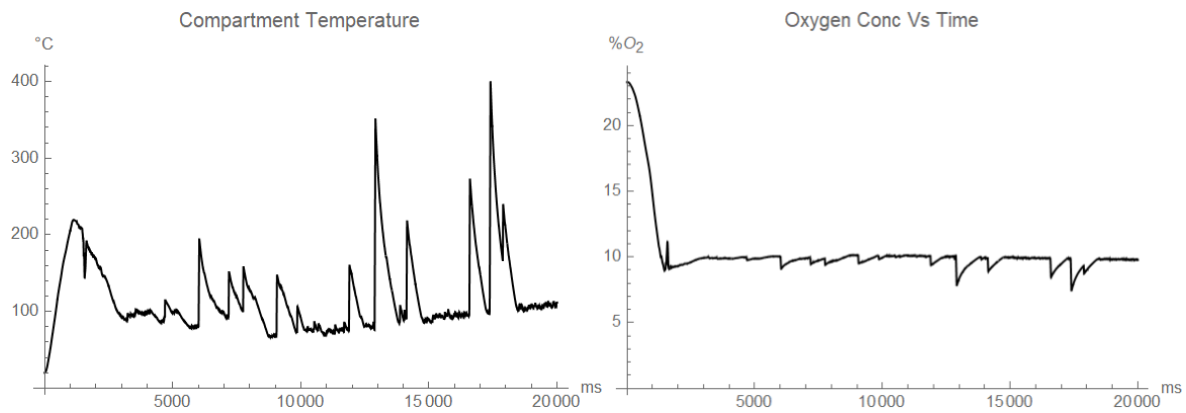
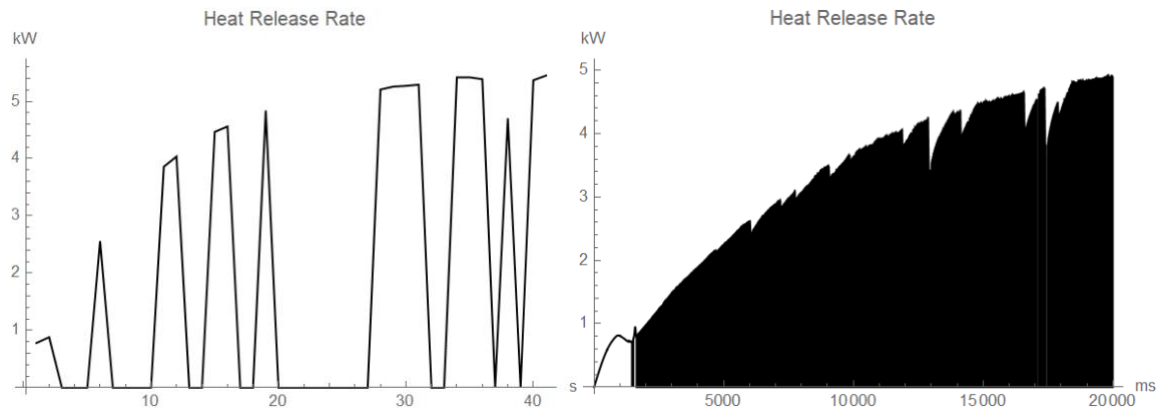
$U/D = 0.5$



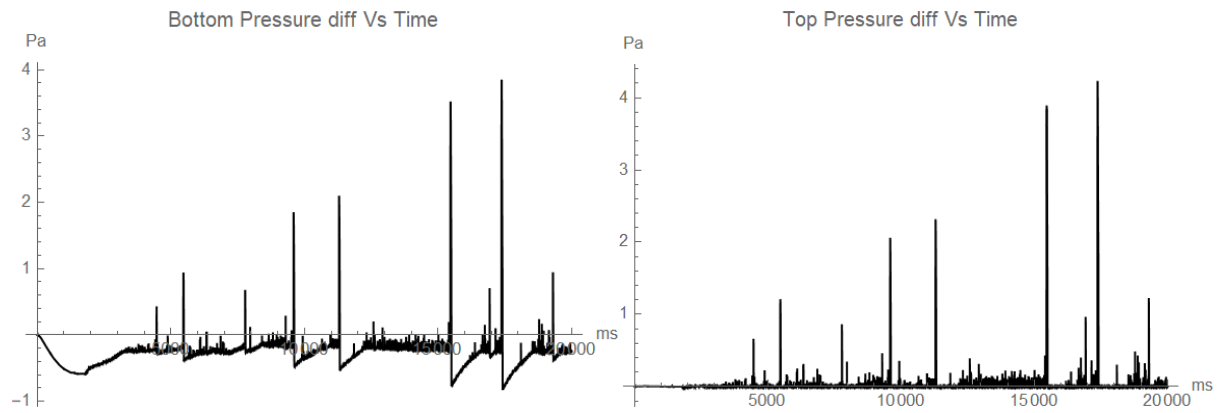
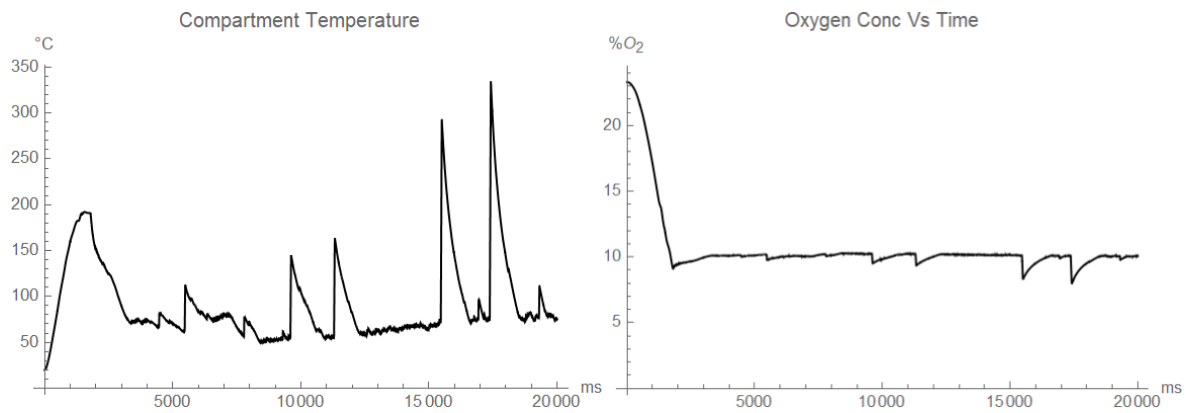
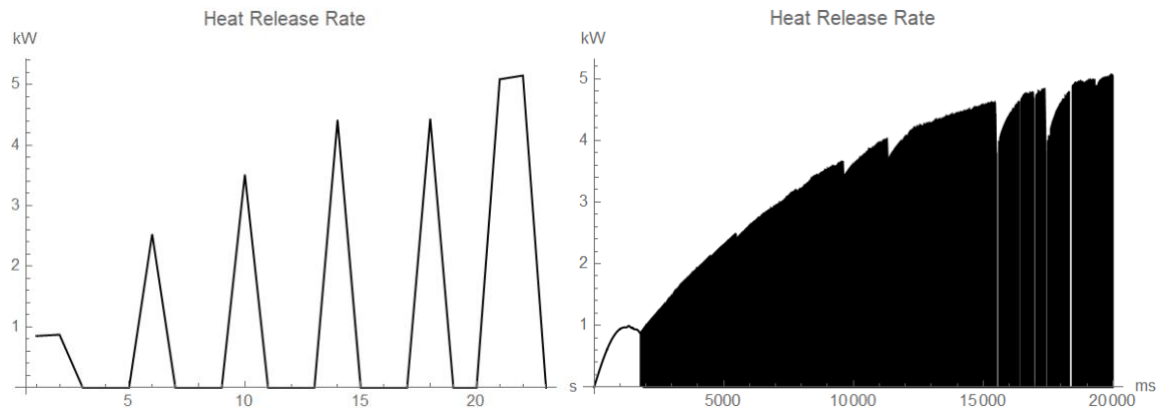
U/D = 0.75



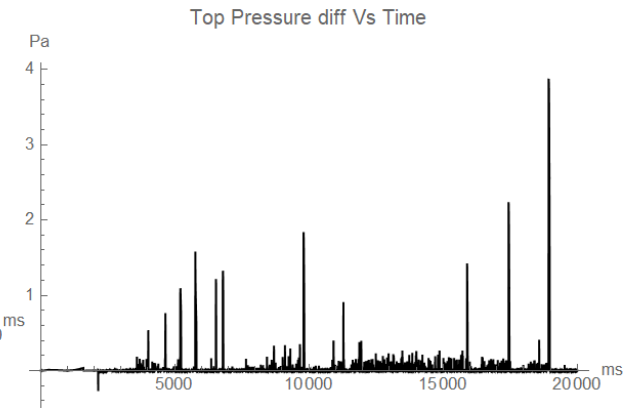
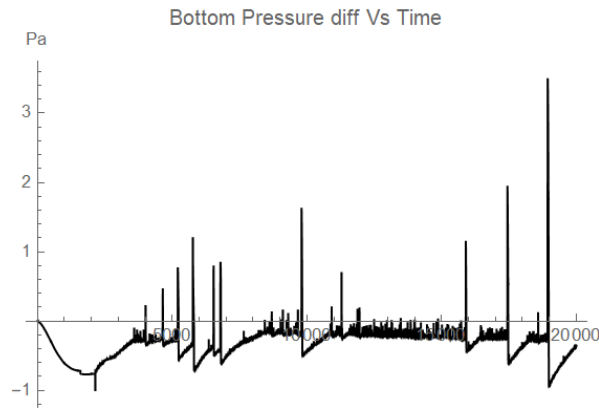
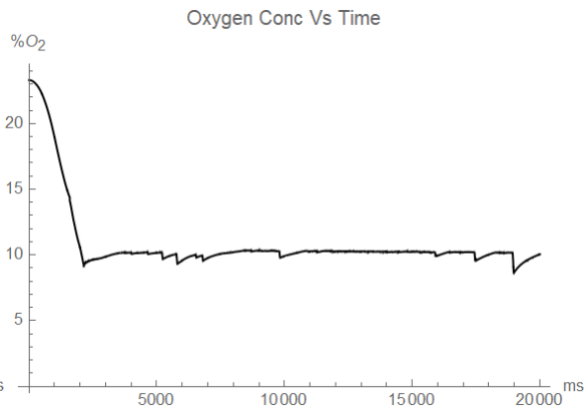
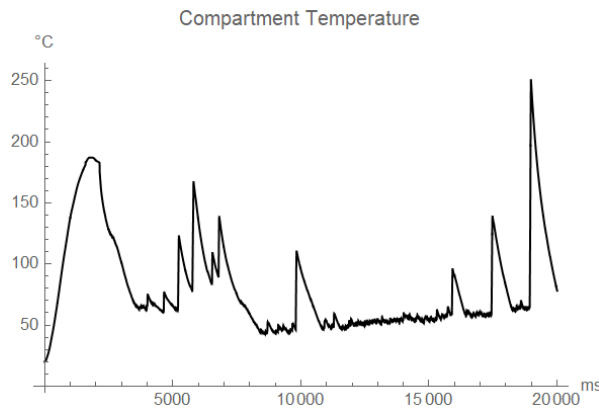
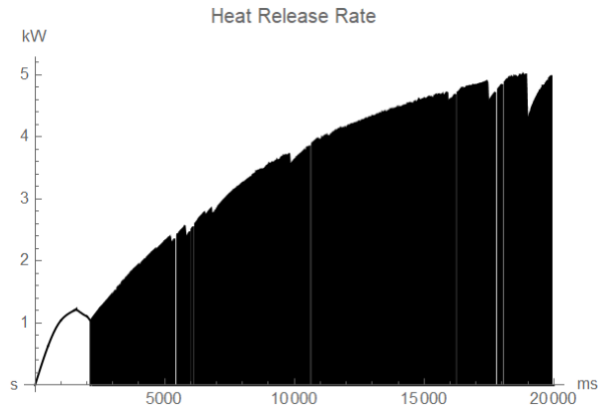
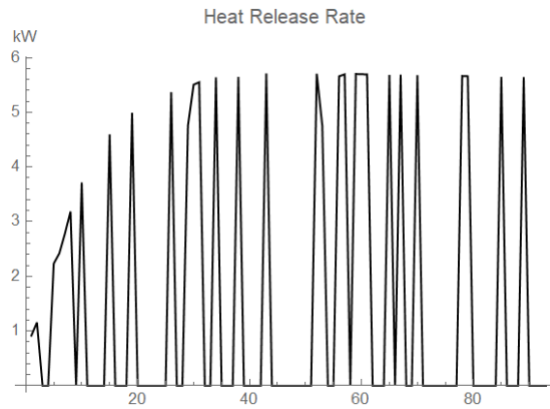
U/D = 1.0



$U/D = 1.5$

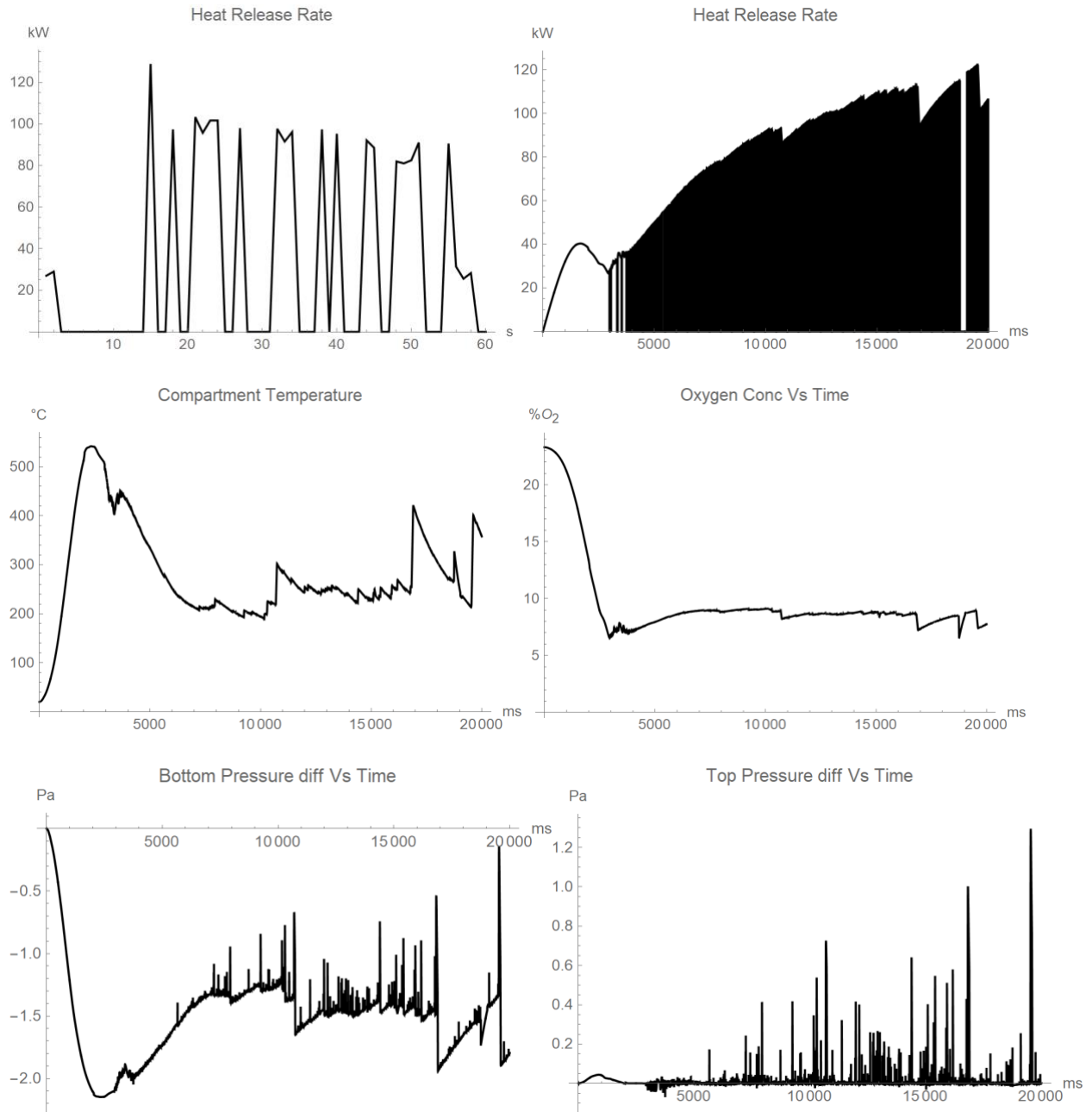


U/D = 2.0

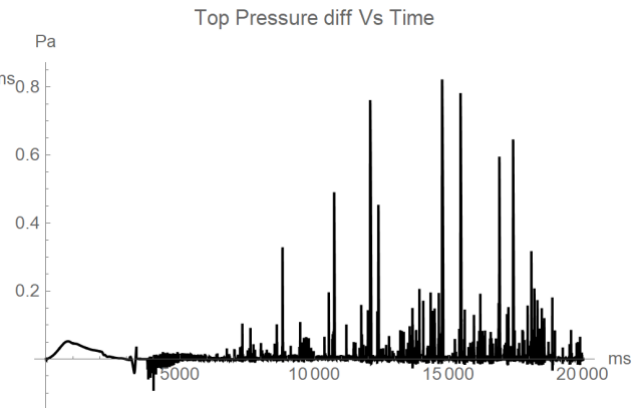
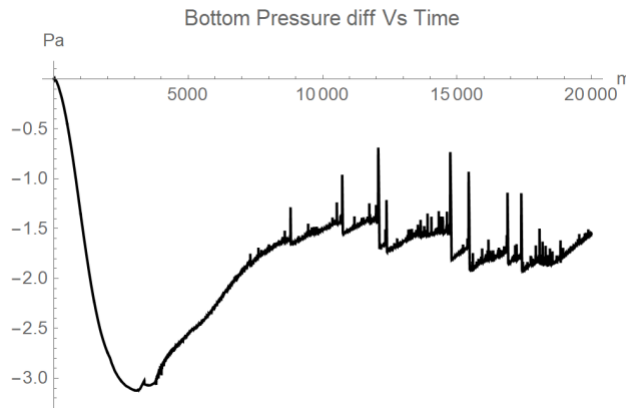
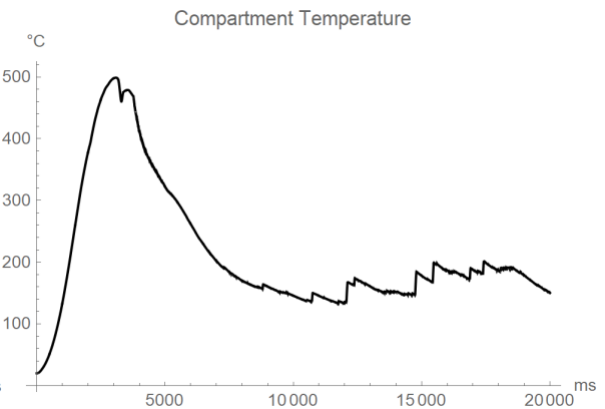
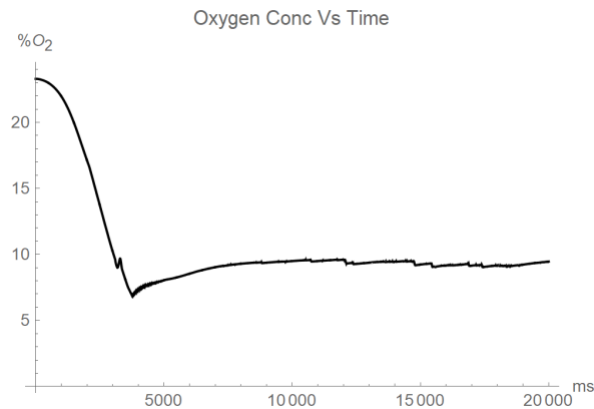
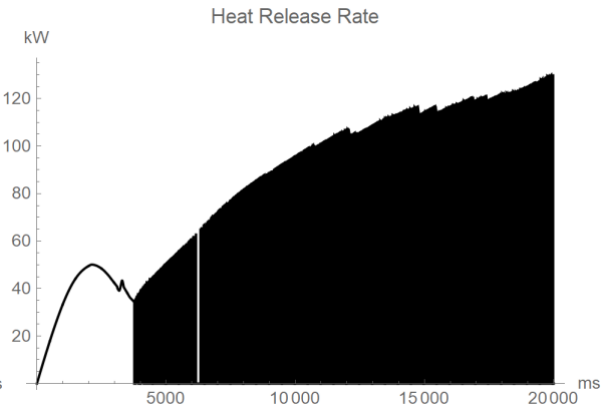
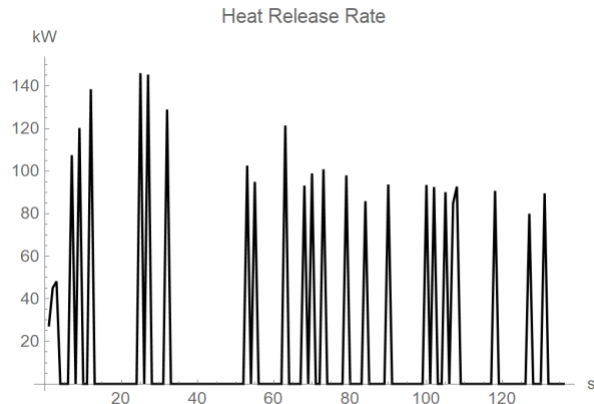


Kerosene

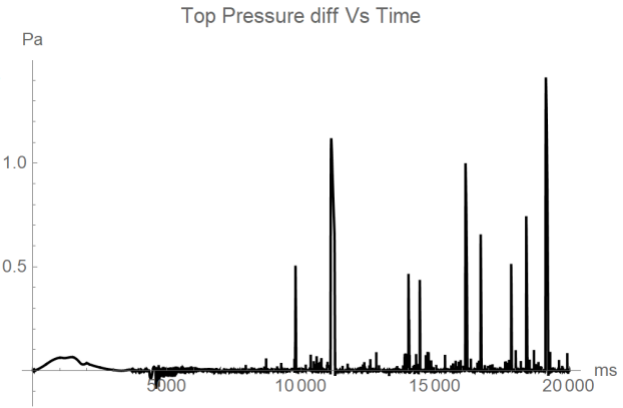
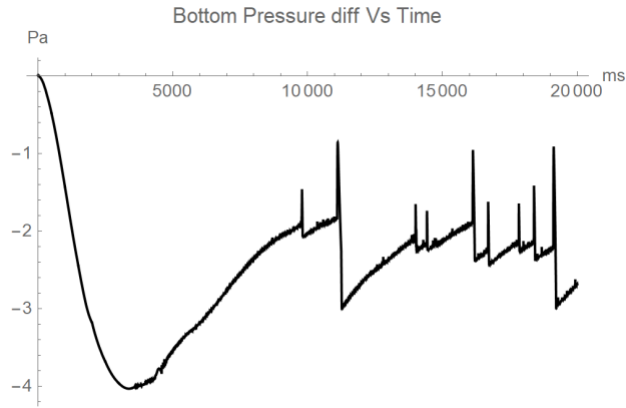
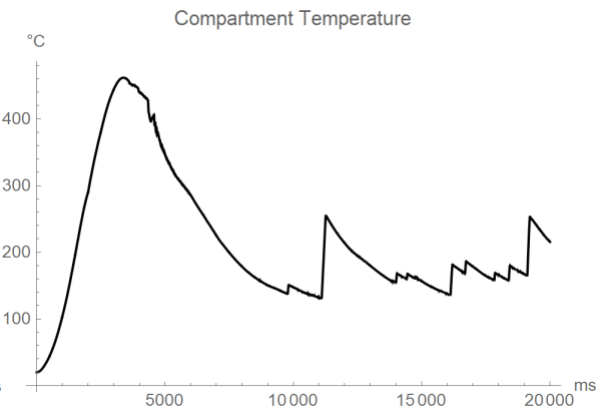
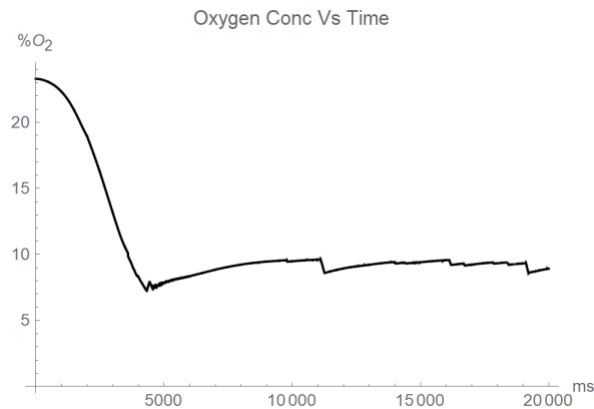
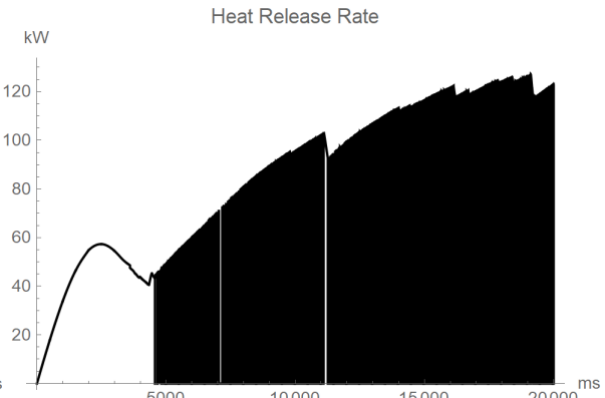
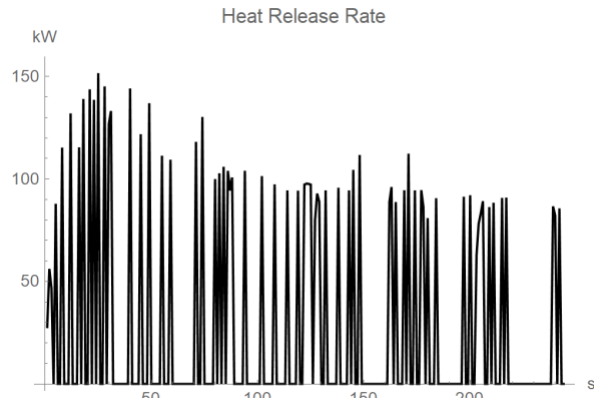
U/D = 0.5



$U/D = 0.75$



$U/D = 1.0$



$U/D = 1.5$

